PSU-IRL-SCI-467
Classification Numbers: [illegible]

THE PENNSYLVANIA STATE UNIVERSITY

IONOSPHERIC RESEARCH

Scientific Report 467

A Global Model of the Neutral Thermosphere in Magnetic Coordinates Based on AE-C Data

by

Carl G. Stehle

September 1980

The research reported in this document has been supported by the National Aeronautics and Space Administration under Grant Nos. [illegible] and [illegible].

IONOSPHERE RESEARCH LABORATORY

University Park, Pennsylvania

SECURITY CLASSIFICATION OF THIS PAGE (When Data Entered)

REPORT DOCUMENTATION PAGE		READ INSTRUCTIONS BEFORE COMPLETING FORM
1. REPORT NUMBER 467	2. GOVT ACCESSION NO.	3. RECIPIENT'S CATALOG NUMBER
4. TITLE (and Subtitle) A Global Model of the Neutral Thermosphere in Magnetic Coordinates Based on AE-C Data		5. TYPE OF REPORT & PERIOD COVERED Scientific Report 467
		6. PERFORMING ORG. REPORT NUMBER PSU-IRL-SCI-467
7. AUTHOR(s) Carl G. Stehle		8. CONTRACT OR GRANT NUMBER(s) NSG-5212 NSG-134-61
9. PERFORMING ORGANIZATION NAME AND ADDRESS National Aeronautics and Space Administration Washington, D. C.		10. PROGRAM ELEMENT, PROJECT, TASK AREA & WORK UNIT NUMBERS
11. CONTROLLING OFFICE NAME AND ADDRESS		12. REPORT DATE September, 1980
		13. NUMBER OF PAGES 143
14. MONITORING AGENCY NAME & ADDRESS(if different from Controlling Office)		15. SECURITY CLASS. (of this report) NONE
		15a. DECLASSIFICATION/DOWNGRADING SCHEDULE

16. DISTRIBUTION STATEMENT (of this Report)

Supporting Agencies

17. DISTRIBUTION STATEMENT (of the abstract entered in Block 20, if different from Report)

18. SUPPLEMENTARY NOTES

19. KEY WORDS (Continue on reverse side if necessary and identify by block number)

Heterosphere

20. ABSTRACT (Continue on reverse side if necessary and identify by block number)

An empirical model of the global atomic oxygen and helium distributions in the thermosphere is developed in a magnetic coordinate system and compared to similar models which are expanded in geographic coordinates. The advantage of using magnetic coordinates is that fewer terms are needed to make predictions which are nearly identical to those which would be obtained from a geographic model with longitude and universal time corrections. Magnetic coordinates are more directly related to the major energy inputs in the polar regions than geographic coordinates and are more convenient to use in studies of high

DD FORM 1 JAN 73 1473 EDITION OF 1 NOV 65 IS OBSOLETE
S/N 0102-014-6601

SECURITY CLASSIFICATION OF THIS PAGE (When Data Entered)

latitude energy deposition processes. This is important for comparison with theoretical models where the number of coordinates is limited.

The effect of magnetic activity on the atomic oxygen distribution in the morning sector of the high latitude thermosphere in the auroral zone is also considered. A magnetic activity indicator (ML) based on an auroral electrojet index (AL) and the 3-hour ap index are used to relate the atomic oxygen density variations to magnetic activity in this region.

PSU-IRL-SCI-467
Classification Numbers: 1.9.3

Scientific Report 467

A Global Model of the Neutral Thermosphere in Magnetic Coordinates Based on AE-C Data

by

Carl G. Stehle

September, 1980

The research reported in this document has been supported by the National Aeronautics and Space Administration under Grant Nos. NSG-5212 and NSG-134-61.

Submitted by:

John S. Nisbet
Director, Ionosphere Research Laboratory

Approved by:

John S. Nisbet
Director, Ionosphere Research Laboratory

Department of Electrical Engineering
Ionosphere Research Laboratory
The Pennsylvania State University
University Park, Pennsylvania 16802

ABSTRACT

An empirical model of the global atomic oxygen and helium distributions in the thermosphere is developed in a magnetic coordinate system and compared to similar models which are expanded in geographic coordinates. The advantage of using magnetic coordinates is that fewer terms are needed to make predictions which are nearly identical to those which would be obtained from a geographic model with longitude and universal time corrections. Magnetic coordinates are more directly related to the major energy inputs in the polar regions than geographic coordinates and are more convenient to use in studies of high latitude energy deposition processes. This is important for comparison with theoretical models where the number of coordinates is limited.

The effect of magnetic activity on the atomic oxygen distribution in the morning sector of the high latitude thermosphere in the auroral zone is also considered. A magnetic activity indicator (ML) based on an auroral electrojet index (AL) and the 3-hour ap index are used to relate the atomic oxygen density variations to magnetic activity in this region.

TABLE OF CONTENTS

LIST OF TABLES

LIST OF FIGURES

ACKNOWLEDGEMENTS

The author wishes to express sincere appreciation to Dr. John S. Nisbet for his imaginative guidance and constant support throughout the course of this work and to Dr. Ernst Bleuler for critical review of the research. Gratitude is extended to Dr. Jack Mitchell for serving on the author's thesis committee and to Drs. A. O. Nier and D. C. Kayser for supplying the data upon which this work is based. This work was presented as it progressed at a series of Atmospheric Explorer team meetings, and the discussions, questions, and comments of the A.E. team and in particular, Dr. A. E. Hedin, are gratefully acknowledged.

Many of the computer programs used here were developed by Mr. Robert Divany and Ms. Beverly Beiswenger and their invaluable programming assistance is greatly appreciated.

Enlightening discussions with Mr. Mark Griffis also contributed to the successful completion of this work.

This research was supported by the National Aeronautics and Space Administration under Grant Numbers NSG-5212 and NSG-134-61.

CHAPTER I

INTRODUCTION

1.1 General Statement of the Problem

Global composition and temperature measurements from mass spectrometer and airglow instruments on Ogo 6 (Carignan and Pinkus, 1968; Blamont and Luton, 1972) and mass spectrometers on Aeros A (Krankowsky et al., 1974) Esro 4 (Trinks and von Zahn, 1975) and the Atmosphere Explorer (AE) satellites (Spencer et al., 1973; Nier et al., 1973; Pelz et al., 1973) have provided a great deal of information about the density and temperature distributions in the thermosphere over a wide range of solar and geophysical conditions. These measurements have been used to construct empirical models (Hedin et al., 1974; Hedin et al., 1977,a, b; von Zahn et al., 1977; Jacchia, 1977; Thuillier et al., 1977) which represent the temperature and density fields in terms of geographic position, altitude, and solar and magnetic activity. At high latitudes, Joule heating, particle inputs, and electrodynamic forces are applied in very restricted areas causing large density and temperature perturbations over small regions of the thermosphere (Hedin and Reber, 1972; Reber and Hedin, 1974; Taeusch and Hinton, 1975; Nisbet and Glenar, 1977; Nisbet et al., 1978). In a geographic coordinate system, these energy sources produce large longitude effects. Towards lower latitudes, ion drag varies with the declination of the magnetic field and, therefore, induces longitudinal variations in the equatorial thermosphere as well (Reber et

al., 1973). A combination of these polar and equatorial influences forces a distinction to be made between local time and longitude. This distinction was realized by Hedin et al. (1979) in the form of longitude correction terms to the MSIS (Mass Spectrometer and Incoherent Scatter) model and by Laux and von Zahn (1979) by similar corrections to the Esro 4 model.

An alternate approach to this problem might consist of analyzing the satellite data in magnetic latitude and magnetic local time instead of geographic coordinates. Although the major energy input to the thermosphere, solar EUV heating, is organized in a geographic coordinate system, latitudinal and longitudinal gradients in this energy input, unlike the magnetic inputs, are small. It would thus seem better to utilize a coordinate system to which the more intense localized energy inputs are related. If a model could be developed in magnetic coordinates which did not require longitudinal corrections and which was of comparable accuracy to a geographic coordinate model developed from the same data base but including longitudinal corrections, it would be very useful for relating energy inputs and transport to their thermospheric consequences. It is the purpose of this work to develop such a model and to compare it to geographic representations of the neutral thermosphere.

1.2 Previous Related Studies

1.2.1 An Overview of Thermospheric Models

Theoretical models seek to explain the observed atmospheric behavior consistent with the laws of physics. Usually, a subset of the transport equations (continuity, momentum, and energy conservation) are solved under various simplifying assumptions. Boundary conditions at the turbopause and exobase are commonly imposed and an isothermal atmosphere above a certain height is often assumed. The difficulty in solving these equations has limited most theoretical treatments to one or two major constituents, although several authors have extended their results to three or more species (Vest, 1973; Harris and Mayr, 1975; Strauss and Christopher, 1979). While these models are becoming increasingly sophisticated, usually only average conditions are treated and the atmospheric fine structure is neglected. This restriction appears to be easing as comparisons between theoretical predictions and actual observations indicate the areas in which the theoretical models are deficient.

Empirical models, on the other hand, inherently offer the advantage of providing better agreement with the observations since it is on the basis of these observations that the models are constructed. This feature is valuable in studies where insight into the causes of atmospheric variations is not critical, but accurate numerical predictions are essential. Caution must be exercised, however, in the application of these models. Extrapolation of model predictions to conditions differing

from those under which the model was derived may give misleading results, although the wealth of ground-based and in situ data accumulated over the last decade has helped to reduce this problem. A discussion of both types of models serves to illustrate what has been done, how current problems are being approached, and what remains to be explained.

1.2.2 Empirical Models of Global Temperature and Composition

The early pioneering efforts of Nicolet (1961), Harris and Priester (1962) and Jacchia (1964, 1965) produced the first empirical thermospheric models using only satellite drag data. Although these models were landmarks in aeronomy, they were somewhat oversimplified. Since that time, the proliferation of aeronomy satellites and their associated databases in the last decade has sparked the development of several new generations of empirical models, some of which use ground-based measurements in addition to in situ observations to represent the density and temperature fields of the earth's upper atmosphere.

Airglow measurements of the 630 nm line of atomic oxygen by the Ogo 6 satellite were used to determine the global exospheric temperature distribution by Blamont et al. (1974). The maximum temperature at 270 km was shown to lie near the summer pole during solstices where there was little diurnal variation. This peak migrated across the equator within about three weeks after the equinoxes under active solar and quiet geomagnetic conditions.

The earliest empirical model based on measurements on several individual constituents was developed by Hedin et al. (1974) from Ogo 6 mass spectrometer measurements. The data base for this model consisted of N_2, O, and He density measurements between 400 km and 600 km near the peak of the 11-year solar cycle (27 June, 1969 to 13 May, 1971). All data were longitudinally (universal time) averaged, but local time variations were retained. Only data taken during quiet geomagnetic periods ($Ap \leq 7$ and $ap \leq 12$ for the same day and previous 6 hours) were included since increased magnetic activity may have caused large fluctuations in the densities. Two schemes were used to model the composition; in one, the densities were extrapolated to 120 km, using exospheric temperatures and a temperature gradient parameter ($s=0.0215\ km^{-1}$) determined from the N_2 measurements and based on a Bates (1959) temperature profile having constant lower boundary (120 km) values. In the other, the densities were extrapolated to 450 km assuming an isothermal regime. A least squares fit of spherical harmonics to the data was made in both cases. These functions were used since it was felt that they were approximate eigenfunctions in the thermosphere and since they were complete. That is, only a small number of terms should be needed, but as much detail as desired could be obtained simply by adding more terms. The theoretical advantages of spherical harmonics are discussed more completely by Mayr and Volland (1971) and Volland and Mayr (1972). The model contained only time independent, solar and magnetic activity, annual, semiannual, diurnal, semidiurnal, and terdiurnal terms. The $F_{10.7}$ variation included nonlinear components, but because the range was small, Ap variations were linearly approximated and a 6-hour lag was

used in accordance with Jacchia (1971).

The accuracy of the temperature representation was estimated to be ±50 K subject to the validity of the boundary conditions. The accuracy of the O and He values at 120 km were dependent on the assumption of diffusive equilibrium as well as on the inferred temperatures. The uncertainty in the actual measurements of the densities, up to 25% for N_2 and O and up to 50% for He, not including a 10-15% calibration uncertainty, also limited the model's accuracy.

A diurnal maximum near 1000 LT was found for He while N_2 peaked near 1600 LT. Winter maxima of He and of the O to N_2 ratio were also observed in addition to a 400 K summer to winter exospheric temperature difference. The inferred temperatures appeared to be about 7% higher than corresponding incoherent scatter measurements (Salah and Evans, 1973) and the diurnal variations compared favorably with the exception of the winter morning values where N_2 data were sparse.

Kasprzak and Newton (1976) compared predictions of the Ogo 6 model (Hedin et al., 1974) to mass spectrometer measurements from San Marco 3. They found that the N_2 values agreed within ±40% while total oxygen and mass density were within ±30%; however, poor agreement between helium values was found and attributed to extrapolation of the Ogo 6 data to the lower altitudes which were covered by San Marco 3. The Ogo 6 model showed a diurnal maximum of He from 1000 to 1100 LT at 450 km while San Marco 3 data displayed a maximum from 0700 to 0800 LT between 220 km and 280 km.

A model similar to Ogo 6 (Hedin et al., 1974) was presented by von Zahn et al. (1977) on the basis of Esro 4 composition measurements. This model used data over the 240-320 km altitude range and covered the lower activity portion of the solar cycle. Exospheric temperatures were inferred from both molecular nitrogen and argon. These averaged 5-9% lower than those predicted by the Ogo 6 model for an $F_{10.7}$ of 120 and were supported by more recent findings (Hedin et al., 1975; Mauersberger et al., 1976; Thuillier et al., 1977). The summer to winter temperature difference was also lower for the Esro 4 (315 K) than for the Ogo 6 model (415 K). The seasonal and diurnal variations of N_2 and Ar in the Esro 4 model were similar, supporting the assumption that both reflect the thermal structure in the upper atmosphere. The seasonal variation of O appeared to be dominated by a semiannual effect and the diurnal amplitude was found to be small. The He distribution showed a noticeable winter bulge of greater than 40 times the summer density and the semiannual component was found to be much larger than the diurnal variation.

An extension to the Ogo 6 model was made by Hedin et al. (1977a, b) using mass spectrometer data from five satellites (AE-B, Ogo 6, San Marco 3, Aeros A, and AE-C) and incoherent scatter measurements from four ground stations (Arecibo, Jicamarca, Millstone Hill and St. Santin). The average exospheric temperature for this MSIS (mass spectrometer and incoherent scatter) model was 1041 K for an $F_{10.7}$ of 150. This was 56 K lower than the Ogo 6 model and 35 K higher than the model of Jacchia (1971). The uncertainty of this value was estimated to be 15-20 K from comparisons between incoherent scatter temperature and N_2 density data. The low

altitude N_2 data also agreed well with rocket data (Offermann, 1974) but the higher altitude N_2 values differed markedly from the Jacchia (1971) values. The other species represented (He, Ar, O_2 and H) and, in particular, O, did not agree so well with low altitude rocket data (Offermann, 1974), possibly due to surface reactions of O in the rocket data and incomplete geographical coverage of He. The high altitude He variations were nearly the same as found by Keating et al. (1974) on the basis of satellite drag analysis and the seasonal variations of atomic oxygen agreed well with the results of Mauersberger et al. (1976).

Thuillier et al. (1977) extensively analyzed the 630 nm airglow data from Ogo 6 and presented a global empirical model of the exospheric temperature derived from this data. The polar heating patterns seen by Blamont et al. (1974) were still present after the database of the model had been edited and these patterns occurred during both solstices and equinoxes. They were particularly strong during magnetically disturbed periods. The airglow derived temperatures were in fair agreement with incoherent scatter results (Salah et al., 1975) and with temperatures inferred from N_2 density data (Hedin et al., 1974) and Ar and N_2 densities (Chandra and Spencer, 1975).

A comparison of exospheric temperatures inferred from total density, N_2 density, and 630 nm airglow data made by Nisbet et al. (1977) showed that temperatures inferred from N_2 densities were in much better agreement with airglow temperatures than they were with those inferred from total densities. This was especially true at high latitudes where the

atmosphere is definitely not in diffusive equilibrium. However, the mass of N_2 is closer to the mean molecular mass than any other constituent and N_2 is the major constituent in the region where eddy diffusion and vertical diffusion are both important and it is a better indicator of temperature than any other species, including the sum of all gases, under the assumption of diffusive equilibrium. The N_2 density inferred temperatures did, however, underestimate the influence of magnetic activity on the temperature at low latitudes while overestimating this effect at high latitudes using CIRA (1972) boundary conditions at 120 km and the polar cap distributions of N_2 and the temperature were rather different.

The effect of the large scale circulation induced by a magnetic storm in February, 1974 on the neutral composition was investigated by Mayr and Hedin (1977) utilizing the model of Mayr and Volland (1973a). High latitude depletions of O and He and enhancements in Ar as well as low latitude increases in O and He and decreases in Ar were predicted and substantially validated by AE-C neutral density measurements. An energy input of 1.7×10^{-3} W m^{-2} above 120 km was needed to bring the theory into agreement with the composition data. The annual changes in the neutral density distribution were said to have an important influence on the dynamics of magnetic storms. It should be noted that this treatment was based on a model having no local time dependence either in the energy input or in the neutral density.

Jacchia et al. (1977) used composition measurements from Esro 4 to create a global thermospheric model for magnetically disturbed conditions. They showed that a variation of the height of the homopause would reproduce the density changes observed during disturbances, though noting that rapid fluctuations of this level might not be likely. They also found that the differences between density values obtained during transient disturbances and sustained magnetic storms could be reproduced by the nonlinear character of the relationship between geomagnetic heating and the variation in homopause height. The sudden heating gave rise to an 'equatorial wave' in addition to the usual thermal effects.

Barlier et al. (1979) compared several thermospheric empirical global models (MSIS, Hedin et al., 1977a, b; Esro 4, von Zahn et al., 1977; J77, Jacchia, 1977; CTM, Barlier et al., 1978b) under various geophysical conditions. Each model performed relatively well overall, but none of the models explained the variations present in the data completely. In particular, diurnal phase and amplitude estimates were noticeably different below 200 km. Also, major discrepancies between He data in areas of low He concentrations from satellite drag analysis and from mass spectrometer measurements could not be reconciled.

Hedin et al. (1979) and Laux and von Zahn (1979) made improvements to the MSIS and Esro 4 models, respectively, by adding longitude corrections to these models which reflected the offset of the geomagnetic poles from the geographic poles. These corrections represented the gross effects of magnetic coordinates on the composition and density, but the role of

increasing magnetic activity was still not satisfactorily delineated.

The annual variations of several neutral constituents (N_2, O, He, Ar, N) were outlined by Köhnlein et al. (1979) using Aeros A and B data taken near 0400 LT and 1600 LT. Agreement with MSIS and Esro 4 predictions was quite good for He although a large scatter (±40%) was present in some of the measurements. The general behavior of N agreed fairly well with Engebretson et al. (1977) although Aeros measurements displayed a polar structure which was quite different. The Aeros, Esro 4, and MSIS models predicted nearly identical values for O except where the measurements were extrapolated to 120 km. The Aeros data on Ar and N_2 showed strong variations with magnetic activity near the poles as was predicted by Esro 4 and MSIS, but the equatorial behavior of Ar was quite different than MSIS estimated.

1.2.3 Theoretical Models

1.2.3.1 Neutral Composition and Temperature

The seasonal behavior of the neutral thermosphere averaged over daily variations was examined by Mayr and Volland (1972a) who outlined the latitudinal structure of the annual and semiannual components by applying small perturbations to the conservation equations and observing the effects of different energy inputs. EUV heating was used as an energy source for the annual component and a term simulating auroral heating, which maximized at the poles, was added to this in order to study the semiannual variations. Although photochemistry was neglected, clear

annual and semiannual trends were found. The annual solar heat input imbalance induced a circulation system with winds blowing from the summer to the winter hemisphere in the upper thermosphere. This first appeared to damp the temperature variation strongly; however, in order to maintain continuity, the lighter minor constituents O and He began to diffuse upward through the major gas molecular nitrogen in the summer hemisphere and became depleted at lower altitudes where the large molecular nitrogen concentration acted as a barrier to diffusion thus decreasing the pressure variation and, consequently, the horizontal wind velocity. This in turn reduced the adiabatic heat transfer from the preferentially heated summer hemisphere to the cooler winter hemisphere allowing the maintenance of a larger temperature imbalance. The semiannual effect appeared as reduced O densities below 450 km and reduced He densities at all thermospheric heights near both poles corresponding to the peak in heat input there; however, the equatorial concentrations of these constituents increased in response to the semiannual circulation cells from the poles to the equator. Surprisingly enough, the annual mass density variation was found to be nearly constant with altitude and the small semiannual variation almost latitude independent; these results were due to the circulation and the resulting diffusion of atomic oxygen and helium through molecular nitrogen. This explained for the first time why satellite drag measurements of total density showed little change in the annual variation with height while mass spectrometer data indicated the opposite.

The diurnal phase difference between the temperature and the O density was investigated by Mayr and Volland (1972b) using a two-dimensional time-dependent model having solar heating as an energy source. The momentum and continuity equations were solved assuming no variation in n(O) at the lower boundary of 90 km and diffusive equilibrium for atomic oxygen above 250 km. Wind-induced variations of n(O) were found to control the atomic oxygen distribution below 200 km whereas thermal expansion became more important above 300 km. The time of the diurnal maximum of atomic oxygen of 1030 LT was nearly equal to that of the wind at low altitudes, increasing slowly towards that of the temperature (1600 LT) throughout the upper thermosphere. The authors noted that a major shortcoming of this model was that energy inputs from magnetic storms, which were not included, could couple with the lower thermosphere and possibly reduce the density-temperature phase difference significantly. Also, the effects of semidiurnal and terdiurnal harmonics, which could be important, were not considered.

This study was extended by Mayr et al. (1973), who used a 'quasi' three-dimensional model and considered diurnal, semidiurnal, and terdiurnal harmonics in the energy input term. These harmonics manifested a latitudinal dependence and peaked at the equator. Nonlinear coupling between the diurnal ion drag term and the diurnal horizontal wind component was also included. The 1600 LT temperature maximum and the mass density peak near 1400 LT were shown to be consistent with the theory. The semidiurnal and, more importantly, the terdiurnal harmonic caused a shift in the temperature maximum at high altitudes to later local times in

close agreement with radar backscatter observations (Carru et al., 1967; Nisbet, 1967; Waldteufel and McClure, 1969; Mahajan, 1969; Salah and Evans, 1973). Lower in the thermosphere, energy redistribution resulting from heat advection tended to shift the temperature peak towards noon. Diffusion of O and He, especially from energy inputs occurring below 120 km, greatly influenced the phase of the mass density above 250 km, shifting it towards earlier hours.

The effects of upper atmospheric flow on the minor gases helium and argon were outlined by Reber and Hays (1973) by combining the momentum and continuity equations to derive density profiles for these gases. Model values were used for the temperature and major gas (N_2) distributions and lower boundary densities were assumed for He and Ar. An expression developed by Hodges and Johnson (1968) was used to determine the upper boundary flux of He. An arbitrary vertical wind profile which induced summer to winter transequatorial flow was chosen as the thermospheric wind field. This hemispherical flux caused a significant increase in the winter to summer helium density ratio. Exospheric transport lessened this value, particularly near the peak of the 11-year solar cycle when the exospheric temperature was high, but a pole to pole ratio of about 10 was still maintained. Equatorial horizontal winds of 100-200 m sec^{-1} at 200 km were found to be consistent with the He densities measured by Ogo 6. The effects of the wind field on Ar were quite different. The Ar density increased in the summer hemisphere by almost a factor of 4 over winter hemisphere values and exospheric flow was found negligible since the Ar density decreased so rapidly with height. No measurements of Ar were

available to compare with this estimate at that time.

The diurnal behavior of the thermosphere was examined by Harris and Mayr (1975) by extending the previous studies of Mayr and Volland (1972a, b; 1973a) involving nonlinear processes and 'mode coupling'. Mode coupling was believed to occur between 100 km and 200 km where the functional form of the solutions to the transport equations changes radically. In this transition region, solutions could only be expressed by a combination of both low altitude and high altitude eigenfunctions. The effects of viscosity, ion drag, diffusion, advection and heat conduction were also included in the analysis. The results showed a decrease in the diurnal variations of temperature and N_2 density at all altitudes with respect to one-dimensional models. The O variation was more complicated; above 200 km the diurnal amplitude decreased, but below 200 km a substantial increase (due to wind-induced diffusion) was observed. The phases of the temperature, N_2 density, and O density decreased at nearly all heights; in particular, the phase of O below 200 km was shifted by more than 12 hours towards morning. The unique amplitude and phase behavior of O were direct results of transport. Further, these results were what Harris and Priester (1962) had attempted to duplicate by invoking a 'second heat source'.

Strauss et al. (1977) constructed a three-dimensional dynamical model of helium in the upper atmosphere which included the effects of exospheric transport, molecular and eddy diffusion, and solar activity. A background gas consisting of O, O_2, and N_2 was assumed and represented by the CIRA

(1972) model, and momentum feedback by He on this gas was considered negligible. The empirical representation of the background gas density and the temperature was considered more realistic than the solution of the energy equation due to uncertainties in the solar flux estimates. The only equations requiring solutions were, therefore, momentum and continuity for He. An upper boundary condition for helium was taken from Hodges and Johnson (1968). The low altitude diurnal maximum in helium was estimated to lie between 0600 and 0800 LT. Although this phase increased somewhat with height, it was still earlier than empirical models predicted. Lower spatial resolution in the theoretical model was suggested as an explanation. The pole to pole helium ratio was calculated for several $F_{10.7}$ values and was found to increase as the $F_{10.7}$ index decreased. A decrease in exospheric transport seemed to be the reason for this as Reber and Hays (1973) had found. Smaller effects on this 'bulge ratio' were observed by varying K, the eddy diffusion coefficient. The ratio increased from 7.2 to 9.0 at 400 km as K was increased from 3×10^2 to 10^3 m^2 s^{-1} for an $F_{10.7}$ of 144×10^{-22} W m^{-2} Hz^{-1}. These results were generally in agreement with empirical models and quantitative differences were attributed to insufficiences of the CIRA (1972) parameters used. The authors suggested that the inclusion of a globally varying eddy diffusivity could have significant effects on the predicted distribution of the minor gases.

Strauss (1977) estimated the global distribution of argon by the same method used to determine the distribution of helium, but without exospheric transport. Calculations were made for both hydrostatic and

dynamic conditions. For dynamic conditions, the diurnal maximum of argon appeared later in the day (1400 LT) and the diurnal 'bulge ratio' was larger (11.5 at 320 km). The model compared favorably in the equatorial regions with San Marco 3 data (Newton et al., 1975) in determining the diurnal phase; however, the diurnal amplitude was overestimated and an inadequate representation by the CIRA (1972) model, which was used to calculate the vertical diffusion velocity of argon, was suggested as the reason for this. Comparison with the MSIS model (Hedin et al., 1977a, b) and with data from Esro 4 (von Zahn et al., 1973) again revealed overestimation of the diurnal variation.

Strauss and Christopher (1979) investigated the influence of transport on the global atomic oxygen, molecular oxygen and molecular nitrogen distributions in the thermosphere. Using O, O_2, and N_2 coupled by collisions and neglecting photochemistry, calculations for hydrostatic and steady state dynamic conditions were made by solving the mass and momentum conservation equations. Departures from diffusive equilibrium for O_2 and N_2 below 200 km were slight, but atomic oxygen showed a substantial variation in this region. All constituents approached diffusive equilibrium towards higher altitudes. A low altitude minimum of the O concentration was found at both poles for equinox and at the summer pole for solstice. The local summer minimum gave way to a maximum in O at higher altitudes ($\geq$375km). These effects were consistent with wind-induced diffusion in the lower thermosphere succumbing to thermal expansion with increasing height.

1.2.3.2. Atmospheric Motion

Theoretical examinations of the thermospheric circulation system have traditionally been based on the solution to the equation of motion for the neutral gas using empirical temperature and pressure distributions and assuming diffusive equilibrium. Although this assumption has been found unrealistic below 150 km (Mayr and Volland, 1972a, b; Mayr et al., 1973), it has, nevertheless, enabled investigators to produce important and useful models of the region of the thermosphere normally investigated by satellites.

One of the earlier attempts to represent the thermospheric wind field was made by Kohl and King (1967) based on a static atmospheric model (Jacchia, 1965) used to estimate pressure gradients resulting from non-uniform solar heating in the upper atmosphere. These estimates of the 'driving force' were applied to the linearized horizontal equation of motion for the neutral gas which included ion drag, viscous, Coriolis and linear inertial terms. Vertical profiles of the horizontal wind velocity in the absence of electric fields were thereby obtained. The calculations were performed for equinox for peak electron densities of 10^{12} m^{-3}, roughly corresponding to daytime and 3×10^{11} m^{-3}, approximately those of nighttime. The wind velocity vector at 300 km corresponding to high electron densities essentially followed the pressure gradient due to the strong influence of ion drag. The Coriolis and inertial terms dominated the circulation pattern for the lower electron density (lower ion drag) conditions. In this case, the high latitude wind direction was distinctly shifted towards the east while the low latitude motions were directed

westward. The authors cautioned that these results were subject to the rather restrictive assumptions of a sinusoidal driving force, fixed electron and ion densities, a single viscosity coefficient profile, coincidence of geographic and magnetic poles, and the neglect of all forces other than that of the pressure gradient (e.g. electric fields).

A similar study was undertaken by Geisler (1967) using a modified pressure distribution (Jacchia and Slowey, 1967) as the driving force. The resulting wind patterns did not vary substantially from those found by Kohl and King (1967) although the wind velocities differed. Variations in ion drag appeared to have much more influence on the meridional wind component than changes in molecular viscosity.

Atmospheric models for both neutral and ionized particle densities (Jacchia, 1965; Nisbet, 1970) formed the basis for the global wind system study completed by Blum and Harris (1975a, b). The Navier-Stokes equations including nonlinear effects were solved to obtain horizontal winds, although the nonlinearities were subsequently shown to be of importance only in the equatorial region. In contrast to previous work, the effects of electric fields were considered, but the simplification of coincident geographic and magnetic poles was retained. The pressure gradient and ion drag terms appeared to have a dominant influence on the solutions, but significant variations from Coriolis, viscosity, and inertial terms at various geographical positions indicated that simplification of the equations of motion was only valid for fixed altitudes or geographic locations. Comparison of theoretical predictions

with wind velocities determined from incoherent scatter measurements were generally favorable. The empirical findings of Harper (1971) at Arecibo (18°N) indicated smaller equatorward velocities than predicted and a diurnal phase about one hour earlier than the theoretical estimate. The observations of Evans (1971) at Millstone Hill (42.6°N) also showed a smaller equatorward average but the lower order harmonics of the local time variation were similar to the theoretical curves. The meridional winds deduced by Amayenc and Vasseur (1972) for equinox also had a smaller equatorward maximum than the theoretical estimates. This discrepancy was not so large for solstice and was thought to have been due to the lower ion densities used in the theoretical treatment.

A similar approach was taken by Creekmore et al. (1975) who used the Jacchia (1971) model for the temperature and neutral densities and the Ching and Chiu (1973) model for the ion concentrations. Modes up to the 4th harmonic were included in the treatment and the results were somewhat similar to those of Blum and Harris (1975a, b) when the differing ion densities assumed were reconciled. Large scale effects appeared to be illustrated reasonably well, but the resolution needed to elucidate the smaller scale features was lacking. The significant contribution of vertical motion to the energy balance at high latitudes was stressed as an important area requiring future work.

The influence of a convection electric field in the polar regions on ion drifts and neutral winds was investigated by Maeda (1976). A dawn to dusk electric field similar to that observed by Ogo 6 (Gurnett, 1972) and

two height independent latitude profiles of the ion density were used to solve the horizontal equations of motion for the neutral and ionized gases between 110 km and 200 km. The neutral wind field of electric field origin was found to depend strongly on the ion density profile and the wind speed was found to be comparable to the thermally driven wind speed (Kohl and King, 1967) of greater than 100 m sec^{-1} at 200 km.

Roble et al. (1977) analyzed the seasonal and solar activity induced variations of the zonal mean circulation for quiet geomagnetic conditions. Extending the model of Dickinson et al. (1975, 1977) to low solar activity, the authors found that the mass flow above 100 km at solstice from the summer to the winter hemisphere was much larger near solar maximum than near solar minimum. The equinoctial transition of the average interhemispheric flow occurred within 2 weeks of equinox and this delay diminished substantially with increasing geomagnetic activity. Although the flow was driven mainly by solar UV and EUV sources, modulation of these sources by high latitude effects which were themselves related to geomagnetic activity appeared likely due to the variation in this transition period. Since the magnitude of the high latitude sources needed to be adjusted over the solar cycle to obtain agreement with measured temperatures and winds, the energy input in these regions was expected to vary with solar activity.

1.2.4 Small Scale Phenomena

1.2.4.1 Temperature and Density Behavior During Periods of Low Magnetic Activity

The spatial and temporal variations of the neutral thermosphere which are highly localized have not yet been included in global empirical models. The large number of terms needed to adequately represent these perturbations in an analytic fashion do not seem justified at this time because of insufficient physical understanding and limited databases. Only specific inquiries into regionalized phenomena can give an accurate picture of the fine structure in the thermosphere at the present time.

Mid- to high-latitude heating sources were observed by Reber and Hedin (1974) by analyzing two years of neutral density measurements from Ogo 6. The molecular nitrogen concentration near 450 km was found to increase, the helium density to decrease, and the atomic oxygen concentration to remain fairly stable in the region of heating. These results appeared consistently during magnetically quiet periods, suggesting that the heating was a permanent feature of the neutral thermosphere. Corotation of this heat source with the geomagnetic pole indicated that some type of geomagnetic control was being exerted although no correlation with the cusp region could be found.

Taeusch and Hinton (1975) related N_2 density variations to electrodynamic and particle heating in the quiet polar thermosphere. Mass spectrometer measurements of the N_2 density from Ogo 6 were normalized to 450 km and then divided by the corresponding Ogo 6 model densities (Hedin et al., 1974) in order to estimate differences from the average

concentration as well as variability in these differences. The behavior of N_2 with respect to invariant latitude (ILAT) and magnetic local time (MLT) was then outlined. The regions having the greatest differences between measurements and model estimates were the cusp area and the 0000-0300 MLT sector. Although the position of the cusp was quite variable, it was usually located near 80° ILAT and 1200 MLT. In addition to large differences from average values, the densities in the cusp were found to be quite variable. The densities in the 0000-0300 MLT region did not display this variability. This suggested that the energy inputs to the cusp, quite possibly the particle precipitation identified by Gustafson (1972), were quite variable while the heat sources in the 0000-0300 MLT region, which are more likely electric fields over a region where particle precipitation has enhanced the conductivity, were very persistent.

Wavelike structure in N_2, Ar, and He was seen by Reber et al. (1975) over several individual orbits of Atmosphere Explorer C (AE-C). The relative amplitude of the Ar waves was about twice that of the N_2 disturbances, but with the same phase. He was usually 180° out of phase with N_2 and had about one-half the N_2 amplitude. The data examined, however, were too limited to determine the nature of the disturbances.

The first experimental evidence of transport by the diurnal tide was presented by Hedin et al. (1978) using AE-E data. A large phase shift in O and He from high to low altitudes, predicted by Mayr and Harris (1977) was substantially validated by these observations although marked

statistical deviations in the data made it difficult to evaluate the agreement between theory and observations quantitatively. The region above 200 km showed no departures from diffusive equilibrium while these were marked in the low altitude regime. A description in terms of eddy diffusion models, which predicted composition variations only below 120 km and diffusive equilibrium above, was found unsatisfactory since the predicted increases of O and He amplitudes from 160 km to 120 km were not observed.

Temperature variations in the polar thermosphere over the 11-year solar cycle were studied by Chanin and Tulinov (1979). Sodium clouds between 120 km and 180 km from rocket flights were used to estimate neutral temperatures. Values obtained near 165 km for the solar minimum were found to be about 500 K larger than those for the solar maximum. A possible explanation of this was increased turbulence in the lower thermosphere and therefore, larger heat flow to the mesosphere during the solar maximum (Roper, 1973). This flow would cause a higher altitude mesopause at the peak of the solar cycle and, therefore, lower temperatures near 120 km. This explanation would be consistent with the observed higher exospheric temperatures of the solar maximum since the temperature gradients would be larger in this case.

1.2.4.2 Temperature and Density Behavior During Periods of High Magnetic Activity

Analysis of orbital drag measurements during geomagnetic storms by Jacchia (1959) first suggested that the neutral thermospheric density increases during these disturbances. The time lag of the response of the composition to heating as well as the details of the response continue to be a topic of considerable interest. Although the theory is still developing, a summary of the advances made is in order.

A theoretical investigation of the density response to auroral heating was launched by Volland and Mayr (1971). A heat input resembling an impulse function in latitude and exponentially decaying in time was positioned in the nighttime auroral zones ($\pm$ 65^{o}LAT) and used to drive a three-dimensional model of the thermospheric density based on a spherical harmonic expansion to see which harmonic components were effectively damped out and which propagated to lower latitudes. Although an inordinate number of harmonics would have been needed to accurately portray the heat input, it was shown that the thermosphere effectively damped all but the four lowest components after the first hour of the storm. The time response of the maximum density change varied from 2.5 hours at the pole to 6 hours at the equator and the amplitude of this variation at the pole was twice that at the equator. The local time behavior of the density changes was found to depend on latitude, maximizing between about 0000 LT and 0600 LT.

Neutral densities from the Ogo 6 mass spectrometer were examined by Taeusch et al. (1971) to determine what variations of composition occurred during the geomagnetic disturbances in the period 27 September to 3 October, 1969. All data were normalized to 500 km and divided by quiet time values before comparisons were made. The ratio of the N_2 density under disturbed conditions to the N_2 density under quiet conditions showed the largest value in the auroral zones and the O ratio increased here as well, but not by so much. The equatorial variations were small during the storms observed. The N_2 and O density variations were used to infer neutral temperature changes by invoking Jacchia (1971) model temperatures corresponding to the neutral density values. Temperature increases of 450 K at high latitudes were inferred from N_2 while increases of only 325 K were inferred from O variations. The smaller increases for O were attributed to changes in the assumed lower boundary conditions. That is, N_2 was expected to be more nearly in diffusive equilibrium at low altitudes than O. In contrast to the high latitude temperature increases, equatorial enhancements of only 25 K for N_2 and 45 K for O were calculated. These values suggested upwelling in the polar regions and subsidence near the equator as predicted by Mayr and Volland (1970) and others. The density changes above 60° geographic latitude appeared to occur less than one hour after the onset of a storm as measured by the geomagnetic field variation. The largest changes occurred near 0600 and 1000 MLT which suggested geomagnetic control of the heat source(s).

A decrease in the lower boundary O to N_2 ratio and changes in thermospheric circulation during magnetic storms were predicted by Chandra and Stubbe (1971) upon solving the equations of motion and heat conduction

for the ions and neutrals and the ion continuity equation. The height of the turbopause was expected to vary and any temperatures derived using fixed boundary conditions were, therefore, considered to be inaccurate. The ion densities were shown to be sensitive to the O to N_2 ratio and it was suggested that ionospheric parameters be used in modeling since they were easier to measure than neutral ones.

Mayr and Volland (1972c) showed that the circulation system set up by a magnetic storm would cause low altitude depletions in n(O) in the polar regions due to diffusion and high altitude enhancements in $n(N_2)$, but not in n(O), at high latitudes. The model of Mayr and Volland (1971) was used for the calculations and two auroral heat sources were assumed to excite thermospheric circulation. One source maximized near 100 km, simulating auroral particle precipitation and the other near 150 km, which was assumed to be similar to Joule heating by electric fields. A constant O density at 90 km and no diffusion above 250 km, where O becomes the major species, were assumed and solutions to the coupled continuity and momentum equations were obtained using up to the second Legendre polynomial for the heat input, temperature and wind fields, and the diffusive flux. Only the Joule heat source was found capable of reproducing the densities measured near 400 km during a magnetic disturbance (Taeusch et al., 1971). The O density variation was separated into temperature and wind components. These were comparable at high altitudes (250-400 km) but the wind effects dominated the temperature induced variations lower down. Since the two mechanisms are basically in opposition, it was expected that O would be depleted at low altitudes (<200 km) due to the vertical wind and slightly

enhanced at high altitudes (>400 km) because of thermal expansion. A quite different situation was predicted for N_2. Being the major species and diffusing negligibly through O, the N_2 gas was found to be controlled mainly by thermal sources throughout the upper atmosphere although the circulation system was responsible for enhancing the concentration at high latitudes while depressing it near the equator.

An increase of the mass density in the thermosphere was linked to enhanced auroral electrojet activity by Forbes and Marcos (1973) who examined accelerometer data taken by the Air Force OV1-15 satellite and orbital decay information on the 1968-64A satellite. The density increases found in the dayside aurora agreed well with Cole's (1962, 1966, 1971) Joule heating theory. A wavelike structure originating in the auroral zone was also observed during periods of electrojet activity.

Several equatorial variations of the composition were discussed by Raber et al. (1973) using Ogo 6 mass spectrometer data. Temperature enhancements of 50-150 K at low latitudes and up to 1000 K at midlatitudes were inferred from N_2 density measurements taken during periods of high magnetic activity. Substantial decreases of n(O) and n(He) and increases of the N_2 concentration coincided with these magnetically disturbed periods. Variations of N_2 with latitude near the equator appeared to correspond with F-region electron density changes which had been associated with the geomagnetic anomaly. The diurnal maximum of He at 450 km was observed near 1000 LT, while N_2 and O peaked nearer to 1500 LT.

Hays et al. (1973) investigated the effects of auroral heating by particle precipitation and by electric fields on the thermospheric composition. In particular, changes of composition resulting from vertical winds which were excited by the heat generated by magnetic storms were estimated by solving the vertical continuity and momentum equations for the period of the sudden heating. Horizontal variations of composition were assumed to be negligible during the onset of a magnetic storm. The mean molecular mass was shown to increase at 500 km regardless of the type of energy input and the largest variations of the composition associated with the particle fluxes resulted from 'soft' (< 0.6 keV) precipitation. This was explained by the fact that winds cause the greatest changes where the vertical composition gradients are largest. The region over which this occurs corresponds to an area of large electric fields and is also the zone of 'soft' particle precipitation (near 130 km). Estimates of the high altitude variation of composition for similar heating profiles showed that this variation was nearly independent of the rate of heating although it did vary significantly with the total energy injected into the system.

The response of the thermosphere to geomagnetic heating was examined in detail by Mayr and Volland (1973b). The theoretical model of Mayr and Volland (1972b) with a modified height distribution of the heat input was used to estimate the variations in thermospheric temperature and density due to Joule heating. The N_2 density increased at all altitudes for every harmonic as would be expected. However, the net increase due to the third harmonic was much smaller than that caused by the first, indicating

substantial damping by advection. The O density decreased at low altitudes (<200 km) as a result of upward diffusion through N_2. The diffusion was caused by the higher harmonics of the heat input (P_2 through P_8) and persisted to high altitudes, becoming offset by thermal expansion only above roughly 400 km. This explained the relatively small variations seen in n(O) at high altitudes (400 km). The situation was completely different for helium. In this case, the diffusive effects controlled the density distribution throughout the thermosphere because of the light mass and low concentration of He. Thermal effects only slightly offset the diffusive influences on He above 300 km. The neutral temperature changes were also quite marked. The first harmonic of the heating source caused an overall increase in the temperature but with little latitudinal dependence. The higher harmonics, through vertical diffusion and horizontal transport, showed large departures from the 'diffusive equilibrium' temperature determined by the first harmonic. These departures were strongly dependent on latitude showing the importance of including diffusion in calculations dealing with the global temperature distribution.

Trinks et al. (1975) inferred from Esro 4 gas analyzer and ground-based ionosonde measurements west of 180° E longitude that the midlatitude O to N_2 ratio between 250 and 400 km substantially decreased during several magnetic disturbances in February, 1973. This ratio was found to decrease even more at high latitudes in a separate and apparently unrelated region. The mid-latitude behavior was attributed to energy deposited below 150 km and transported from the high latitude auroral

ovals, possibly by winds or gravity waves.

Empirical evidence of compositional changes during a period of increasing magnetic activity was obtained by Prölss and Fricke (1976) from Esro 4 mass spectrometer samples. The disturbed to quiet time density ratio R(n) served as an indicator of compositional changes throughout the period studied. R(n) increased above 1 for N_2 and for Ar at high latitudes and became especially large near the peak of the magnetic disturbance; R(n) decreased below 1 for He in the same region becoming as small as 0.1. The behavior of O was more complex and both increases and decreases of R(n) were observed. Generally the decreases appeared at lower altitudes. An upper limit of one orbital period (ninety minutes) was placed on the high latitude response time by the authors based on the results of this study.

Mayr and Volland (1976) again used Joule heating as an auroral energy input to determine what role density waves excited by the aurora played in modifying the composition in the thermosphere. Diffusion was found to be responsible for the large phase difference of about 220° between He and N_2 waves and of their relatively equal amplitude. The phase difference was in agreement with Reber et al. (1975) although there remained some question as to the actual amplitudes. The wavelengths considered were of the order of 1000 km and other modes, if present, were said to be able to significantly alter these results.

Neutral N_2, O, Ar, and He data taken down to 160 km by Atmosphere Explorer C during a magnetic storm in February 1974 were analyzed by Hedin et al. (1977c) in order to determine the response of the composition at low altitudes to magnetic disturbances. The N_2 and Ar concentrations were found to increase and the O and He densities to decrease above 45°N geographic latitude, while below this latitude all densities increased during the storm. A very slow return to normal conditions after the disturbance indicated that the atmosphere has a time integration effect with respect to this type of energy input. There was no apparent correlation of the neutrals to the 3-hour ap index, but a correlation with magnetic latitude was seen. The authors noted that this correlation was asymmetrical suggesting a possible magnetic local time, universal time, or longitude influence. The O to N_2 ratio was also found to be closely correlated with in-situ electron densities and F_2 peak densities as measured by ionosondes.

1.2.4.3 Neutral Wind Observations

Theoretical models of the global circulation system do not yet accurately represent the small scale features. This inaccuracy stems from the global empirical pressure and temperature models used to determine the circulation patterns. The global model of Jacchia (1971), which is based on satellite drag data, exhibits a diurnal pressure maximum near 1400 LT while incoherent scatter results (Nisbet, 1967) show the temperature maximum to be near 1600 LT. Studies of the Ogo 6 airglow data (Blamont et al., 1974; Thuillier et al., 1977; Nisbet et al., 1977) have revealed that

the maximum temperatures occur near the local summer pole at solstice and not near the equator as was previously assumed. Further, Mayr and Volland (1972b) have determined that the temperature and mass density do not maximize at the same local time because of transport effects; the temperature appears to peak near 1600 LT while the diurnal maximum of the mass density is nearer to 1400 LT.

While more recent models of the thermosphere (Hedin et al., 1977a, b; von Zahn et al., 1977) have improved the pressure and temperature estimates, the wind field is still too variable to be accurately represented on the basis on global models. For example, meridional winds of substantial magnitude have been shown to flow from the polar cap. Nisbet and Glenar (1977) have found that these winds are not uniform but depend strongly on magnetic local time. It is precisely this type of dependence that the models have yet to incorporate. For this reason, only empirical results will be considered here.

Kent (1970) has discussed two techniques for determining neutral winds. One is based on ion drift calculations, which are used to infer neutral velocities and the other is direct measurement of the neutral motion. Ion velocities can be found using incoherent scatter facilities while rocket vapor trail measurements are often employed as a direct approach. Other direct methods have been developed and will be discussed later.

Reddy (1974) observed a meridional circulation pattern using incoherent scatter data from St. Santin (44.7°N) during several days in February, 1969, when a magnetic storm was in progress. Equatorward winds were seen, above roughly 120 km, while a poleward flow appeared nearer to 100 km. Estimates of the momentum balance showed that the 100 km 'return flow' could support the higher altitude equatorward flux. An interesting observation of the wind structure made was that the difference in velocity between quiet and distrubed days peaked at 165 km and decreased above this altitude. The implications of this observation towards understanding the nature of the wind source were not known.

Support to the circulation theory of magnetic storms was lent by Brekke et al. (1974) who inferred neutral wind speeds from incoherent scatter data taken at Chatanika, Alaska (ILAT=65°) during the magnetospheric storm of 3 August to 9 August, 1972. The magnitude of the daytime antisolar flow reported by Brekke et al. (1973) decreased during the storm and, at one point, even reversed direction. This implied that strong local forces at high latitudes were effectively competing with the predominant day-to-night flow caused by solar heating. Since ion drag was not expected to cause such a change, a heat source north of Chatanika which produced a local pressure gradient was postulated. The nighttime equatorward flow resulting primarily from the solar tide was reduced, presumably due to an increase in ion drag, while the afternoon and early morning winds experienced a shift in direction towards the equator during the storm. These effects were thought to influence the motion far from the auroral zones, and it was suggested that they be included in future

investigations of the global wind system.

Roble et al. (1977) used incoherent scatter measurements of the electron and ion temperatures, electron density and vertical plasma drift to determine neutral winds over Millstone Hill (42.6°N, 71.5°W) for three winter and three summer geomagnetically quiet days in 1969 and 1970. The calculations were made following Roble et al. (1974). These authors had deduced neutral winds over Millstone Hill for two quiet days near equinox and found diurnal averages of the zonal wind to be westward at about 30 m s^{-1}. In the more recent work, the nighttime equatorward winds found were larger for summer that for winter, but the daytime poleward winds were smaller during summer than in winter. The diurnal average summer winds were 15 m s^{-1} westward for the zonal and 45 m s^{-1} equatorward for the meridional component. The winter averages were 15 m s^{-1} eastward for the zonal but a highly irregular meridional component was found. All velocities were calculated in a form consistent with the Ogo 6 model density values. These values were used in the ion heating and cooling rate estimates which yielded neutral temperatures based on a locally balanced ion energy equation. The contributions of electric fields to the wind system were not included since fields on the order of 1-2 mV m^{-1} at this location (Kirchoff and Carpenter, 1975) were felt to cause only small velocity changes.

Midlatitude winds do not appear to depend critically upon electric fields, but high latitude motions are much more tightly coupled to the E-fields, particularly in the auroral zones, through ion drag and Joule

heating (Fedder and Banks, 1972). Therefore, high latitude analyses must take the ion drag force into account.

Simultaneous measurements of ion drifts and neutral flows at high magnetic latitudes ($\geq 65^{\circ}$) and high altitudes (>200 km) were carried out by Meriwether et al. (1973) using barium clouds from rocket releases to monitor the motions. Optical triangulation allowed a determination of both drift and wind velocities in the auroral zones, polar cap, and the transition region. Ion drag forces were sufficient to explain most of the wind measurements in the evening and midnight regions while other forces, including a large inertial component, were needed to explain the morning flows. Spatial rotation of the wind direction from the auroral zones to the polar cap in the evening and midnight regions was quite noticeable. The westward to eastward ion convection reversal near the Harang discontinuity before midnight was particularly outstanding.

Hays and Roble (1971) obtained meridional wind speeds representative of the 250 km region at Michigan (42.3°N, 83.7°W) during two geomagnetic storms by measuring the Doppler shift of the 630 nm line of atomic oxygen. Southward velocities of 250 to 400 ms^{-1} were observed throughout the night during both storms. A combination of diurnal and enhanced auroral zone sources were suspected to be responsible for these intense flows.

Nagy et al. (1974) also measured the Doppler shift of the 630 nm line of atomic oxygen from Ester Dome, Alaska (ILAT=65°) in order to infer neutral wind velocities while simultaneously measuring ion drifts by incoherent scatter radar at Chatanika, Alaska. The ion drift reversal

near magnetic midnight seen by Meriwether et al. (1973) was quite prominent and the westward ion drift in the premidnight region appeared to control the neutral zonal flow, although no such control was apparent in the neutral meridional winds since the north-south ion flux is much smaller. The postmidnight magnetic local time region displayed virtually no neutral zonal motion and there appeared to be no simple explanation for this. The authors noted in conclusion that a thorough investigation of the wind system would require estimates of several driving forces: electric fields of magnetospheric origin, diurnal pressure gradients from solar heating, Joule and particle heating in the auroral zones, and Coriolis terms.

Monthly variations in nighttime neutral winds and temperature near 250 km during solar minimum were catalogued by Hernandez and Roble (1977) using airglow data taken at Fritz Peak Observatory (39.9°N, 105.5°W) from April, 1975 through March, 1976. Measurements during quiet geomagnetic conditions were compared to values calculated from Ogo 6 model pressure gradients (Hedin et al., 1974). The zonal flow was predominantly eastward during winter nights while shifting westward during the mornings. This transition became progressively earlier towards summer and approached midnight at the solstice. The diurnally averaged flow was eastward (35-50 m s^{-1}) during winter and westward (25-30 m s^{-1}) in summer. The equatorial meridional winds were largest near midnight in summer and smallest during winter. The daytime poleward flows maximized in winter and minimized in summer. Diurnal averages of these were 40 m s^{-1} equatorward and 25-35 m s^{-1} poleward during summer and winter, respectively. The nighttime

temperatures were lowest in January and highest during May, July, and August. Agreement between measured and calculated wind speeds was generally good; in fact, the diurnal averages of the calculated wind speeds were taken as representative of the measured diurnal averages. Nighttime temperatures did not agree so well. The measured values were 100-150 K higher than model estimates for summer and equinox and 50-75 K higher for winter. Daytime differences were unknown. The authors suggested that differences between measured and calculated motions might be reduced by including an auroral heating term in the wind system model, the magnitude of this term to be determined as that which would bring calculated and measured values into agreement.

An interesting new way of measuring neutral wind velocities based on mass spectrometer sampling was developed by Knutson et al. (1977). Vertical velocity estimates were obtained by using the open source spectrometer on the AE-C satellite. A determination of the periods between successive maxima of the spectrometer signal, which were quite sharp, as the satellite spun allowed the wind component perpendicular to the spin plane to be approximated. Horizontal wind contributions were eliminated by using only low altitude measurements since in this case, only vertical motions were perpendicular to the spin plane. The largest vertical wind variations were found in the post magnetic midnight auroral region. Velocity changes as large as 65 m s^{-1} were observed although no simple relationships with altitude or magnetic activity were obtained due to insufficient data. These values were not always consistent with tracking measurements, but the tracking data were restricted to dawn and

dusk. The authors noted that their method did not suffer these restrictions and that horizontal winds could be found by placing the satellite spin axis in the vertical direction.

CHAPTER II

DATABASE OF THE MODEL AND COORDINATE SYSTEM

2.1 Description of the Satellite and Operating Conditions

The Atmosphere Explorer-C satellite was launched into a 68.1° inclination orbit on December 16, 1973 with an initial apogee of 4300 km and an initial perigee of approximately 157 km. The initial perigee latitude changed by .5° per day from 10°N and the local time of perigee decreased by about 8 minutes per day from 1430 hours local time due to orbital precession. The satellite was maintained in this highly elliptical orbit until November, 1974, when the orbit was made circular at altitudes between 220 km and 320 km. The orbital period was then about 90 minutes so that successive passes were separated in longitude by about 22 degrees. Until this maneuver, numerous low altitude excursions were made in order that data could be taken to altitudes below 140 km.

The AE-C neutral density measurements used in this study were obtained from January, 1974 to June, 1975, a period which corresponded to the low activity portion of the 11-year solar cycle. The daily burst adjusted 10.7 cm solar radio flux at 1 A.U. was between 66.5 and 144.7 x 10^{-22} W m^{-2} Hz^{-1} throughout this period.

2.2 Instrumentation - The Open Source Mass Spectrometer

Several neutral mass spectrometers were included in the payload of AE-C. Only the Open Source Spectrometer (OSS) was used in the present study in order to maintain consistency throughout the database. This instrument has been described in detail by Nier et al. (1973). Briefly, the spatial resolution of the OSS was 3.2 km along the orbital path for a sampling rate of 16 samples per second, the normal operating rate. The accuracy of the number density measurements was estimated to be within ±20% and much better relative values of the concentration were presumed. Gases measured by the instrument included N_2, O, O_2, He, Ar and several minor species.

2.3 Data Selection and Corrections

The OSS instrument generated several thousand spectra for each gas sampled during one 30-minute perigee pass of the satellite in the elliptical phase. This amount of high resolution data was considerably larger than desired for the present purposes; therefore, a way of unifying the measurements was needed. The original database of the AE satellite series included Telemetry (TM) files, Geophysical Unit (GU) files, and Unified Abstract (UA) files. The TM files consisted of satellite orbital information and raw instrument voltages. The GU files contained high resolution data, which consisted of spectra in the case of the OSS. The UA files were made up of 15-second averages of the high resolution spectra and as such were well suited for the present study. By definition, these averages were centered on the universal time specified for the measurement

so that the satellite was within about 65 km (along the orbital path) of the position corresponding to this universal time when the samples comprising the averages were taken.

Measurements of N_2 and He by the OSS were accomplished in a fairly straightforward manner since both of these gases are reasonably inert. Estimation of the O density was much more difficult due to the interactions that this highly reactive gas underwent on the surfaces of the instrument. In fact, in the normal mode of operation, O was actually measured as it would have been in a closed source instrument. That is, as O_2, after recombination on the walls of the OSS ionizing region. Unfortunately, the recombination of O into O_2 was incomplete and the measurements had to be scaled to reflect this. A correction for ambient O_2 in the atmosphere was also made. Both corrections were applied as described by Kayser (1977). More information concerning the analysis and calibration of the OSS as well as techniques used to measure O and O_2 via mass spectrometers have been supplied by Nier et al. (1974, 1976), French et al. (1975), and Kayser and Potter (1976).

Lower limits were set on the concentrations as suggested by Kayser (1977) to reduce the problems of outgassing and low multiplier counting rates at high altitudes. The minimum values used were 5×10^{12} m^{-3}, 10^{11} m^{-3}, and 5×10^{10} m^{-3} for O, He, and N_2, respectively. The altitudes at which these concentrations were reached depended strongly upon the time of sampling, the geographical position of the satellite, the magnetic and solar activities at the time the measurements were taken, and the neutral

gas sampled.

2.4 The Magnetic Coordinate System

Many aeronomic studies have organized data in coordinate systems which are based on the magnetic field of the earth. The 'geomagnetic' coordinate system is derived from a centered dipole approximation to the magnetic field. This representation is equivalent to the superposition of two dipoles located at the center of the earth, one aligned along the geographic axis and the other lying in the equatorial plane. Geomagnetic latitude is defined analogously to geographic latitude. The geomagnetic equator is defined as the great circle around a spherical earth which is normal to the centered dipole. Geomagnetic local time is defined in terms of the angle formed between the plane containing the earth-sun line and a vector parallel to the dipole, and the plane containing a vector from the center of the dipole to an observer and a vector parallel to the dipole.

'Magnetic', 'eccentric dipole', or 'offset dipole' coordinates are derived by displacing the centered dipole some distance from the center of the earth in order to minimize the second term in the harmonic expansion of the magnetic field without affecting the first term. Magnetic latitude and magnetic local time are then defined analogously to their geomagnetic counterparts.

The transformation from geographic to geomagnetic coordinates is simpler than that from geographic to magnetic or eccentric dipole coordinates. For this reason, geomagnetic coordinates were preferable to

magnetic coordinates before computers were widely used. Eccentric dipole coordinates, however, are much more closely related to the magnetic field configuration at high latitudes, in the auroral zones, and in the polar cap. Because they yield a better representation, eccentric dipole latitude and magnetic local time will be used exclusively in the present analysis.

The equations used to transfer from geographic to magnetic coordinates were given by Agy (1965) and appear in Appendix 1 of Matsushita and Campbell (1967). These equations used the direction of the centered dipole derived by Finch and Leaton (1957) and the displacement of the eccentric dipole calculated by Parkinson and Cleary (1958). Secular variations in the magnetic field cause quantities to change with time and it was found desirable to update them to more recent values. The I.G.R.F. 1975 magnetic field model in conjunction with the method described by Bartels (1936) was used to do this. The updated equations for magnetic latitude and magnetic local time are:

$$\text{Magnetic latitude} = \sin^{-1}(\hat{g} \cdot \hat{m}) \tag{2.1}$$

$$\text{Magnetic local time} = \frac{1}{\omega}\left(\tan^{-1}\left[-\frac{\hat{b} \times \hat{c}}{\hat{m}(\hat{b} \cdot \hat{c})}\right] + 180^{\circ}\right) \tag{2.2}$$

where

$\bar{b} = \hat{s} \times \hat{m}$ = vector in magnetic equatorial plane perpendicular to earth-sun line

$\bar{c} = \hat{g} \times \hat{m}$ = vector in magnetic equatorial plane perpendicular to magnetic position vector

$\hat{m}$ = unit vector in direction of (negative) dipole

$= \hat{i} \cos 289.5^\circ \cos 78.6^\circ + \hat{j} \sin 289.5^\circ \cos 78.6^\circ + \hat{k} \sin 78.6^\circ$ [based on I.G.R.F 1975]

$\bar{d} = \hat{i}\, d \cos 146.9^\circ \cos 19.5^\circ + \hat{j}\, d \sin 146.9^\circ \cos 19.5^\circ + \hat{k}\, d \sin 19.5^\circ$ [based on I.G.R.F. 1975]

d = magnitude of displacement of eccentric dipole

$= 474$ km [based on I.G.R.F. 1975]

$\bar{g}$ = position vector relative to dipole (magnetic position vector)

$= \bar{p} - \bar{d}$

$\bar{p}$ = position radius vector

$= \hat{i}\, r \cos \lambda \cos \phi + \hat{j}\, r \sin \lambda \cos \phi + \hat{k}\, r \sin \phi$

$\hat{s}$ = unit vector in direction of (infinitely distant) sun

$= \hat{i} \cos (180^\circ - \omega T) \cos \delta + \hat{j} \sin (180^\circ - \omega T) \cos \delta + \hat{k} \sin \delta$

$\hat{i}, \hat{j}, \hat{k}$ = unit vectors from center of spherical earth along direction indicated: $\hat{i}$ to intersection of equator and Greenwich meridian, $\hat{j}$ to intersection of equator and 90° east geographic meridian, $\hat{k}$ to north pole

R = radius of earth = 6371.2 km

h = height above the earth, km

$r = R + h$

ϕ = geographic latitude

λ = geographic longitude (east)

T = Greenwich local solar time, hours

ω = 15 deg h^{-1} ($180^{\circ} - \omega T$ = Greenwich hour angle of sun)

δ = solar declination

In these equations, the position used for the geomagnetic north pole was 78.6°N, 289.5°E and the displacement of the dipole eccentric from the center of the earth was calculated to be 474 km towards 19.5°N, 146.9°E.

CHAPTER III

EXAMINATION OF THE LONG-TERM TRENDS OF THE COMPOSITION IN THE MAGNETIC COORDINATE SYSTEM

3.1 Determination of Average Density Structure

The behavior of the neutral thermospheric composition has sometimes been described on the basis of data taken from individual satellite orbits or groups of orbits. Such limited information must be interpreted very carefully, however, since temporal variations due to magnetic storms and large gravity waves can cause large orbit to orbit variations which mask the global and seasonal variations.

One way to unmask the basic structure is to reduce these local effects by analyzing data taken over long periods of time which have been corrected for long-term solar and geophysical variations. These data should then be more representative of average conditions making it much easier to separate persistent from transient distributions of the neutral gas more clearly. In order to study the density structure in the magnetic coordinate system and to find persistent effects this approach will be followed here.

Several solar and geophysical influences on the composition need to be considered before averages are taken. The contribution of solar activity variations towards neutral density changes during 1974 and the first 6 months of 1975 did not seem to be of great importance. The 11-year solar cycle was near minimum and the $F_{10.7}$ index generally changed

by less than 40×10^{-22} W m^{-2} Hz^{-1}. Based on the MSIS model (Hedin et al., 1977a, b), it can be estimated that such changes in solar flux translate into less than 10% variations in neutral temperature and density. These fluctuations are much smaller than those arising from other major sources and were, therefore, neglected.

The influence of the level of magnetic activity on the neutral atmosphere, on the other hand, was found to be extremely important and was included in this study. The 3-hour planetary ap index was used as an indicator of magnetic activity because it applies globally and is readily available, although it is by no means the best indicator of auroral disturbances as will be shown later. Three levels of magnetic activity were considered and delineated by the following ranges of ap values: 0 to 4, 5 to 15, and 18 to 67. These ranges were chosen to be representative of low, medium and high magnetic activity conditions, respectively. It should be noted that there were fewer data and more variable data taken over the high range of ap but much meaningful information is still obtained for these conditions. The dependencies of the atomic oxygen and helium data on altitude were treated individually and the reasons for this are described below. In each case, all data were reduced to a common altitude (Sections 3.2, 3.3) to aid in representation and interpretation. Later, these fixed altitude results are generalized.

The period over which all measurements were treated as a single (data) set was quite long. All neutral density values taken within 45 days of a given equinox or solstice were chosen to comprise a 'season'.

In order to determine the appropriate corrections for annual effects in the densities taken at the extremes of these periods, scatter plots were made of the data at fixed altitudes within a small range of magnetic latitudes ($\pm 5^{\circ}$) and magnetic local times (± 3 hours) as a function of day number for the entire database.

The helium data showed a winter pole to summer pole ratio of about 40 to 1 at 300 km (Figure 1). This large variation was also quite regular permitting a logarithmic correction to the equinox data to be made based on the day number of the measurements and the magnetic latitude band into which the data fell. The solstice helium data were not corrected in this way since a deviation from uniform coverage for these seasons would have a much smaller effect than at equinox. The scatter in the atomic oxygen measurements was greater than any annual variations which might be present (Figure 2); therefore, no corrections were made to these data.

Finally, the magnetic coordinates at which the measurements were taken were considered by forming 5° 'bins' of magnetic latitude and one hour bins of magnetic local time centered at 5° intervals from the equator and on the hour, respectively. All data taken within a particular range of ap and corresponding to a given season falling into the same bin were averaged. The number of points in each bin ranged from 0 to over 100. Bins which had no data, including those poleward of about 78° MLAT in the northern hemisphere and 82° MLAT in the southern hemisphere, where the satellite did not reach, were filled by logarithmic interpolation. Once this global 'grid' was established, contour plots of the data in each

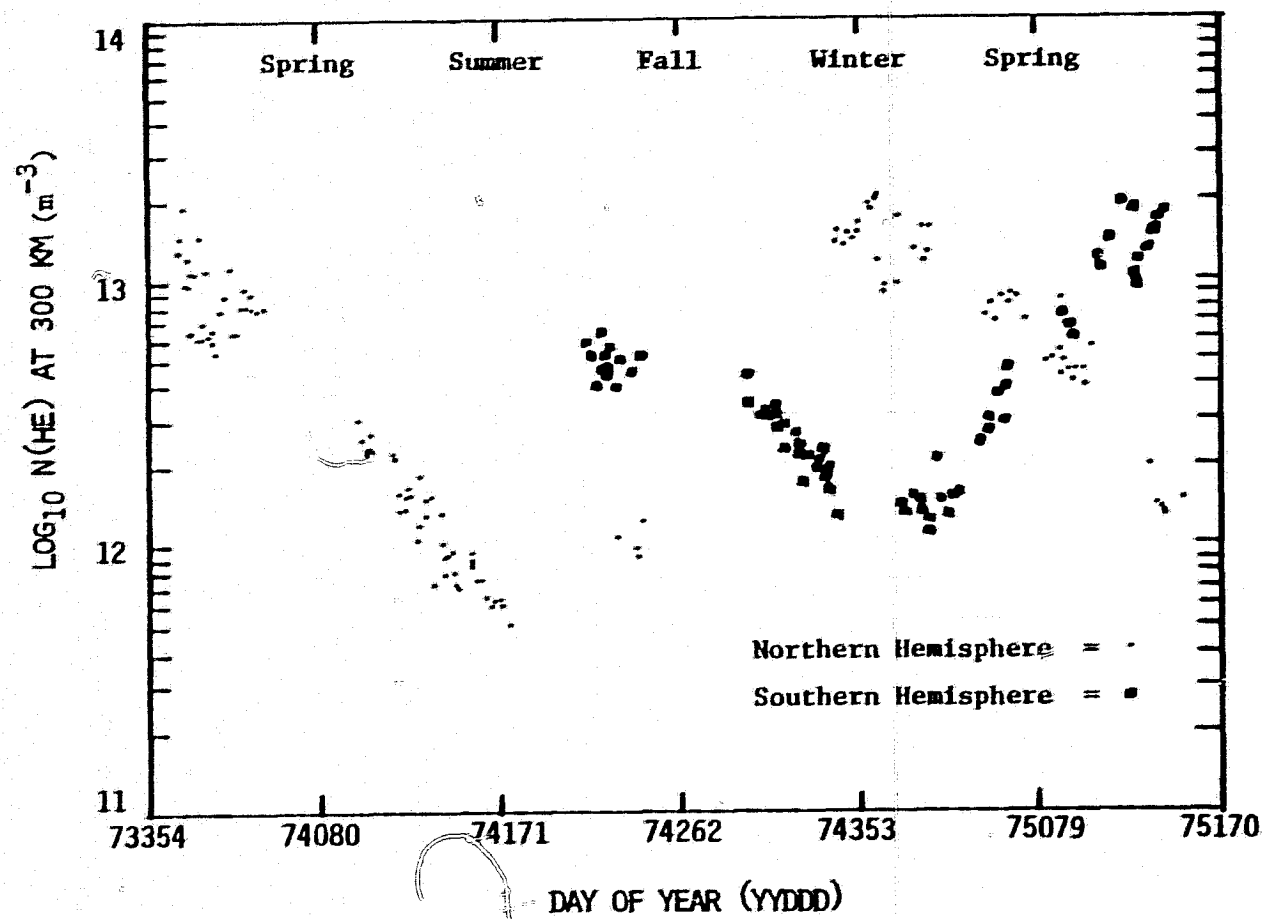

Figure 1 Scatter plot of $\log_{10}$ n(He) at 300 km as a function of day number. All data were taken from 50 - 60° magnetic latitude and between 1200 and 1800 hours magnetic local time. Similar plots for other latitude ranges were used to derive a correction factor for helium data depending on number of days from equinox.

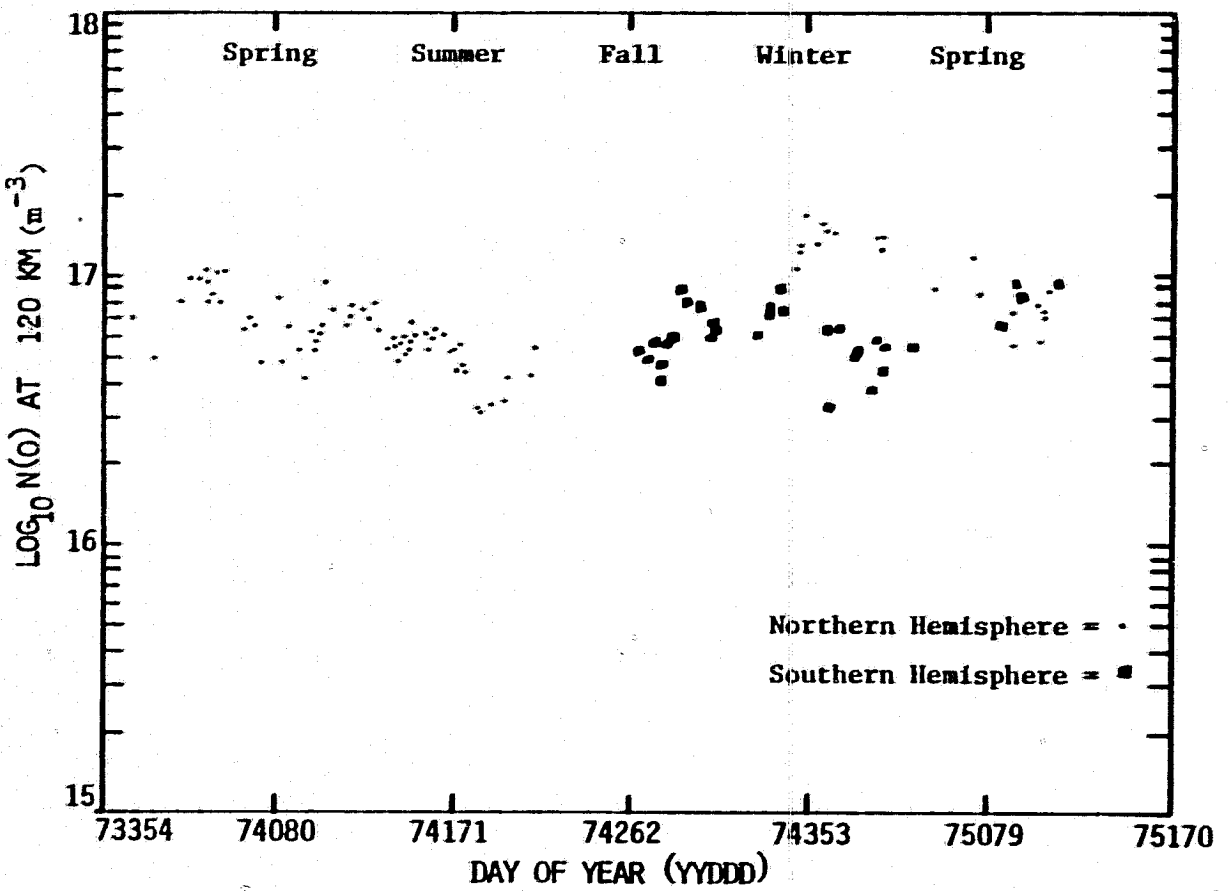

Figure 2 Scatter plot of $\log_{10}$ n(O) at 120 km as a function of year and day number (yyddd). All data were taken from 50 - 60° magnetic latitude and 1200 - 1800 hours magnetic local time. The large scatter in the data makes it difficult to correct for seasonal variations.

hemisphere were made. These plots are displayed in polar form as functions of magnetic latitude and magnetic local time for various seasons and ap ranges and will be described in detail in Section 3.4.

3.2 Reduction of Atomic Oxygen to 120 km

Atomic oxygen is the main constituent in the middle thermosphere and at altitudes of the order of 300 km winds cause the horizontal density gradients to be small. This results in vertical transport in regions of energy input where the exospheric temperatures are high. In order to separate the effects of scale height variations due to temperature variations from those due to vertical diffusion at low altitudes it is convenient to use an equivalent atomic oxygen density at 120 km that would reproduce the observed variations at satellite altitudes assuming a diffusive equilibrium profile. These densities are a sensitive indicator of vertical transport and heating in the thermosphere and provide simpler boundary conditions for a model. Care must, of course, be taken not to interpret these literally as measurements of the actual atomic oxygen densities at 120 km which may be different due to the effects of relative diffusion above 120 km as discussed by Nisbet and Glenar (1977).

These authors have shown that measurements of the atomic oxygen and molecular nitrogen density at any altitude may be combined with a neutral temperature in a straightforward manner so as to give estimates of the O density at 120 km if an N_2 density and a neutral temperature are assumed at this lower boundary. They have also shown that the resulting O values at 120 km are relatively insensitive to the value used for the neutral

temperature at the height at which the measurements were taken (less than a 4% change in density for a 100 K temperature change). This result allows model temperatures to be used in place of actual measurements with very little change in accuracy. Their method will be followed here.

The density of a neutral gas in diffusive equilibrium at any height z above a certain base level z_o may be found ignoring thermal diffusion effects, which are negligible for O, from the equation,

$$n_i(z) = n_i(z_o) \left[\frac{T(z_o)}{T(z)}\right] \exp\left(\left[\frac{-M_i}{R}\right] \int_{z_o}^{z} \frac{g(z)}{T(z)}\, dz\right) \qquad (3.1)$$

where

z level where density is desired, km

M_i molecular weight, g $mole^{-1}$

R gas constant, J $mole^{-1}K^{-1}$

Using N_2 in this equation, the integral can be written as,

$$\int_{z_o}^{z} \frac{g(z)}{T(z)}\, dz = \frac{R}{M_{N_2}} \left(\ln \left[\frac{T(z_o)}{T(z)}\right] - \ln \left[\frac{n_{N_2}(z)}{n_{N_2}(z_o)}\right]\right) \qquad (3.2)$$

Substituting this into the first equation with O instead of N_2 as the gas,

$$\ln n_O(z_o) = \ln n_O(z) - \left[\frac{M_O}{M_{N_2}}\right] \ln \left[\frac{n_{N_2}(z)}{n_{N_2}(z_o)}\right] + \left[\frac{M_O}{M_{N_2}} - 1\right] \ln \left[\frac{T(z_o)}{T(z)}\right] \quad (3.3)$$

Now, for a base level $z_o = 120$ km and $M_O = 16$, $M_{N_2} = 28$, this equation becomes,

$$\log_{10} n_O(120) = \log_{10} n_O(z) + \frac{4}{7}[\log_{10} n_{N_2}(120) - \log_{10} n_{N_2}(z)] + \frac{3}{7} \log_{10} \left[\frac{T(z)}{T(z_o)}\right] \quad (3.4)$$

where the common logarithm of the density has been used.

If the N_2 density and neutral temperature are taken from the CIRA (1972) 1000 K model ($n_{N_2} = 3.79 \times 10^{17}$ m^{-3}, $T_{120} = 334.5$ K),

$$\log_{10} n_O(120) = \log_{10} n_O(z) + \frac{4}{7}[17.579 - \log_{10} n_{N_2}(z)] + \frac{3}{7} \log_{10} \left[\frac{T(z)}{334.5}\right] \quad (3.5)$$

This equation was used to reduce the O data to 120 km.

3.3 Reduction of Helium to 300 km

Helium is one of the lightest constituents in the thermosphere and as such has a very large scale height. Under the assumption of hydrostatic equilibrium, the global helium distribution will be fairly similar at most

thermospheric heights. Therefore, an intermediate altitude such as 300 km serves as a convenient reference height to study the variations in neutral helium. Further, since satellite measurements need only be extrapolated over less than about one scale height to reach this altitude, it may be expected that the inferred distribution at 300 km will reflect the distribution over the height range of the satellite measurements fairly well. At this altitude, the thermospheric temperatures have almost reached exospheric values. The assumption of an isothermal atmosphere is, therefore, reasonable and will be made.

The neutral density of He in diffusive equilibrium is given by

$$n_{He}(z) = n_{He}(z_o)\ \left[\frac{T(z)}{T(z_o)}\right]\ \exp\left\{\left[\frac{-M_{He}}{R}\right]\int_{z_o}^{z}\frac{g(z)dz}{T(z)}\right.$$

$$\left. - \alpha\int_{z_o}^{z}\frac{dT}{T(z)}\right] \qquad (3.6)$$

where α is the thermal diffusion factor,

-.38 (Banks and Kockarts, 1973)

In an isothermal atmosphere, this reduces to

$$n_{He}(z) = n_{He}(z_o)\ \exp\left\{\left[\frac{-M_{He}}{RT_\infty}\right]\int_{z_o}^{z} g(z)dz\right\} \qquad (3.7)$$

where T_∞ is the exospheric temperature.

After integration and substitution of z_0 = 300 km into the above expression, the helium density at 300 km may be calculated as,

$$n_{He}(300) = n_{He}(z) \exp\left(-\frac{M_{He} g(0)}{RT} [h(z) - h(300)]\right) \quad (3.8)$$

where

h(z) is geopotential height of z, km

g(0) is acceleration of gravity at earth's surface, 9.81 m sec^{-1}

This expression and the MSIS model neutral temperature (Hedin et al., 1977a) corresponding to the position of the satellite and the solar and geophysical conditions present for a given measurement were used to determine the 300 km helium densities.

3.4 Comparison of the Density Averages Under High and Low Solar Activity Conditions

3.4.1 Atomic Oxygen Densities at 120 km

Long-term averages of the atomic oxygen densities for spring equinox conditions are shown in Figures 3, 4, and 5. Data from the AE-C satellite were used to make the low solar activity contours (top) and Ogo 6 satellite measurements (Stehle et al., 1979), which represented high solar activities ($F_{10.7}$ = 101 to 239), were used to construct the contours for the solar maximum (bottom). The density variations for low magnetic activity levels, ap = 0 to 4, are illustrated in Figure 3. Atomic oxygen shows similar high latitude structure for both high and low solar

activities. The minimum of n(O) at 120 km extends from the magnetic poles through the postmidnight magnetic local time (MLT) sectors in both cases, although this minimum is less restricted for Ogo 6. This is probably due to fewer measurements in this region by the Ogo 6 satellite. The densities in these minima are about 50% of the respective hemispherical averages, but the absolute values of the AE-C data are nearly 40% lower than the Ogo 6 measurements. This is in agreement with Hedin et al. (1977b), who predict an increase in n(O) with increasing solar activity. The high latitude structure becomes sharper for medium magnetic activity levels, ap = 5 to 15, and the density minima persist in the postmidnight MLT region under both high and low solar activities (Figure 4). The densities in these minima become smaller than for low magnetic activities, being only about 40% of the hemispherical averages. The atomic oxygen densities show even more structure for high magnetic activity levels, ap = 18 to 67 (Figure 5). For both solar activities, the densities are smallest near 0700 MLT in the polar regions. The values in these minima are less than 30% of the hemispherical averages and only about 50% of the corresponding low magnetic activity values. The postmidnight MLT density minimum persists for the summer solstice atomic oxygen data (Figure 6). For this season, the AE-C minimum densities are about 30% of the northern hemispherical average but the Ogo 6 values are nearer to 40% of this average, suggesting a stronger annual effect for low solar activity conditions. The winter n(O) values (Figure 7), while showing somewhat different MLT structure near the magnetic poles, support this as the winter to summer pole-to-pole ratio for AE-C is about 2 to 1

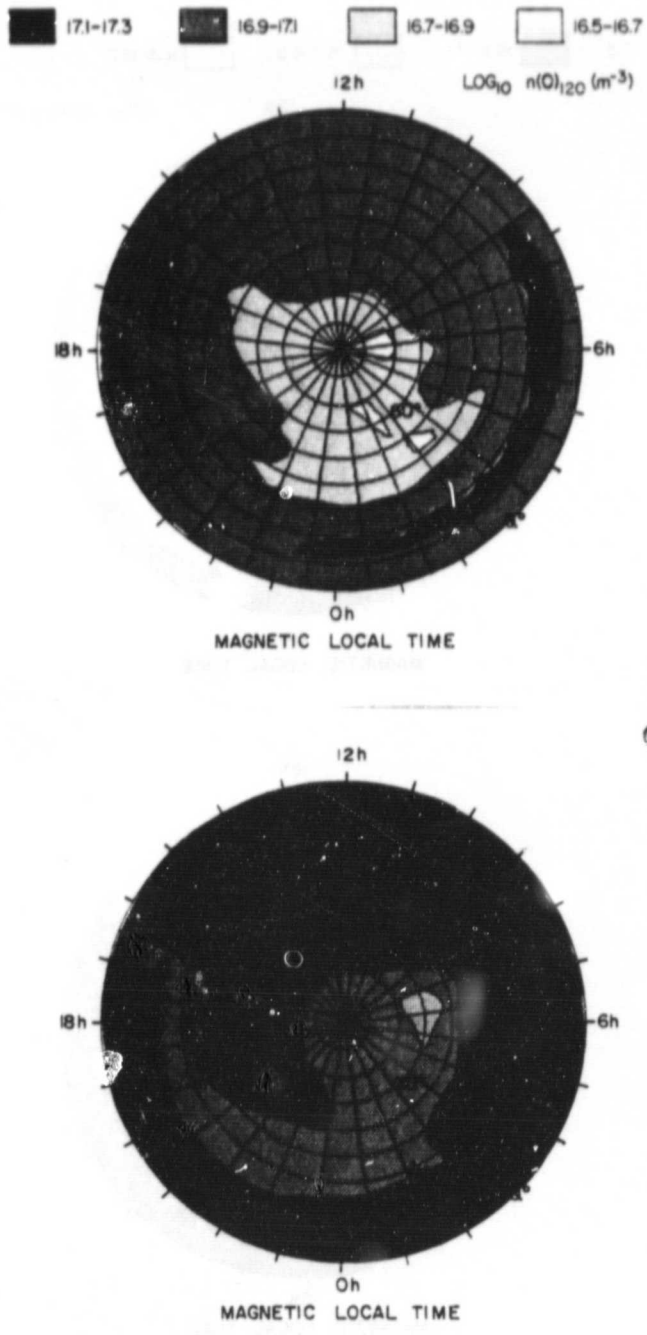

Figure 3 Atomic oxygen density at 120 km for spring equinox and ap values between 0 and 4 as a function of magnetic latitude and magnetic local time. Top represents low solar activity conditions (1974) and AE-C data and bottom shows high solar activity conditions (1970) and Ogo 6 data (Stehle et al., 1979).

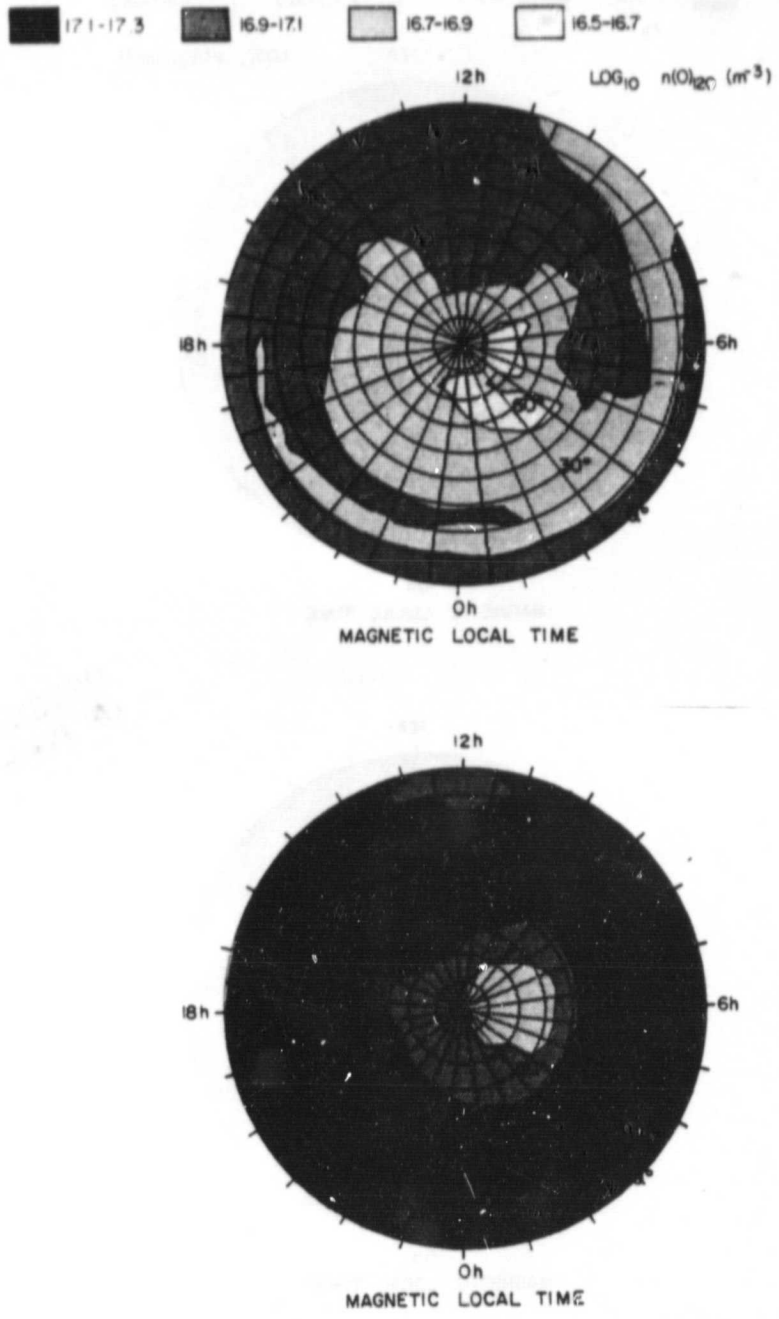

Figure 4 Atomic oxygen density at 120 km for spring equinox and ap values between 5 and 15 as a function of magnetic latitude and magnetic local time. Top represents low solar activity conditions (1974) and AE-C data and bottom shows high solar activity conditions (1970) and Ogo 6 data (Stehle et al., 1979).

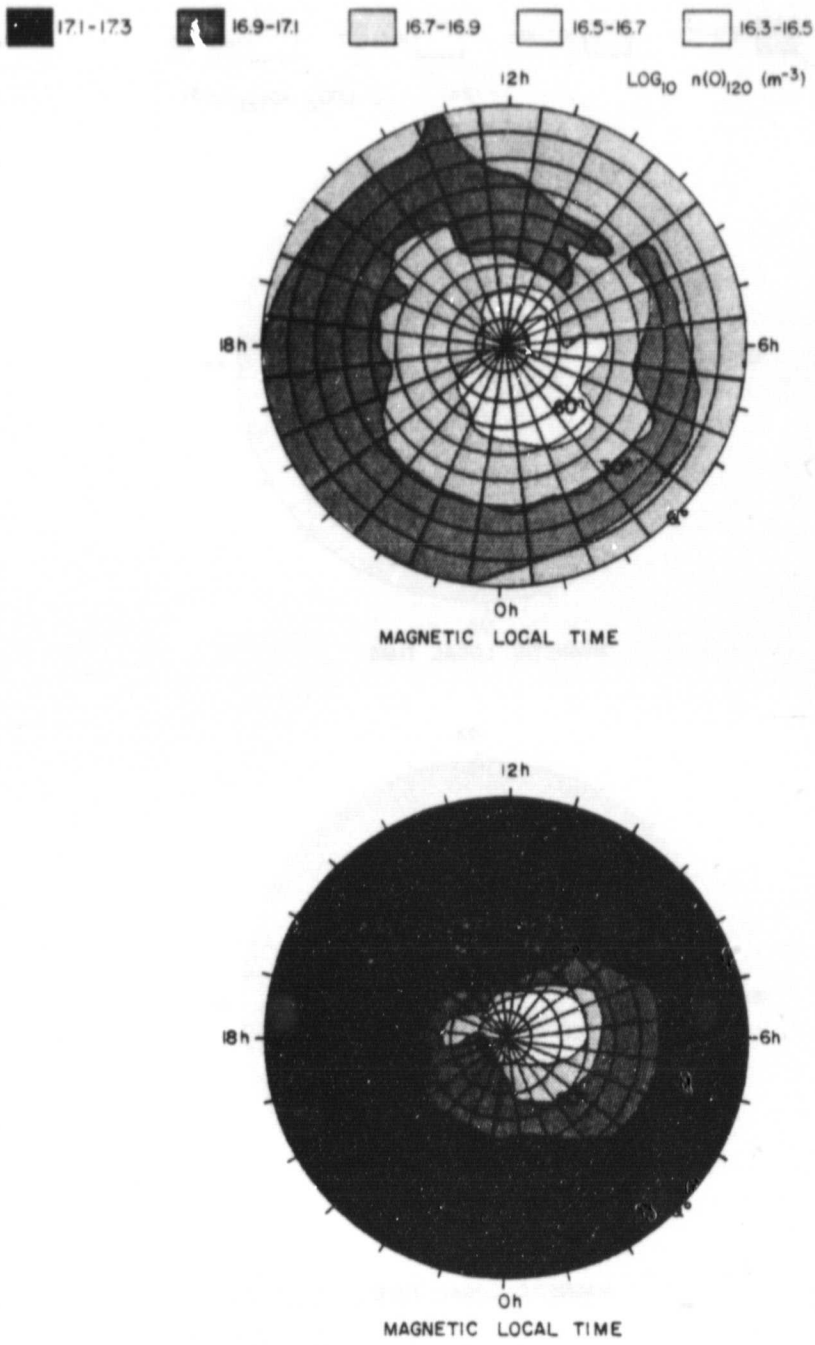

Figure 5 Atomic oxygen density at 120 km for spring equinox and ap values between 18 and 67 as a function of magnetic latitude and magnetic local time. Top represents low solar activity conditions (1974) and AE-C data and bottom shows high solar activity conditions (1970) and Ogo 6 data (Stehle et al., 1979).

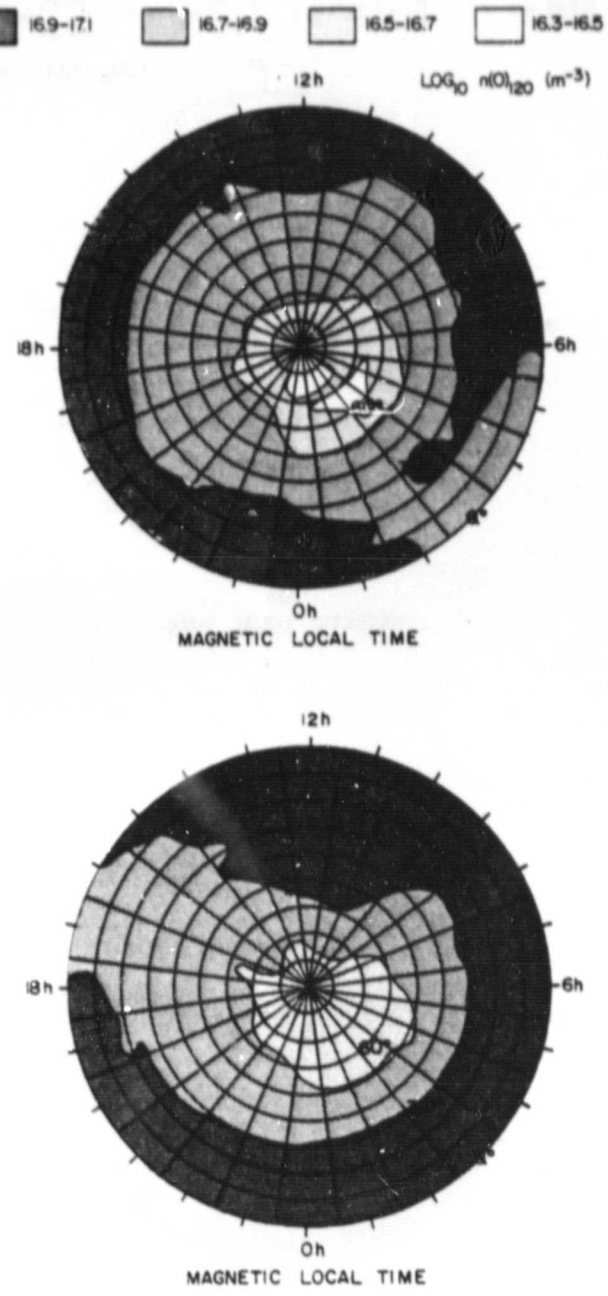

Figure 6 Atomic oxygen density at 120 km for summer solstice and ap values between 5 and 15 as a function of magnetic latitude and magnetic local time. Top represents low solar activity conditions (1974) and AE-C data and bottom shows high solar activity conditions (1970) and Ogo 6 data (Stehle et al., 1979).

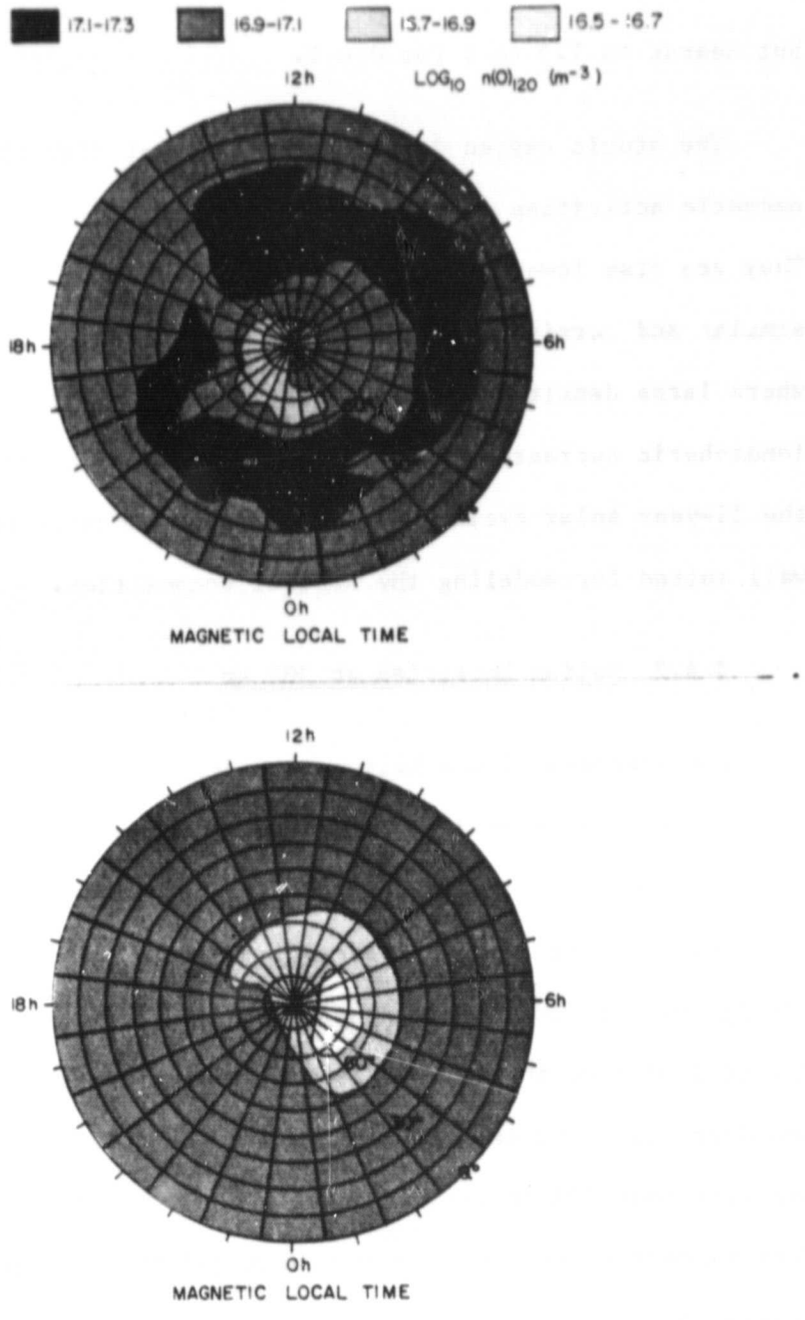

Figure 7 Atomic oxygen density at 120 km for winter solstice and ap values between 5 and 15 as a function of magnetic latitude and magnetic local time. Top represents low solar activity conditions (1974) and AE-C data and bottom shows high solar activity conditions (1969) and Ogo 6 data (Stehle et al., 1979).

but nearer to 1.5 to 1 for Ogo 6.

The atomic oxygen densities decrease at high latitudes for increasing magnetic activities under both high and low solar activity conditions. They are also lower in summer than in winter for both cases and show similar and persistent structure in the region of the westward electrojet where large density variations are expected due to Joule heating from ionospheric currents. That this structure is maintained over one-half of the 11-year solar cycle suggests that the magnetic coordinate system is well suited for modeling the neutral composition.

3.4.2 Helium Densities at 300 km

The averages of the helium data for AE-C and Ogo 6 during spring equinox are represented by Figures 8, 9, and 10. The low magnetic activity, ap = 0 to 4, structure of helium at high latitudes is not apparent in these contours probably due to a paucity of data, especially for Ogo 6. At medium levels of magnetic activity, ap = 5 to 15, the spring densities show high latitude minima near the magnetic pole for AE-C and over the magnetic pole for Ogo 6. The n(He) values in these regions are less than 20% of their respective hemispherical averages. These density depressions become more pronounced at high magnetic activity levels, ap = 18 to 67, although they are no smaller in magnitude than the densities for medium ap. This 'saturation' of density variations with increasing ap has also been seen by Hedin et al. (1977c) in AE-C data taken during a magnetic strom in February, 1974. The helium concentrations in the postmidnight minima for high ap levels decrease to

about 40% of the low magnetic activity values for both quiet and active solar conditions.

Summer solstice helium averages (Figure 11) maintain the high latitude equinox structure having minima in the postmidnight MLT area under high and low solar activities although the Ogo 6 density depression extends into the premidnight MLT region near the eastward electrojet. The winter solstice data (Figure 12), on the other hand, maximize over the magnetic pole and a very strong annual effect seems to be the reason for this. The winter to summer pole-to-pole ratio for the AE-C helium data is greater than 25 which is close to that reported by Mauersberger et al. (1976) and Straus et al. (1977), the latter from a theoretical model including dynamical effects. This ratio is less than 10 for the Ogo 6 data and an increase in exospheric transport with increasing exospheric temperatures and solar activity as suggested by Reber and Hays (1973) and Strauss et al. (1977) would explain this since smaller density gradients in latitude would be maintained in this case.

The helium density averages and the atomic oxygen density averages show very similar behavior at high latitudes under both quiet and active solar conditions for nearly all levels of magnetic activity, except during winter when the large annual variation of helium obscures this structure. These two constituents have masses less than molecular nitrogen and are very good indicators of horizontal winds, thermospheric heating and upwelling. Since their structure is much he same in the magnetic coordinate system under widely varying solar and

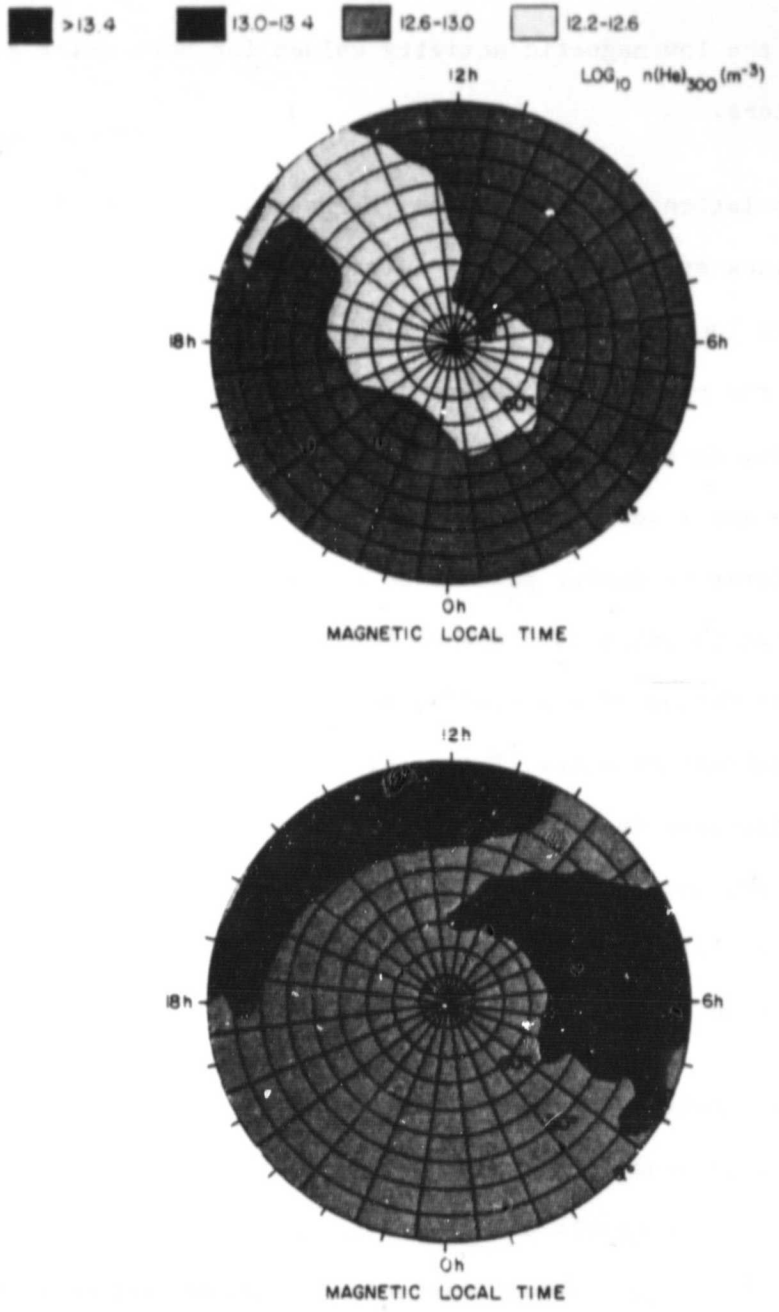

Figure 8 Helium density at 300 km for spring equinox and ap values between 0 and 4 as a function of magnetic latitude and magnetic local time. Top represents low solar activity conditions (1974) and AE-C data and bottom shows high solar activity conditions (1970)and Ogo 6 data (Stehle et al., 1979).

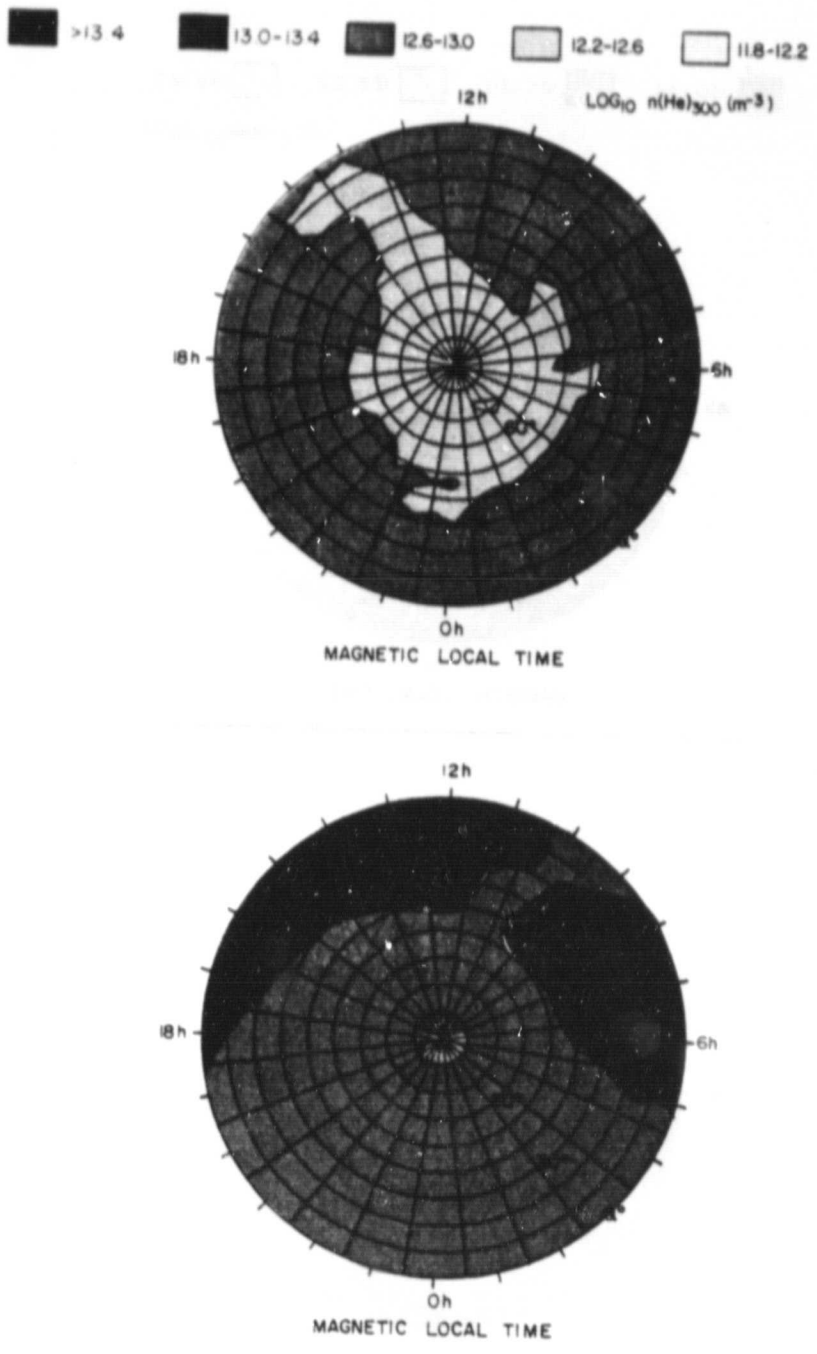

Figure 9 Helium density at 300 km for spring equinox and ap values between 5 and 15 as a function of magnetic latitude and magnetic local time. Top represents low solar activity conditions (1974) and AE-C data and bottom shows high solar activity conditions (1970) and Ogo 6 data (Stehle et al., 1979).

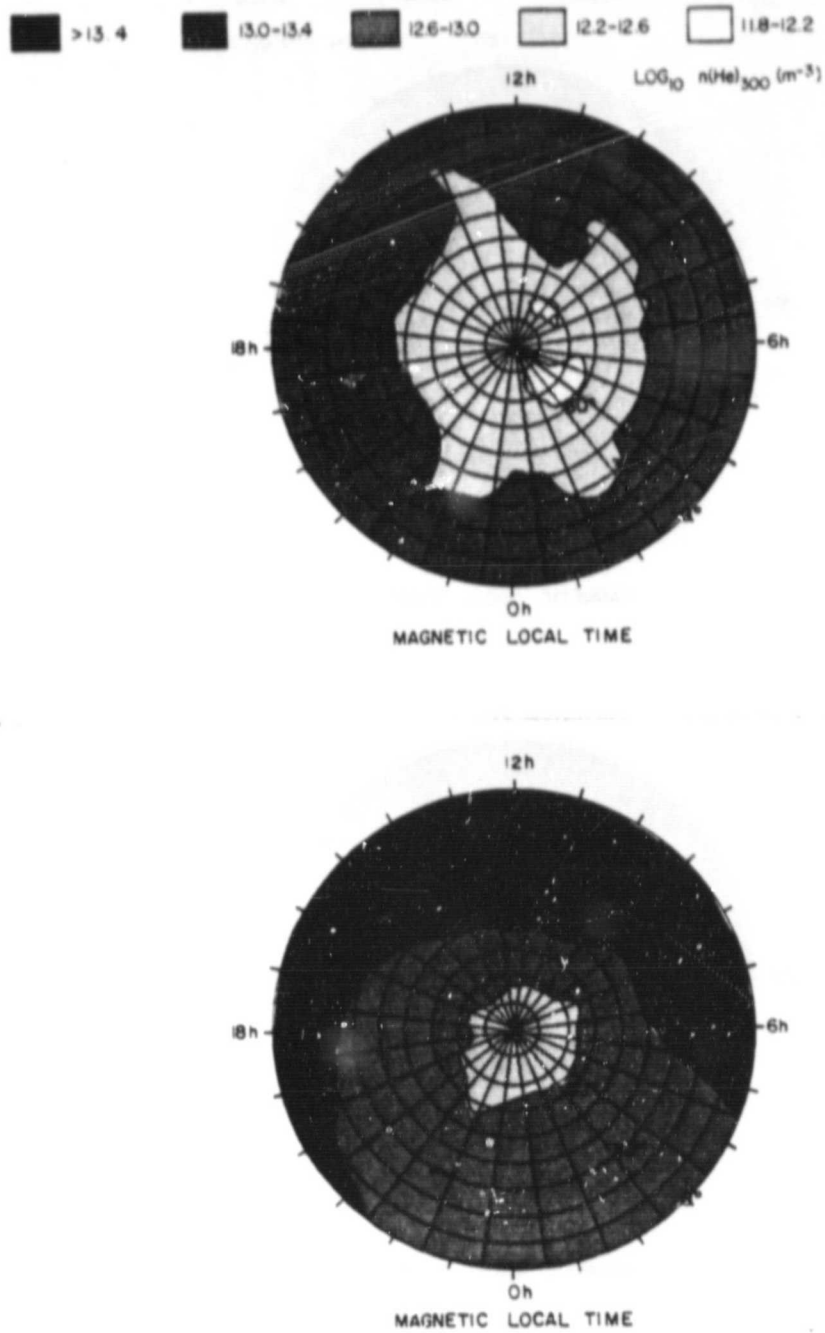

Figure 10 Helium density at 300 km for spring equinox and ap values between 18 and 67 as a function of magnetic latitude and magnetic local time. Top represents low solar activity conditions (1974) and AE-C data and bottom shows high solar activity conditions (1970) and Ogo 6 data (Stehle et al., 1979).

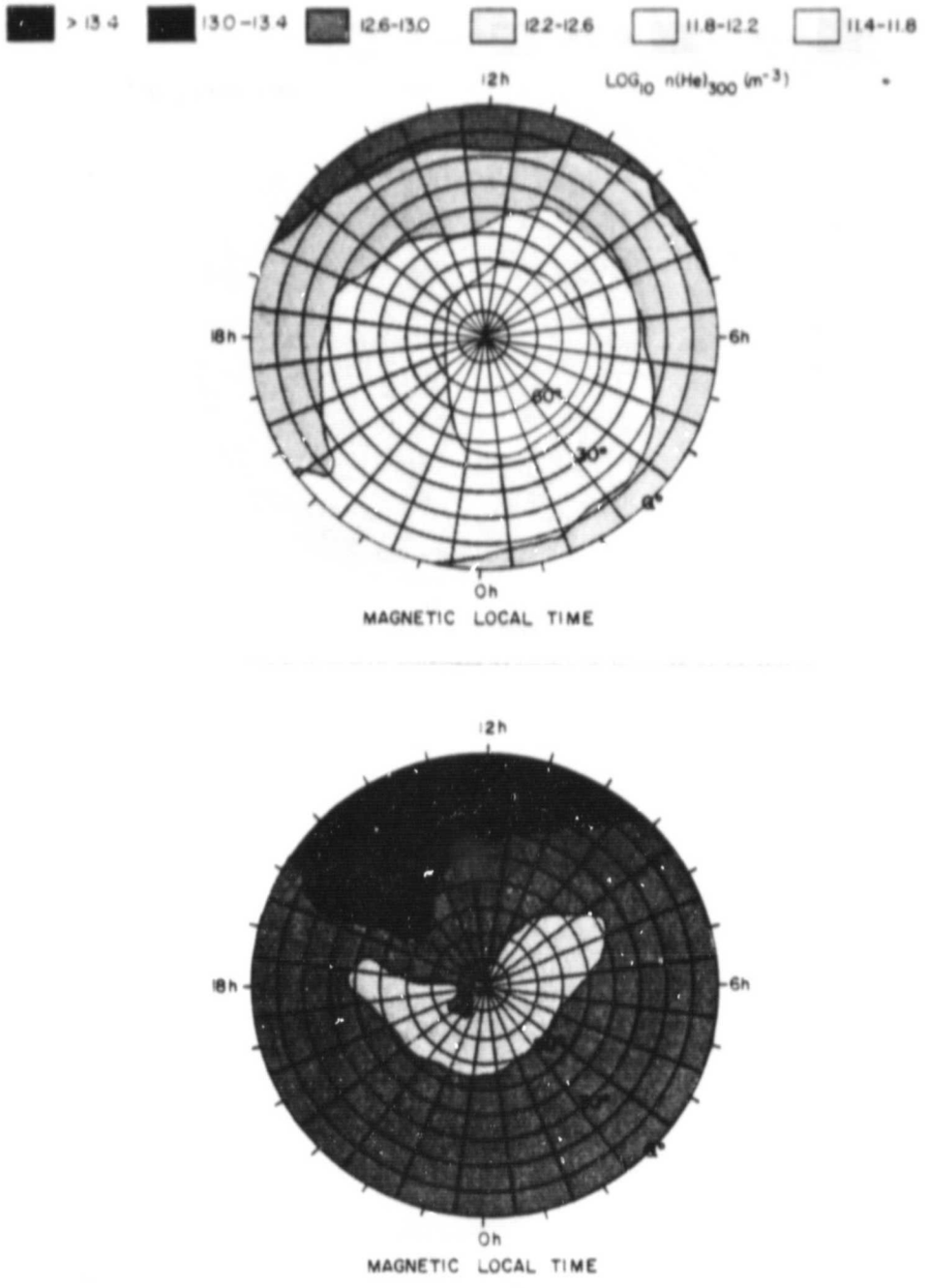

Figure 11 Helium density at 300 km for summer solstice and ap values between 5 and 15 as a function of magnetic latitude and magnetic local time. Top represents low solar activity conditions (1974) and AE-C data and bottom shows high solar activity conditions (1970) and Ogo 6 data (Stehle et al., 1979).

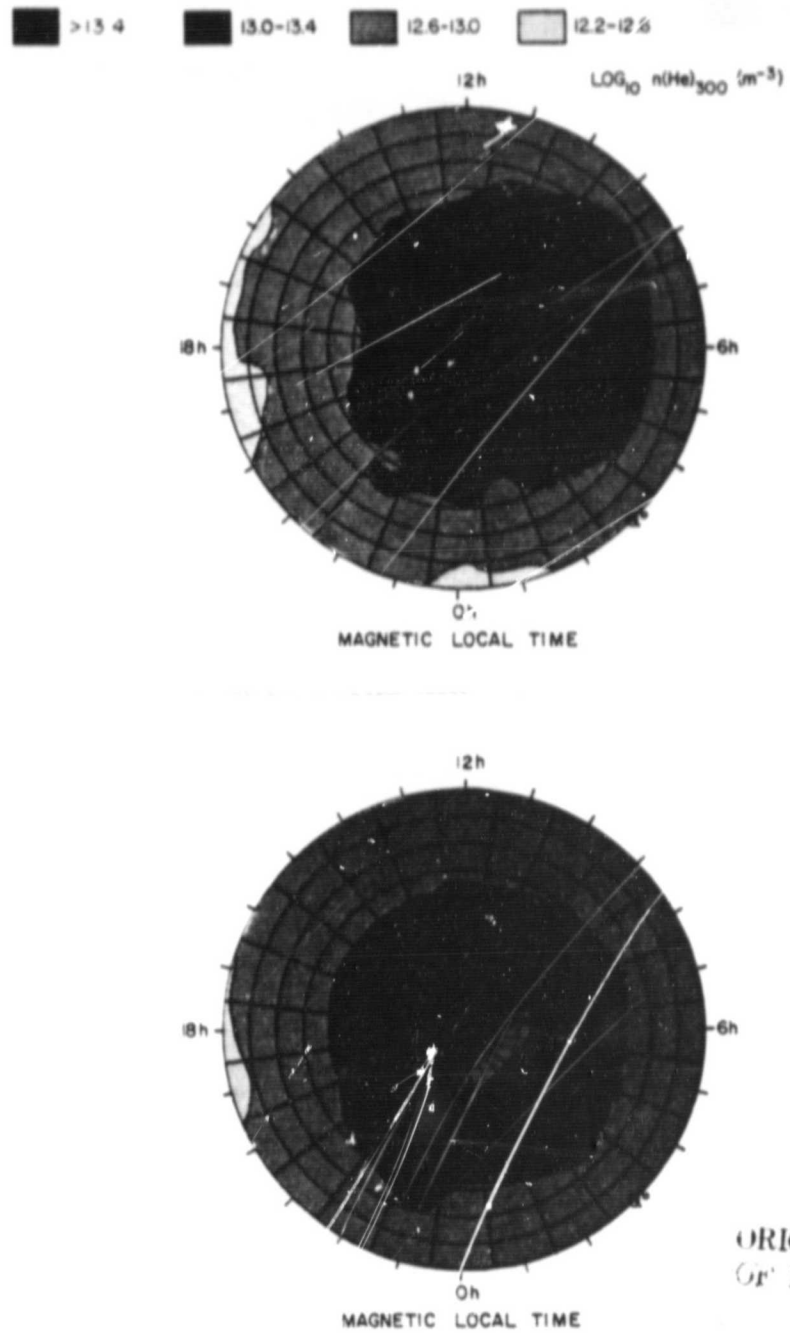

Figure 12 Helium density at 300 km for winter solstice and ap values between 5 and 15 as a function of magnetic latitude and magnetic local time. Top represents low solar activity conditions (1974) and AE-C data and bottom shows high solar activity conditions (1969) and Ogo 6 data (Stehle et al., (1979).

geophysical conditions, it would appear that a general analytic model of their distribution in this system would be of value in studies of energy deposition processes and dynamics of the polar thermosphere. Such a model is developed in the next section (Chapter IV).

CHAPTER IV

METHOD OF ANALYSIS AND CONSTRUCTION OF A MODEL

4.1 The Neutral Magnetic Coordinate Model

The long-term averages of the atomic oxygen and helium densities showed consistent structure at high latitudes for various seasons and magnetic activity levels. Extraction of annual variations from these averages is difficult due to the long time periods used and determination of semiannual variations, if any, is impossible. In order to include these effects in the representation of the atomic oxygen and helium distributions, individual data points were used to construct the global model. Enough measurements were included (over 2500) that the large and highly localized temporal variations discussed earlier should not adversely affect the results. Of course, all small scale effects will not be faithfully reproduced by a model of this type, but a wide range of solar and geophysical conditions will be covered globally.

4.2 Temperature Distribution

Molecular nitrogen is the major constituent in the region between 90 km and 150 km where relative diffusion of the atmosphere constituents is of importance. The mass of N_2 is very close to the mean molecular mass in this region which means that N_2 is not greatly affected by the transition from the realm in which the distribution is controlled by eddy diffusion

to the area where free molecular diffusion dominates. The N_2 altitude profile can, therefore, be approximated at all heights by the characteristics of a hydrostatic distribution even when large velocity fields are present. The approximation allows a neutral temperature profile to be inferred from the N_2 measurements. In particular, each N_2 density value was used to calculate an equivalent exospheric temperature, referred to as NT. Only data taken above 190 km were used so that a unique exospheric temperature could be inferred from each N_2 density value. Since the database of AE-C was well over 100,000 points, it was found impractical to use the entire data set and only one of every ten admissible data points was actually used in calculating NT. The locations of these points in the magnetic coordinate system within 45 days of the equinoxes and solstices are shown in Figures 13 and 14.

A Bates (1959) temperature profile was assumed for calculating NT and it was necessary to assume lower boundary values for the temperature and the N_2 density and a shape parameter for the temperature profile in order to determine NT. These values were taken from the MSIS model (Hedin et al., 1977a). NT was computed by iteration with the aid of equation 4.3. Since the molecular nitrogen data used here were obtained at times of low solar activity, it was difficult to estimate the effects of EUV variations on the temperatures. The parameters reflecting these effects were also taken from the MSIS model which was based on data taken during various phases of the 11-year solar activity cycle.

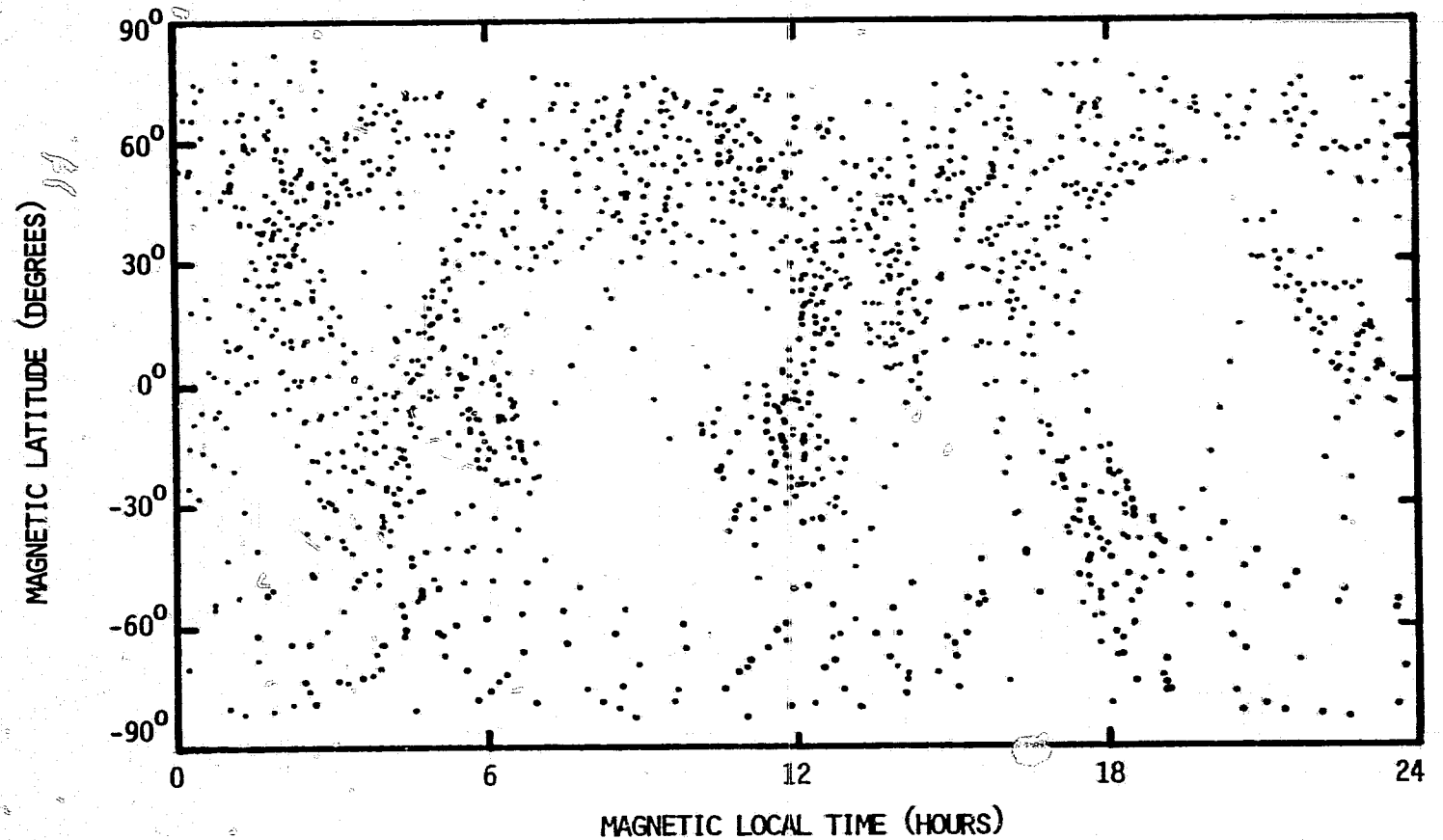

Figure 13 Data used in the global model depending on magnetic latitude and magnetic local time. Points shown were taken within 45 days of the equinoxes and above 190 km for Ap values less than or equal to ten. Northern hemisphere represents local spring.

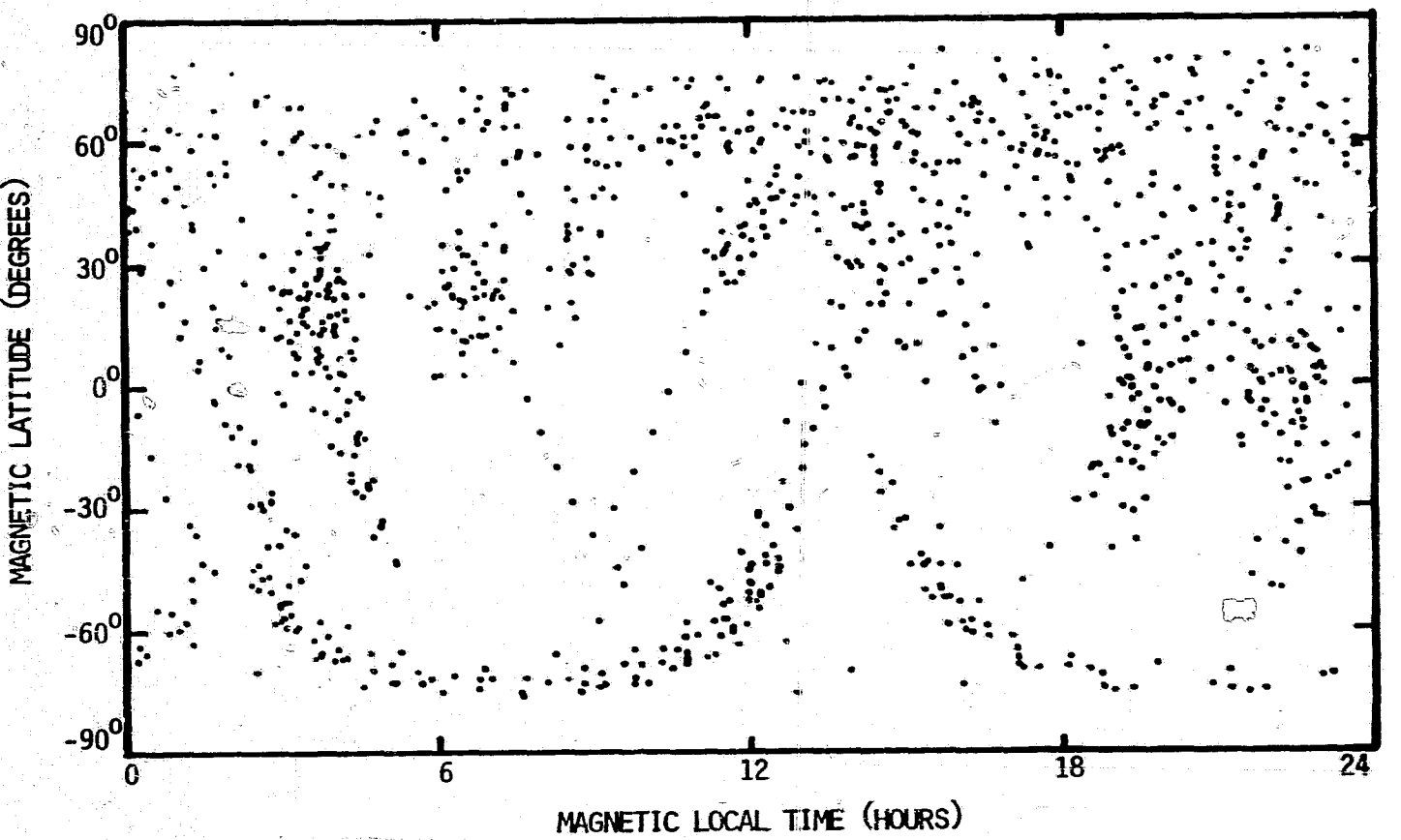

Figure 14 Data used in the global model depending on magnetic latitude and magnetic local time. Points shown were taken within 45 days of the solstices and above 190 km for Ap values less than or equal to ten. Northern hemisphere represents local summer.

The expression used for the neutral temperature profile, taken largely from the MSIS model, was of the form,

$$T(z,L) = T_\infty(L) - [T_\infty(L) - T_{120}] \exp\{-s[z-120]\}$$

$$T_\infty(L) = \overline{T}_\infty G_T(L) \tag{4.1}$$

The spherical harmonic expansion, $G_T(L)$, can be written, with brief descriptions of the terms involved, as

$$G_T = 1 \tag{4.2}$$

Time Independent Terms

$$+ a_{10}P_{10} + a_{20}P_{20} + a_{40}P_{40}$$

Solar Activity Terms

$$+ f_{00}^{a1}\Delta F + f_{00}^{a2}(\Delta F)^2 + \overline{f}_{00}^{a1}\Delta\overline{F}$$

Annual Terms

$$+ c_{00}^{1} \cos \Omega(t_d - t_{00}^{c1}) + (c_{10}^{1}P_{10} + c_{30}^{1}P_{30})$$
$$(1 + \overline{f}_{10}^{c}\Delta\overline{F}) \cos \Omega(t_d - t_{10}^{c1})$$

Semiannual terms

$$+ (c_{00}^{2} + c_{20}^{2}P_{20}) \cos 2\Omega(t_d - t_{00}^{c2}) + c_{10}^{2}P_{10} \cos 2\Omega(t_d - t_{10}^{c2})$$

Diurnal Terms

$$+ [a_{11}P_{11} + a_{31}P_{31} + a_{51}P_{51} + (c_{11}^{1}P_{11} + c_{21}^{1}P_{21}) \cos \Omega(t_d - t_{10}^{c1})]$$
$$(1 + \overline{f}_{11}^{a}\Delta\overline{F}) \cos \omega\tau$$

$$+ [b_{11}P_{11} + b_{31}P_{31} + b_{51}P_{51} + (d_{11}^{1}P_{11} + d_{21}^{1}P_{21}) \cos \Omega(t_d - t_{10}^{c1})]$$
$$(1 + \overline{f}_{11}^{a}\Delta\overline{F}) \sin \omega\tau$$

Semidiurnal Terms

$$+ a_{22}P_{22}\,(1 + \overline{f}^{a}_{11}\Delta\overline{F})\cos 2\omega\tau + b_{22}P_{22}\,(1 + \overline{f}^{a}_{11}\Delta\overline{F})\sin 2\omega\tau$$

Magnetic Activity Terms

$$+ (k^{a}_{oo} + k^{a}_{20}\,P_{20})\,\Delta A$$

where

$\Delta A = (Ap - 4)$

$\Delta F = F_{10.7} - \overline{F}_{10.7}$

$\Delta\overline{F} = \overline{F}_{10.7} - 150$

P_{nm} associated Legendre polynomials equal to $(1 - x^2)^{m/2} / 2^n\, n!\ \ (d^{n+m}/dx^{n+m})\ (x^2 - 1)^n$,

x = cosine of magnetic colatitude.

$\Omega = 2\pi/365$ day^{-1}

$\omega = 2\pi/24$ hour^{-1}

τ = magnetic local time, hours

L list of solar and geophysical parameters

z altitude, km

t_d day of year

Ap daily magnetic index

$F_{10.7}$ 10.7 cm solar flux on previous day, 10^{-22} W m^{-2} Hz^{-1}

$\overline{F}_{10.7}$ average of $F_{10.7}$ over 3 solar rotations centered on t_d

$\overline{T}_\infty$ average exospheric temperature, K

T temperature at height z

T_{120} lower boundary temperature, 386 K

s temperature gradient parameter, 2.548×10^{-2} km^{-1}

The coefficients of the spherical harmonic expansion for $T_\infty(L)$ were determined by calculating a nonweighted least squares fit of NT to $\bar{T}_\infty G_T(L)$. This fit was done in two steps. The first step included only data where Ap≤10 and all coefficients except those due to magnetic activity were determined. The second step used all data where Ap≤130 (one third of those are above an Ap of ten) to determine the magnetic activity coefficients. The coefficients and their standard deviations are listed in Table 1.

4.3 Atomic Oxygen and Helium Density Distributions

The global distribution of the neutral composition can be represented over a range of altitudes once the temperature profile has been determined and lower boundary densities have been specified. The extrapolation in altitude is made through the diffusive equilibrium profiles of Walker (1965), given by

$$n(z,L) = n_{120}(L)\, D[z,s,T_{120},T_\infty(L)]$$

$$D[z,s,T_{120},\, T_\infty(L)] = [(1-a)/(1-ae^{-s\xi})]^{1+\gamma+\alpha} \exp(-s\xi) \qquad (4.3)$$

$$\xi = \frac{(z - 120)(R_E + 120)}{R_E + z}$$

where

$$n_{120}(L) = \bar{n}_{120} \exp[G_M(L) - 1]$$

$$\gamma = Mg_{120}/sRT\ (L)$$

$$a = 1 - T_{120}/T_\infty(L)$$

$$g_{120} = 9.44663\ m\ s^{-2}$$

n ambient density, m^{-3}

$\bar{n}_{120}$ average 120 km density

for N_2, $n_{120} = 2.81 \times 10^{17}\ m^{-3}$ and $G_{28} = 1$

M mass number of constituent, g $mole^{-1}$

In order to determine the atomic oxygen distribution at the 120 km lower boundary, the n(O) values at satellite altitudes were reduced to 120 km using corresponding N_2 values as discussed previously (Section 3.2). The neutral temperatures, T_z, were inferred from the N_2 data rather than calculated from the MSIS model. The 120 km helium densities were found similarly and the effects of thermal diffusion for He were included in the reduction expression,

$$\ln n_{He}(120) = \ln n_{He}(z) + \tfrac{1}{7}[\ln n_{N_2}(120) - \ln n_{N_2}(z)]$$

$$+ [\tfrac{6}{7} + \alpha]\ \ln[\frac{T_z}{\bar{T}_{120}}] \qquad (4.4)$$

The 120 km boundary densities were used to determine the coefficients (Table 2) of the spherical harmonic expansion $G_M(L)$, chosen to be identical in form to that used for the inferred exospheric temperatures

Table 1. Spherical harmonic coefficients for the inferred exospheric temperature

Coefficients	T_∞	Coefficients	T_∞
Average	1.045E+3±3.E+0	c_{00}^{2}	-3.007E-2±2.E-3
a_{10}	-1.271E-2±3.E-3	c_{20}^{c2}	-2.795E-2±4.E-3
a_{20}	5.407E-2±3.E-3	t_{00}^{c2}	2.405E+1±2.E+0
a_{40}	3.566E-2±4.E-3	c_{10}^{2}	-3.104E-2±4.E-3
$*f_{00}^{a1}$	1.198E-3±4.E-5	t_{10}^{c2}	-3.195E+0±3.E+0
$*f_{00}^{a2}$	-5.374E-6±1.E-6	a_{11}	-6.652E-2±4.E-3
$*\bar{f}_{00}^{a1}$	3.197E-3±3.E-5	a_{31}	-9.515E-3±2.E-3
$*\bar{f}_{10}^{c}$	5.620E-3±3.E-4	a_{51}	1.114E-5±2.E-3
$*\bar{f}_{11}^{a}$	5.582E-3±2.E-4	c_{11}^{1}	-2.238E-2±7.E-3
k_{00}^{a}	2.500E-3±5.E-5	c_{21}^{1}	1.767E-2±4.E-3
k_{20}^{a}	2.375E-3±1.E-4	b_{11}	-8.004E-2±4.E-3
c_{00}^{1}	2.874E-2±3.E-3	b_{31}	6.322E-3±2.E-3
t_{00}^{c1}	-2.726E+1±5.E+0	b_{51}	1.111E-2±2.E-3
c_{10}^{1}	-1.660E-1±8.E-3	d_{11}^{1}	-1.029E-3±7.E-3
c_{30}^{1}	-2.134E-2±8.E-3	d_{21}^{1}	-1.307E-2±4.E-3
t_{10}^{c1}	-1.406E+0±2.E+0	a_{22}	6.055E-4±1.E-3
		b_{22}	6.211E-3±2.E-3

*MSIS model value

Table 2. Spherical harmonic coefficients for the atomic oxygen and helium concentrations at 120 km

Coefficients	O	He
Average (m^{-3})	7.875E+16±5.E+14	1.981E+13±1.E+11
a_{10}	-1.178E-2 ±1.E-2	-1.641E-1 ±1.E-2
a_{20}	-3.763E-1 ±1.E-2	-1.825E-1 ±1.E-2
a_{40}	-2.181E-1 ±1.E-2	-2.278E-1 ±1.E-2
$*f_{00}^{a1}$	9.588E-4 ±2.E-4	-6.927E-4 ±2.E-4
$*f_{00}^{a2}$	0	0
$*\bar{f}_{00}^{a1}$	2.261E-3 ±2.E-4	0
$*\bar{f}_{10}^{c}$	1.892E-3 ±8.E-4	1.373E-4 ±3.E-4
$*\bar{f}_{11}^{a}$	2.160E-3 ±1.E-3	6.400E-3 ±5.E-4
k_{00}^{a}	-1.773E-3 ±1.E-3	-2.382E-3 ±4.E-4
k_{20}^{a}	-8.695E-3 ±3.E-3	-1.470E-2 ±8.E-4
c_{00}^{1}	1.178E-1 ±1.E-2	-3.647E-1 ±1.E-2
t_{00}^{c1}	2.157E+1 ±4.E+0	-1.565E+2 ±1.E+0
c_{10}^{1}	3.430E-1 ±2.E-2	1.730E+0 ±2.E-2
c_{30}^{1}	1.272E-2 ±2.E-2	1.933E-1 ±2.E-2
t_{10}^{c1}	5.949E+0 ±3.E+0	-5.945E+0 ±5.E+0
c_{00}^{2}	1.251E-1 ±7.E-3	4.093E-1 ±7.E-3
c_{20}^{2}	-1.268E-1 ±1.E-2	-2.073E-1 ±1.E-2
t_{00}^{c2}	1.030E+2 ±2.E+0	1.069E+2 ±7.E-1

Table 2. (Continued)

Coefficients	O	He
c_{10}^{2}	-1.574E-1 ±1.E-2	-8.549E-2 ±1.E-2
t_{10}^{c2}	-8.260E+1 ±2.E+0	-6.594E+1 ±5.E+0
a_{11}	-1.273E-2 ±1.E-2	-7.072E-2 ±2.E-2
a_{31}	-1.826E-2 ±6.E-3	-5.019E-2 ±8.E-3
a_{51}	-1.163E-2 ±4.E-3	-5.425E-2 ±6.E-3
c_{11}^{1}	1.813E-2 ±2.E-2	2.380E-2 ±3.E-2
c_{21}^{1}	2.223E-2 ±1.E-2	4.914E-2 ±2.E-2
b_{11}	3.600E-2 ±1.E-2	4.618E-1 ±2.E-2
b_{31}	-6.465E-2 ±6.E-3	-3.722E-2 ±9.E-3
b_{51}	-3.277E-2 ±4.E-3	-4.316E-2 ±6.E-3
d_{11}^{1}	5.734E-2 ±2.E-2	1.319E-1 ±3.E-2
d_{21}^{1}	2.339E-2 ±1.E-2	2.220E-1 ±2.E-2
a_{22}	8.638E-3 ±4.E-3	2.404E-2 ±6.E-3
b_{22}	-3.489E-3 ±5.E-3	2.181E-3 ±7.E-3

*MSIS Model Value

for consistency. These coefficients were determined in the same way as those for the exospheric temperatures. First, a quiet model was formed using data taken when the Ap index was less than or equal to ten. Then, the magnetic activity coefficients were determined using all data with Ap $\leq$ 130. No measurements obtained below 190 km were used. The reason for this is that atomic oxygen and helium very likely show departures from diffusive equilibrium at low altitudes. Since the model represents the hydrostatic distributions, a correction term for a non-zero diffusion velocity, such as that used by Hedin et al. (1977b), would be needed in order to incorporate low altitude measurements into this model. No attempt to use a non-zero diffusion velocity was made here. The 120 km lower boundary was chosen because it is a convenient level for modeling the upper thermosphere through the Walker (1965) profiles. Actual 120 km values may be above or below the model estimates.

As in the case of molecular nitrogen, the atomic oxygen and helium data were limited to low solar activity conditions so that the effect of EUV variations could not be found simply. In order to allow the model to be used under higher solar activities, the coefficients of the MSIS model describing the density variations with solar flux changes were used here.

CHAPTER V

DISCUSSION OF THE RESULTS OF THE MODEL

5.1 Accuracy of the Magnetic Model

The overall performance of the magnetic coordinate model was examined by computing the residuals (data to model ratios) of the atomic oxygen and helium measurements as functions of day number, magnetic latitude, magnetic local time, and magnetic activity (Ap) in order to search for systematic removal of density variations with these parameters by the harmonic expansion. No attempt to estimate possible correlations between parameters was made. A subset (one of five points) of the quiet time data ($Ap \leq 10$) comprised the density ratio plots, except for the magnetic activity residuals which were computed using data with Ap values as large as thirty. Only measurements obtained between 200 km and 400 km were included since the satellite coverage was best over this height range.

The atomic oxygen residuals for 1974 and the first half of 1975 are shown in Figure 15a. Most of the data lie within a factor of 1.3 of the model, although several points are more than a factor of two below unity. These could be due to the slow return of the densities to quiet time values after a magnetic storm while the Ap index returns much more rapidly as is discussed in Chapter VI. There does not appear to be a systematic change in the residuals with day number indicating that the annual and semiannual effects have been largely included in the model.

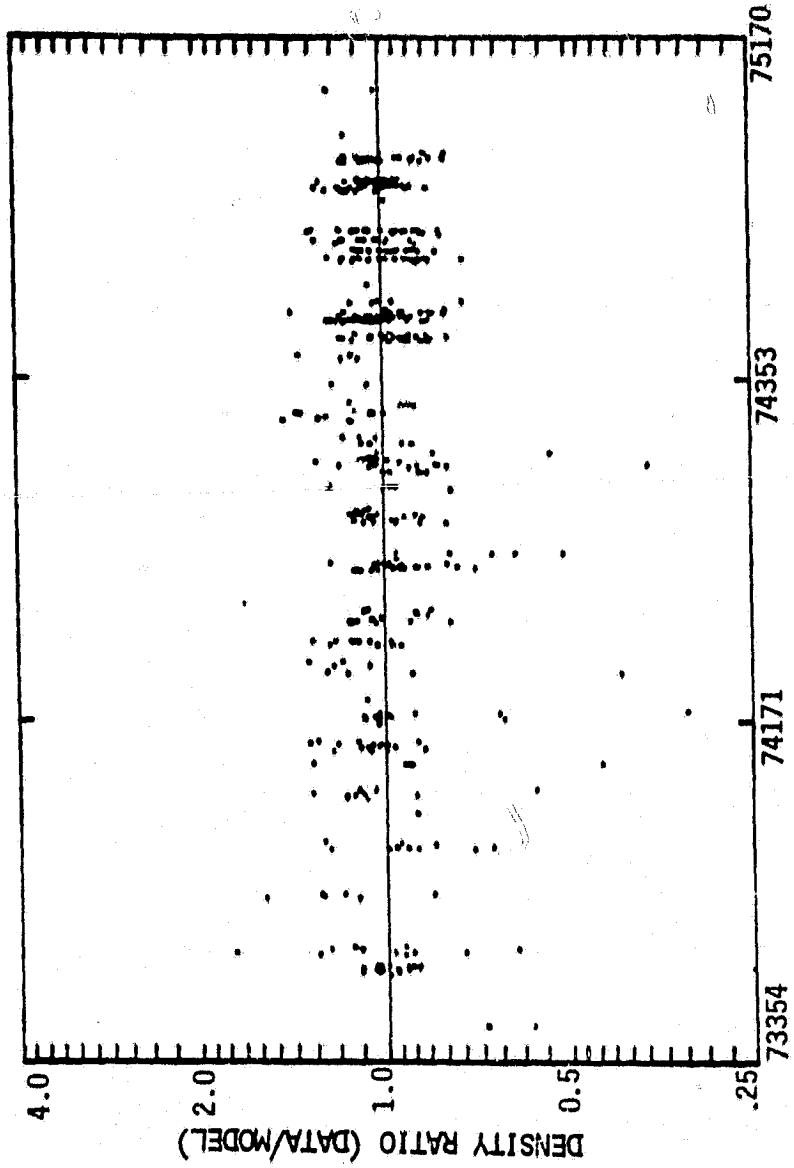

Figure 15a Ratios of model predictions to atomic oxygen data between 200 and 400 km for Ap values less than or equal to ten as a function of year and day number (yyddd).

Magnetic latitude behavior of the residuals is plotted in Figure 15b. The average scatter is fairly uniform over the entire globe, although the northern hemisphere contains most of the data which differ substantially from the model predictions.

Density ratios for various magnetic local times appear in Figure 15c. There does not seem to be any systematic change in the average scatter with MLT but the overall deviations are smallest between 1200 MLT and 1800 MLT and largest between 2200 MLT and 0400 MLT. The latter region is one in which steep density gradients exist resulting from auroral heating. Because of the sensitivity of the O densities in this region to the magnetic activity level rapid fluctuations of the densities would be expected in this area.

The scatter of the residuals for Ap values up to thirty (Figure 15d) does not increase greatly with magnetic activity which is somewhat surprising since this model was developed for primarily quiet magnetic conditions. There are more data which fall below a factor of 1.3 of the model for Ap values between ten and twenty but most of these lie less than a factor of two from unity. Above twenty the number of points is much smaller so that fewer points having large deviations are expected.

For the majority of the data, the model is expected to reproduce the data to within a factor of 1.3. Some points fall well outside this range and these may be related to the delay of the composition in response to magnetic heating which is not represented by the Ap index.

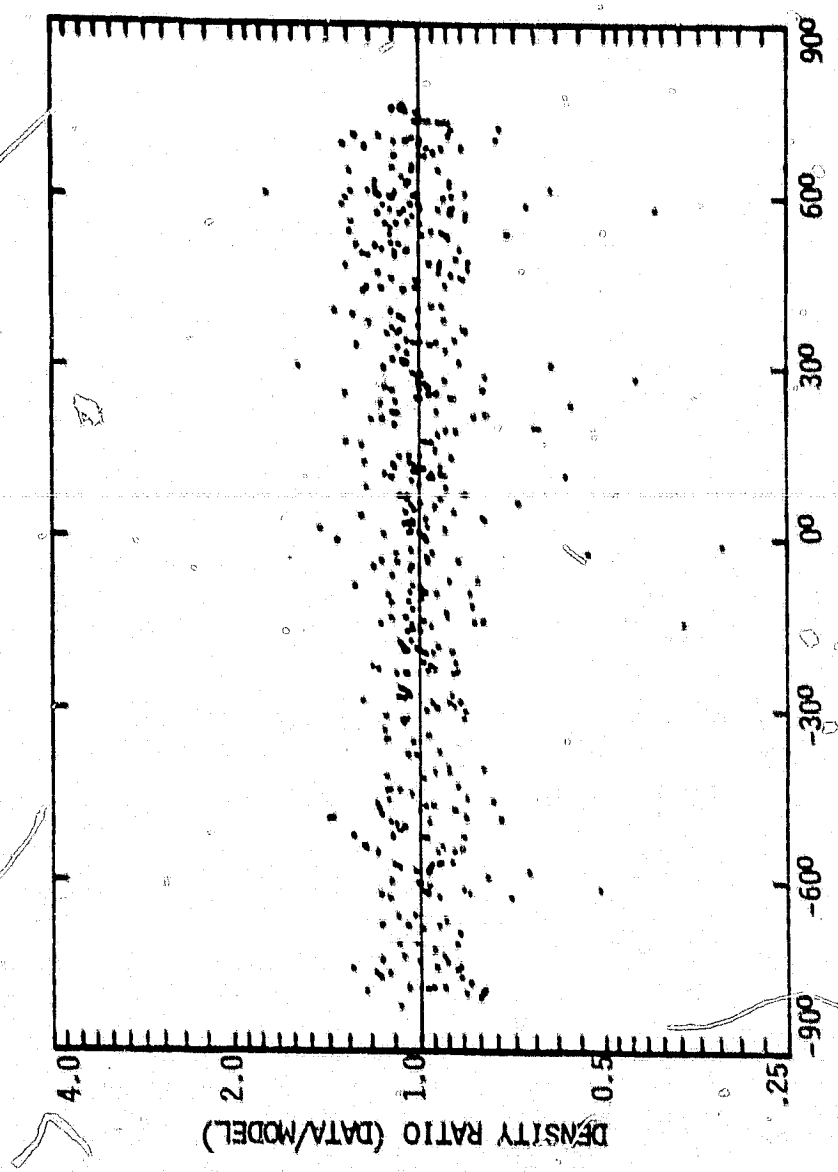

Figure 15b Ratios of model predictions to atomic oxygen data between 200 and 400 km for Ap values less than or equal to ten as a function magnetic latitude.

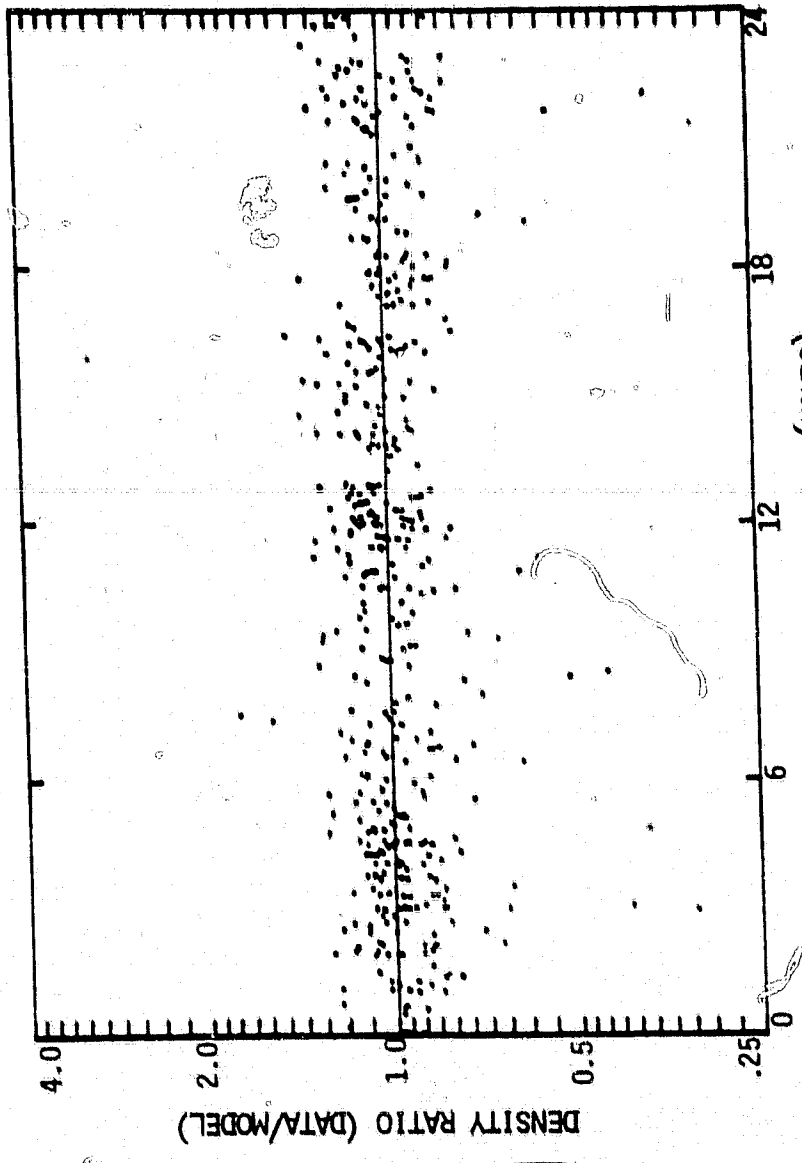

Figure 15c Ratios of model predictions to atomic oxygen data between 200 and 400 km for Ap values less than or equal to ten as a function of magnetic local time.

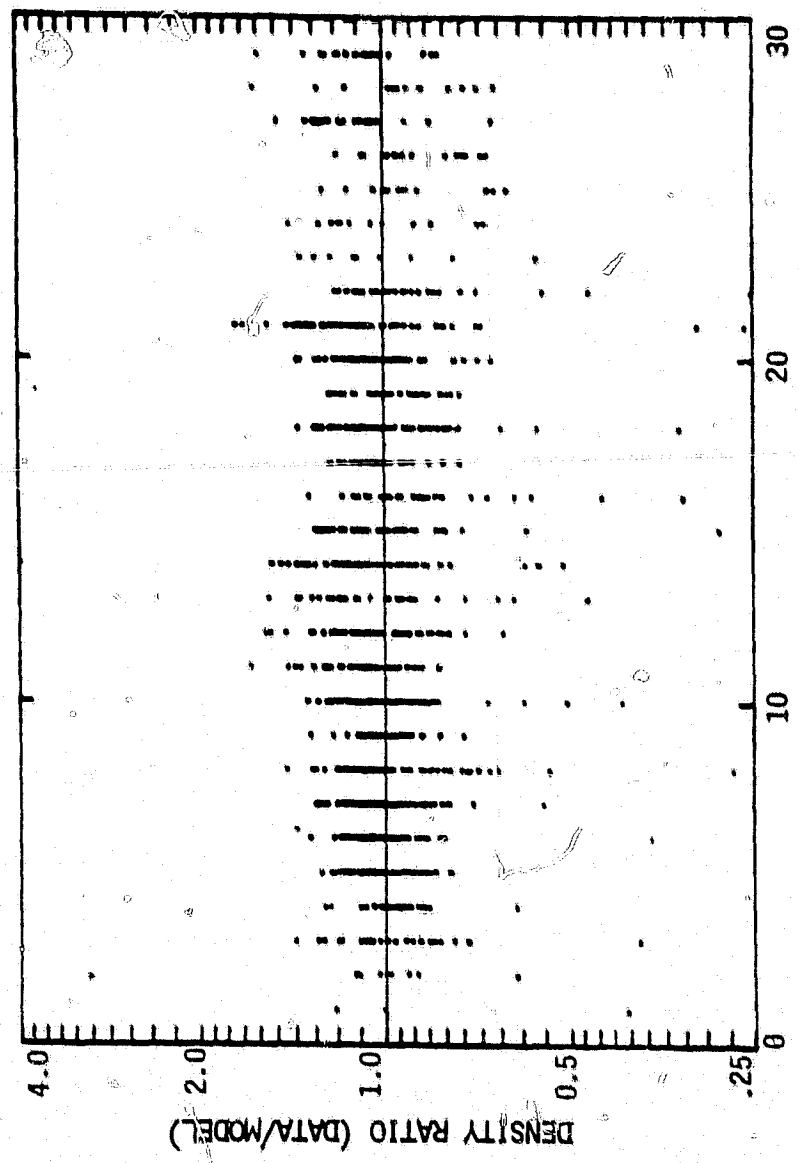

Figure 15d Ratios of model predictions to atomic oxygen data between 200 and 400 km as a function of Ap.

The helium density ratios over the period spanned by the AE-C database (Figure 16a) show somewhat more average scatter than those for atomic oxygen but the number of points differing greatly from the model is much smaller. The majority of the data fall within a factor of 1.5 of the model. The slight rise in the average estimate with day number may be due to the adopted solar activity coefficients or may be spurious.

Average scatter of the density ratio with magnetic latitude (Figure 16b) is greatest in the polar region. This is expected since the densities are the most variable in the auroral zones.

The 0000 MLT to 0800 MLT region shows the largest deviations of the data from the model although several points near 1800 MLT are also much lower than estimated (Figure 16c). These points lie near the high latitude minimum observed in the long-term density study, an area of very large density changes. The composition is very sensitive to magnetic activity here and the same problems occur in modeling helium as occured with atomic oxygen.

The helium density ratios for higher Ap values are not appreciably further from the model in general than those for lower Ap values although several points are well outside a factor of two from unity for Ap values above ten (Figure 16d). These points are few in number, though, and may be caused by local effects.

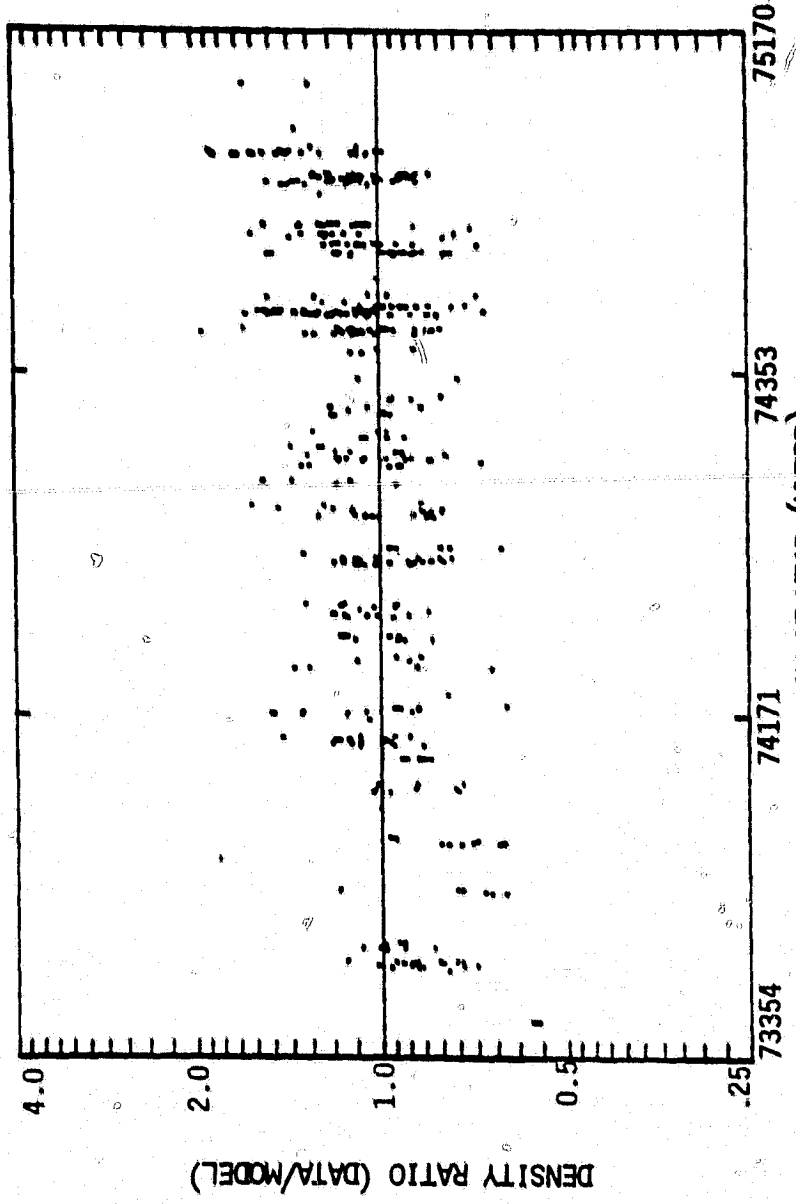

Figure 16a Ratios of model predictions to helium data between 200 and 400 km for Ap values less than or equal to ten as a function of year and day number (yyddd).

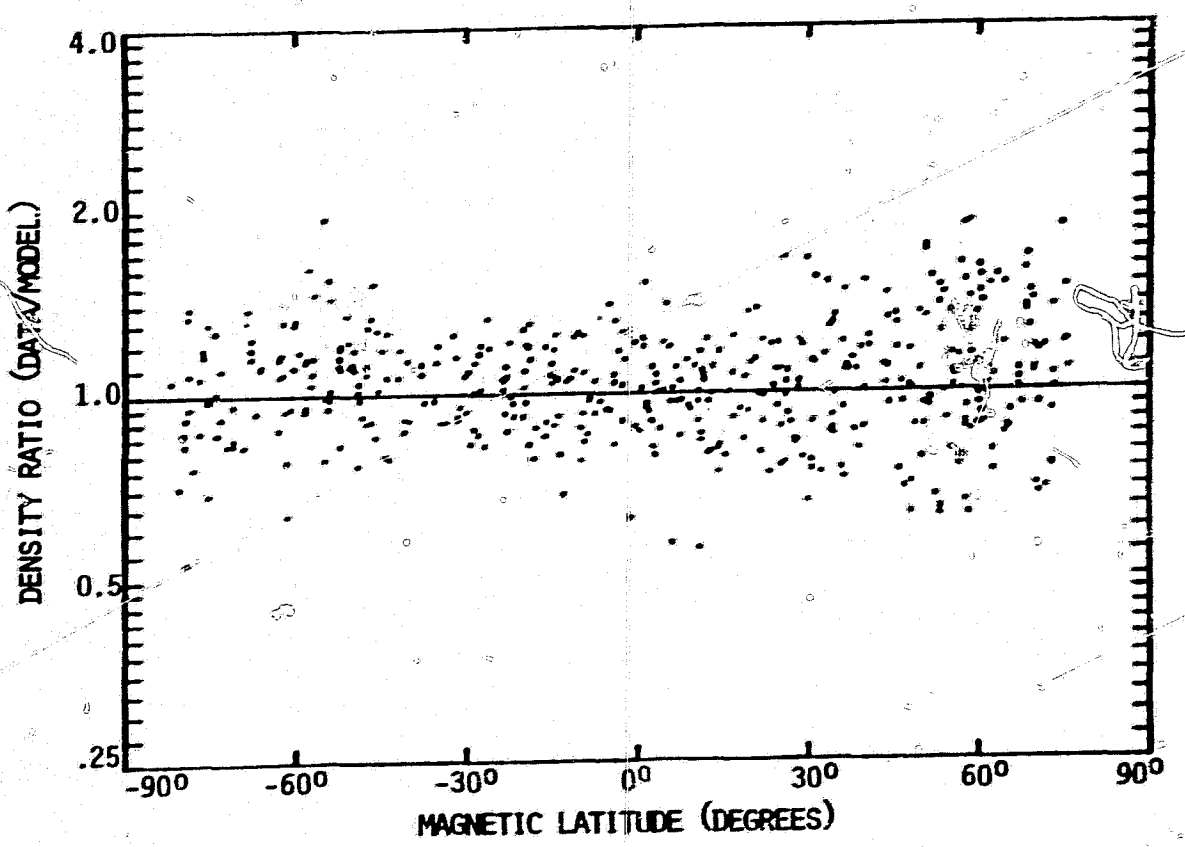

Figure 16b Ratios of model predictions to helium data between 200 and 400 km for Ap values less than or equal to ten as a function of magnetic latitude.

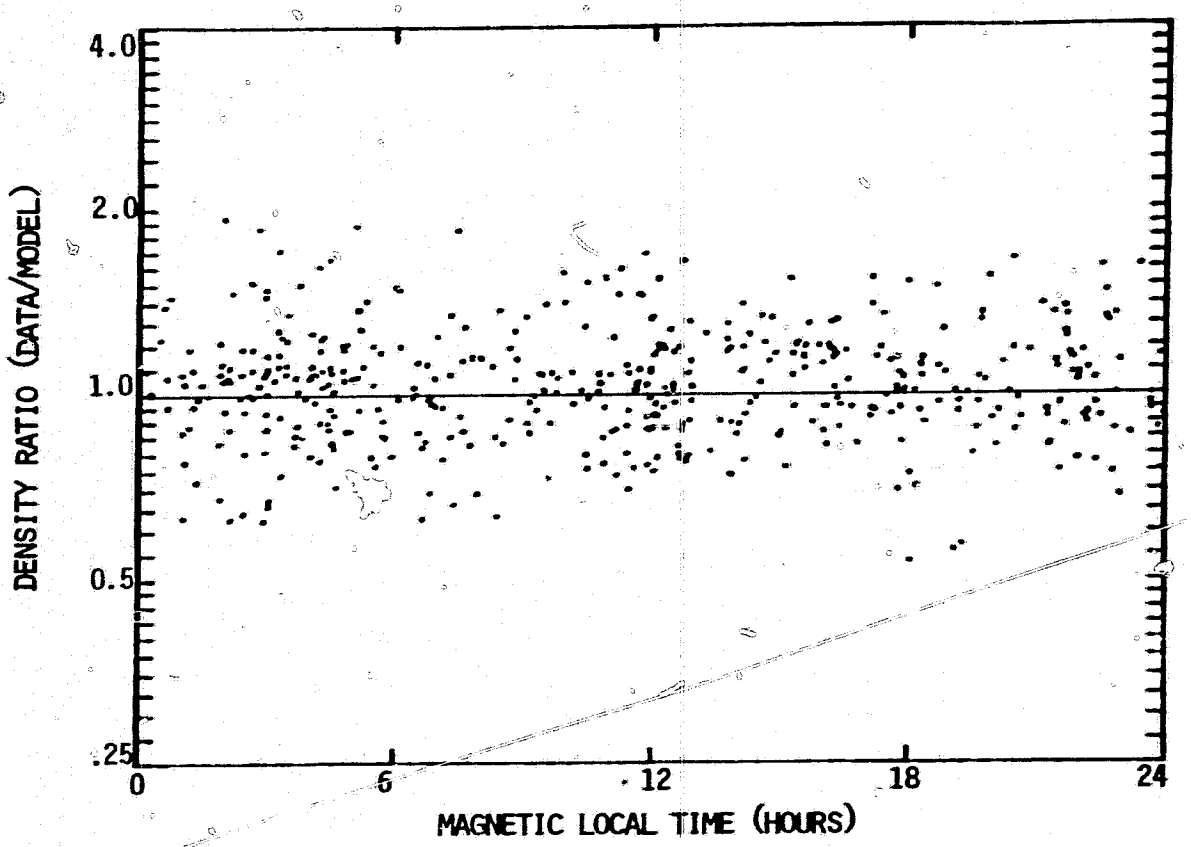

Figure 16c Ratios of model predictions to helium data between 200 and 400 km for Ap values less than or equal to ten as a function of magnetic local time.

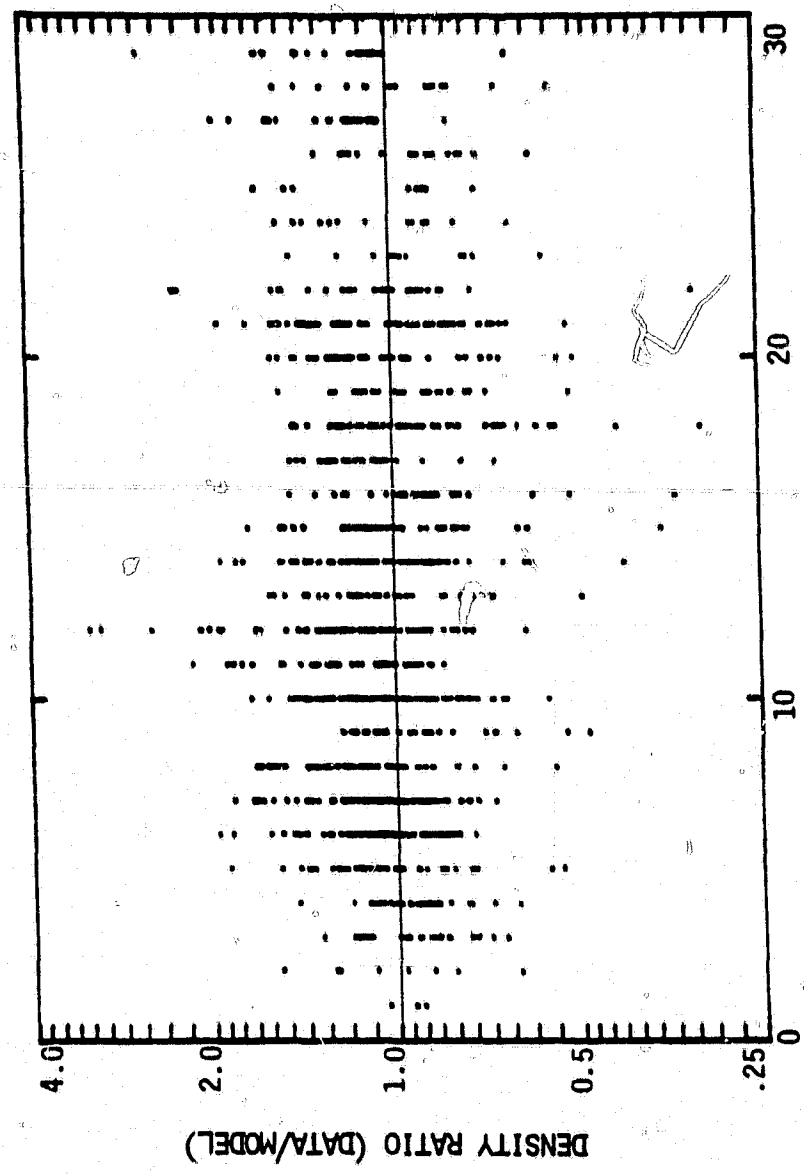

Figure 16d Ratios of model predictions to helium data between 200 and 400 km as a function of Ap.

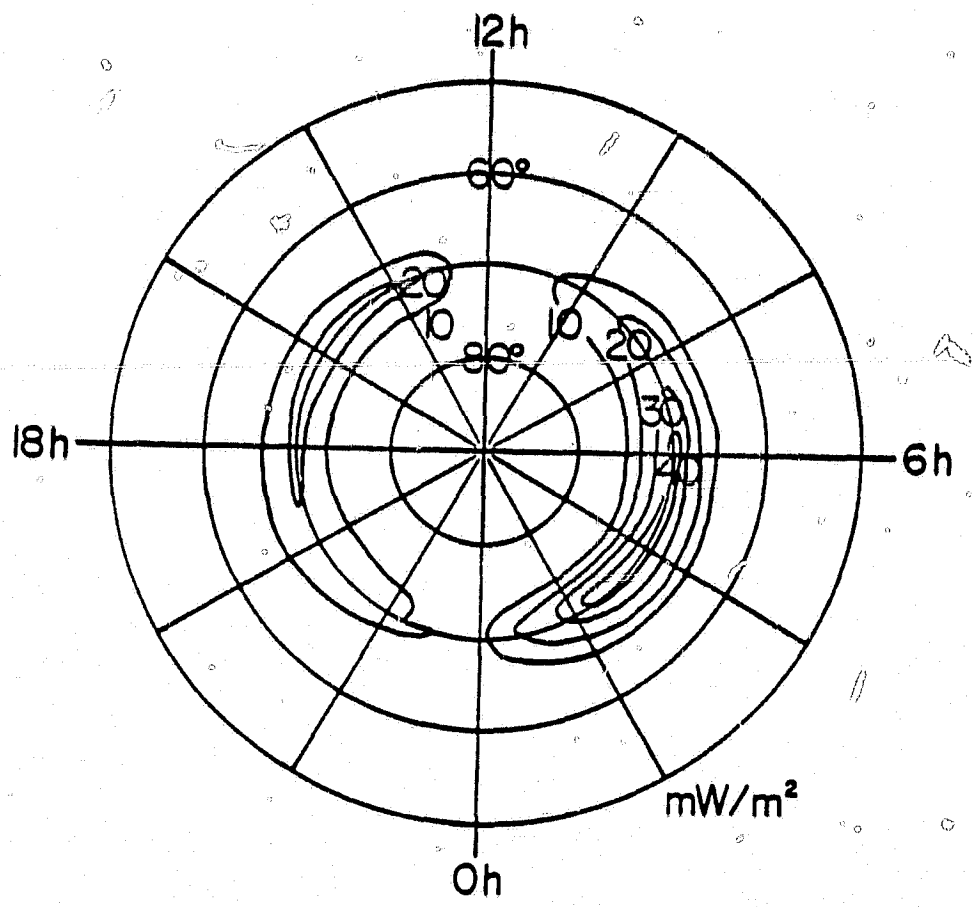

Figure 17 Power input in the polar region at June solstice due to Joule heating (Nisbet et al., 1978).

The helium model represents the major portion of the data to within a factor of 1.5 up to Ap values of thirty. The largest discrepancies appear to be in the polar regions, mostly between 0000 MLT and 0800 MLT, an area of strong magnetic heating associated with the westward electrojet. The power input into the region is relatively large as shown by Figure 17 (Nisbet et al., 1978) and substantial changes in the composition during magnetic storms occur too rapidly to be adequately represented by the model in this region.

5.2 Comparison of the Magnetic Model and the MSIS Geographic Model with Longitude Terms to the Data

The major differences between an empirical model organized in magnetic coordinates and one developed in a geographic system might be expected to occur in the polar region since the greatest density variations appear in these areas as a result of restricted but intense magnetic heating in the auroral zones. The two coordinate systems also differ the most at high latitudes. If the density variations are not adequately described by magnetic latitude and magnetic local time components, but manifest significant universal time dependencies, the data should exhibit periodic changes with universal time. No such periodic structure is apparent in either the atomic oxygen or the helium residuals above 60° N or below 60° S geographic latitude as shown in Figures 18 and 19. The MSIS model with longitude terms (Hedin et al., 1979) shows no significant periodicities either, of course, but the scatter of helium is somewhat greater. This may be the result of using a larger database to construct the MSIS model.

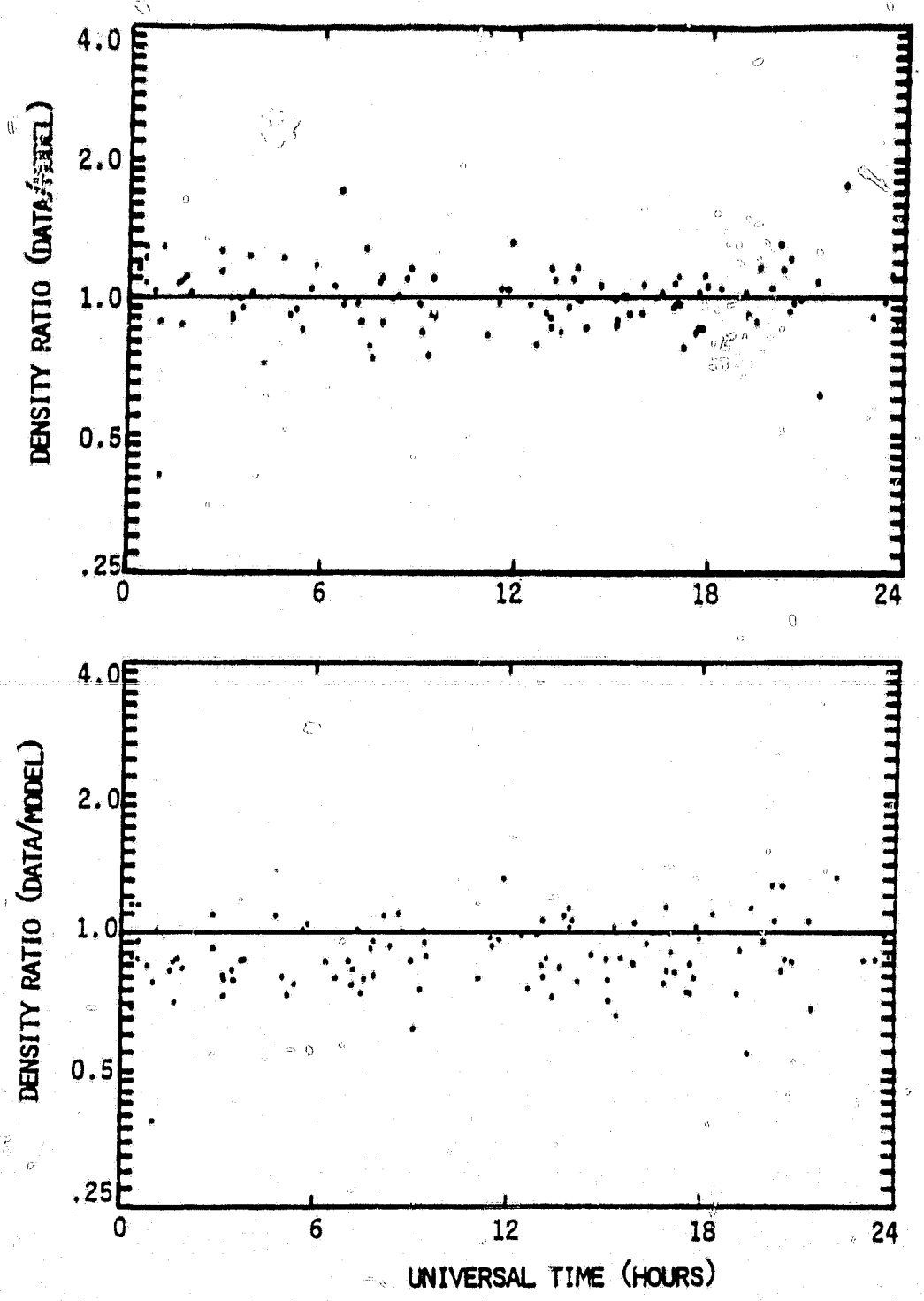

Figure 18 Ratios of magnetic model predictions (top) and estimates of the MSIS geographic model with longitude terms (bottom) to atomic oxygen data between 200 and 400 km for Ap values less than or equal to ten above |LAT| of 60°.

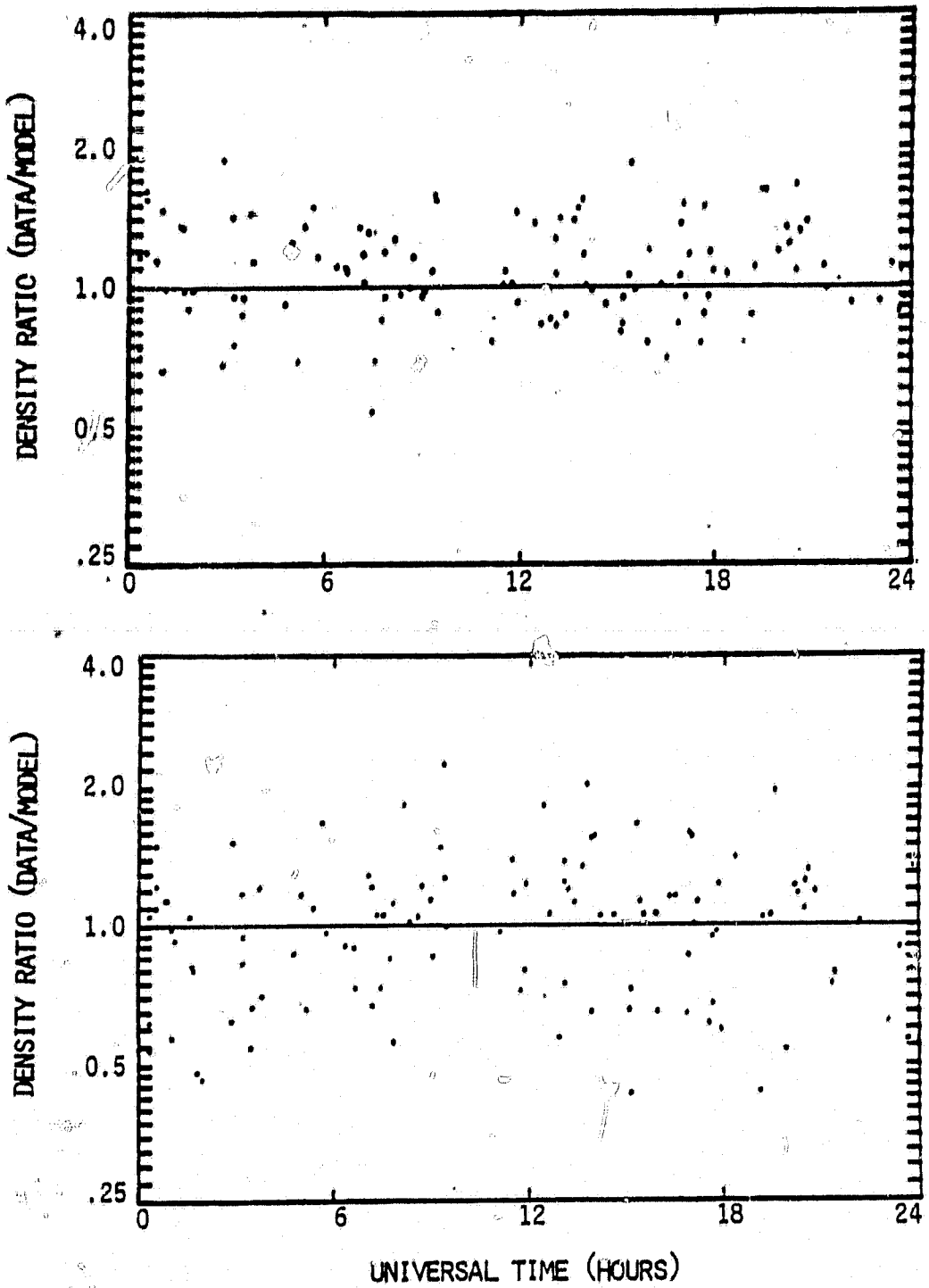

Figure 19 Ratios of magnetic model predictions (top) and estimate of the MSIS geographic model with longitude terms (bottom) to helium data between 200 and 400 km for Ap values less than or equal to ten above |LAT| of 60°.

For the AE-C data, the magnetic model seems to reproduce the high latitude composition variations at least as well as the MSIS model with longitude terms while using fewer parameters. It is also much more convenient to use in particle and Joule heating studies since density estimates can easily be made in the coordinate system to which these energy deposition processes are related. This is particularly important for comparison to theoretical models, where the number of coordinates is limited.

The low latitude behavior of the magnetic model is also quite important and must be considered since the major energy input in the equatorial region, solar heating, is geographically controlled. This energy source has a much more uniform global structure than the auroral heat input and the main variations can be represented using lower order harmonics. For these terms the magnetic and the geographic coordinates are about the same towards the equator so that either system should be satisfactory for modeling the composition. The density ratios of data taken within 30° of the geographic equator for the magnetic model show no significant periodicities in UT (Figures 20 and 21) and, in fact, are generally smaller than the residuals associated with the MSIS model, possibly for the same reason that the high latitude residuals differ. From the scatter in these residuals, it can be seen that the magnetic model represents the density variations as well as the MSIS geographic model with longitude terms at low latitudes.

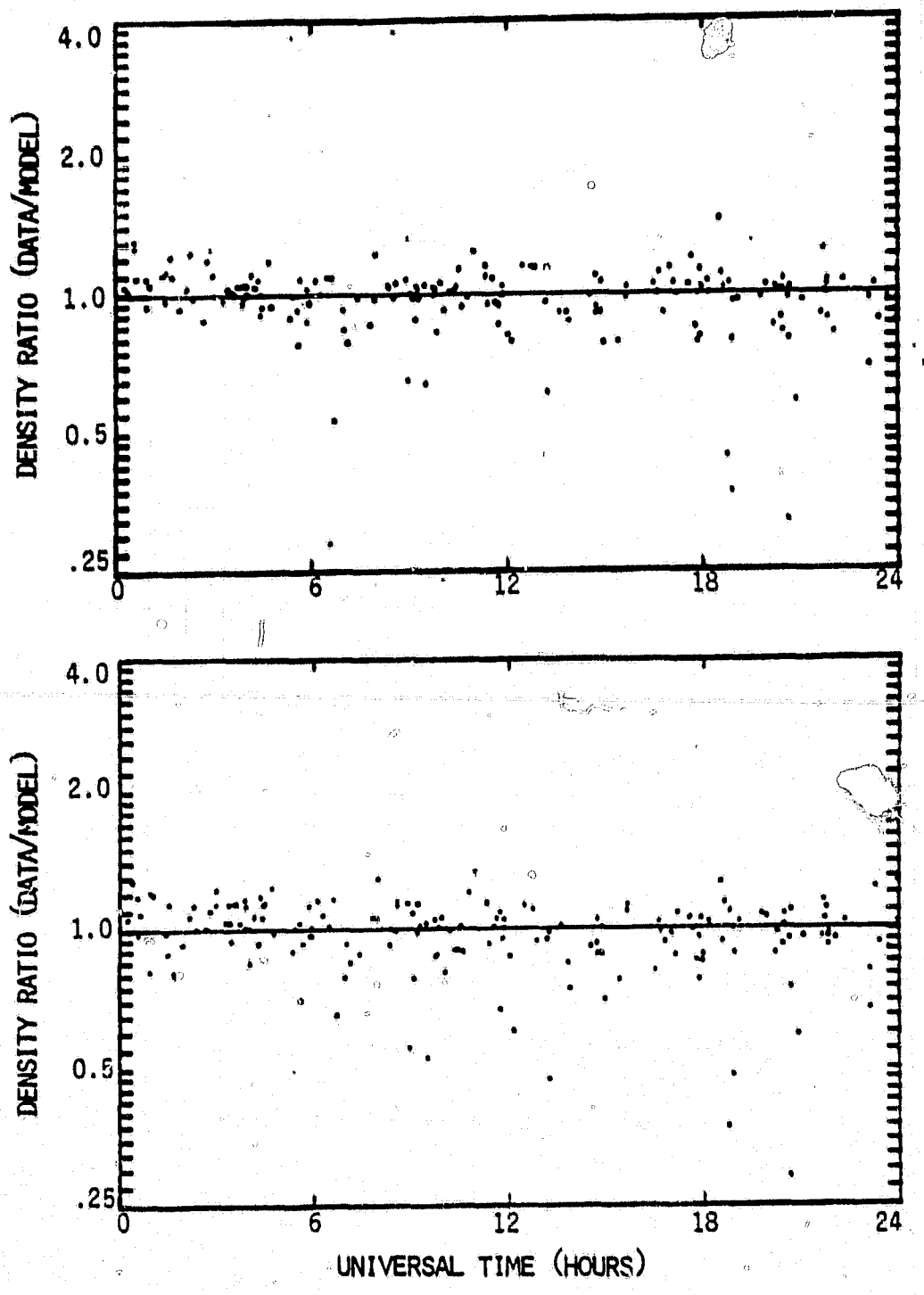

Figure 20 Ratios of magnetic model predictions (top) and estimates of the MSIS geographic model with longitude terms (bottom) to atomic oxygen data between 200 and 400 km for Ap values less than or equal to ten below |LAT| of 30°.

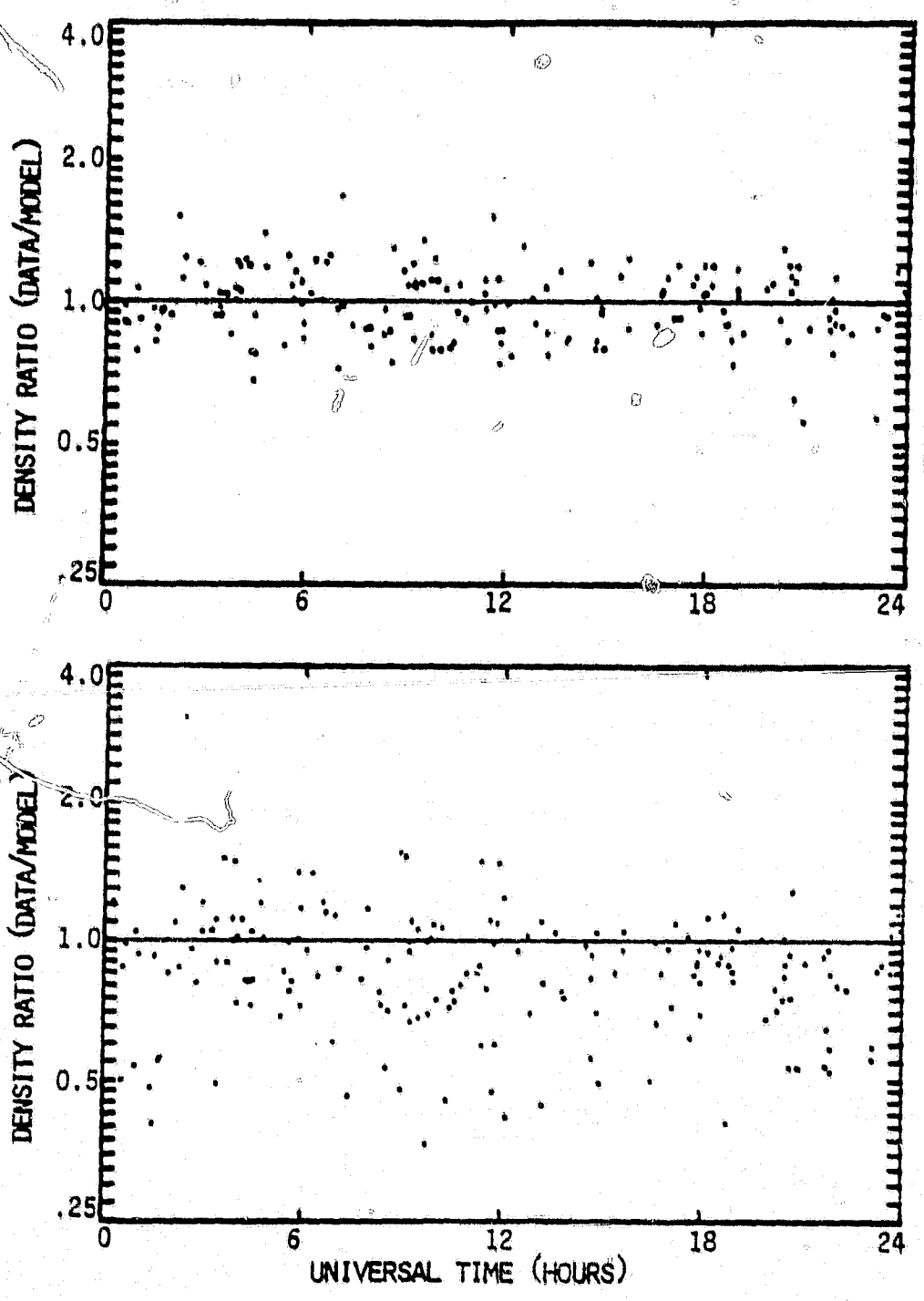

Figure 21 Ratios of magnetic model predictions (top) and estimates of the MSIS geographic model with longitude terms (bottom) to helium data between 200 and 400 km for Ap values less than or equal to ten below |LAT| of 30°.

5.3 Predictions of the Magnetic Model, the MSIS Geographic Model without Longitude Terms, and the MSIS Geographic Model with Longitude Terms

A comparison between the magnetic model estimates and those of the two geographic models by contour plotting the 120 km distributions in magnetic latitude-magnetic local time coordinates illustrates clearly the major differences between the models.

Figures 22, 23, and 24 show the helium densities for all three models for the same solar and magnetic activity conditions in the magnetic coordinate system. The predictions of the MSIS geographic models for various longitudes and universal times were transferred to the magnetic coordinate system and put into bins of one hour MLT and 5^{o} MLAT and then averaged in order to make these plots. The high latitude structure is quite similar for the magnetic model and the MSIS geographic model with longitude terms, but it is almost completely smoothed out in the MSIS geographic model without longitude terms. The importance of magnetic position in modeling the neutral concentrations in the polar regions is seriously underestimated in the geographic model which has no longitude or universal time dependencies.

Although the MSIS model with longitude terms has the capability of reproducing both universal time and longitude variations simultaneously, the magnetic model reproduces the main features of the data with fewer terms. It also does not smooth out the high latitude density variations as does the MSIS model without longitude terms, which has about the same number of coefficients as the magnetic model. The advantage of having a

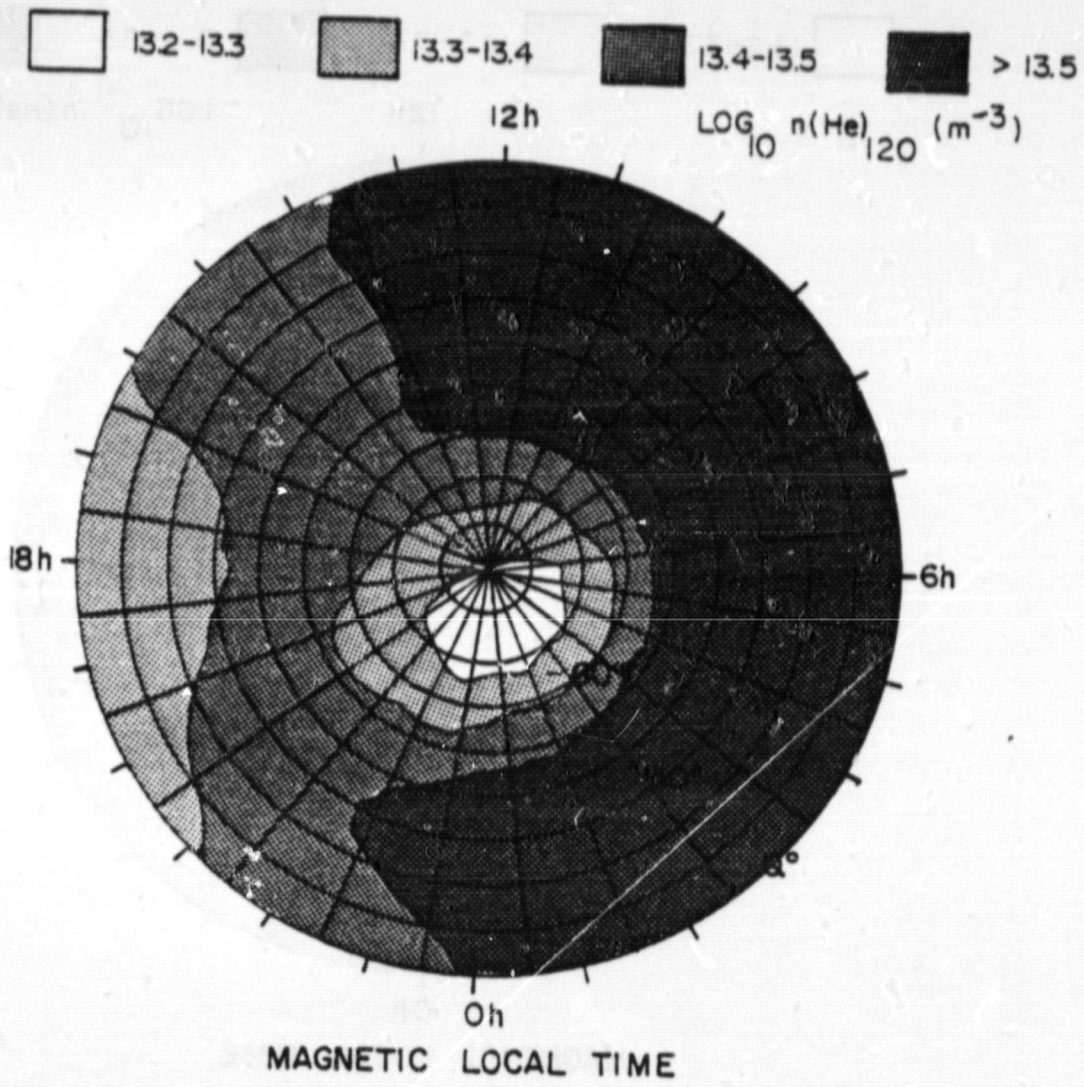

Figure 22 Contour representation of $\log_{10}$ n(He) at 120 km in the southern hemisphere for the magnetic model at spring equinox for $F_{10.7}$ = 100 and Ap = 4.

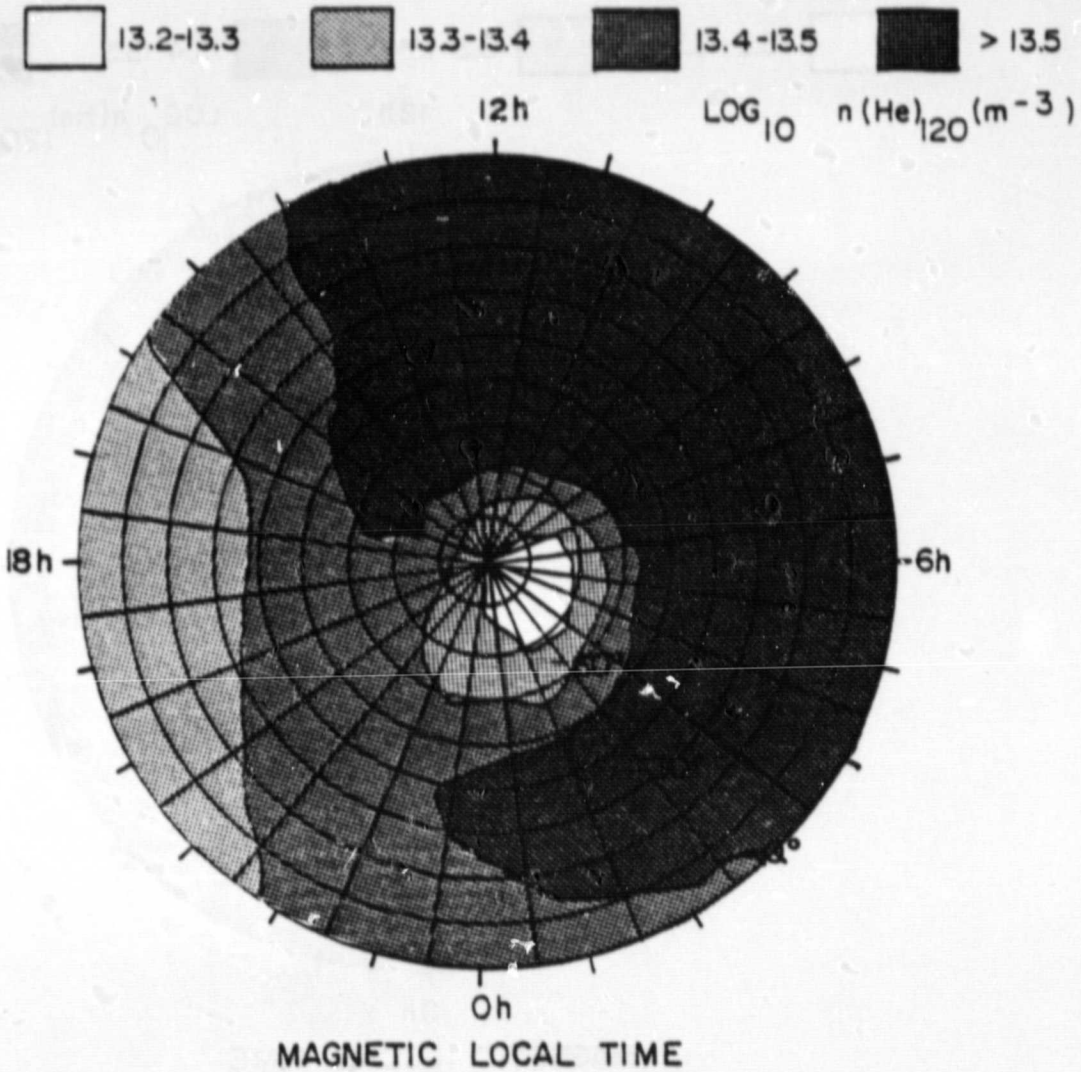

Figure 23 Contour representation of $\log_{10}$ n(He) at 120 km in the southern hemisphere for the MSIS geographic model with longitude terms at spring equinox for $F_{10.7}$ = 100 and Ap = 4.

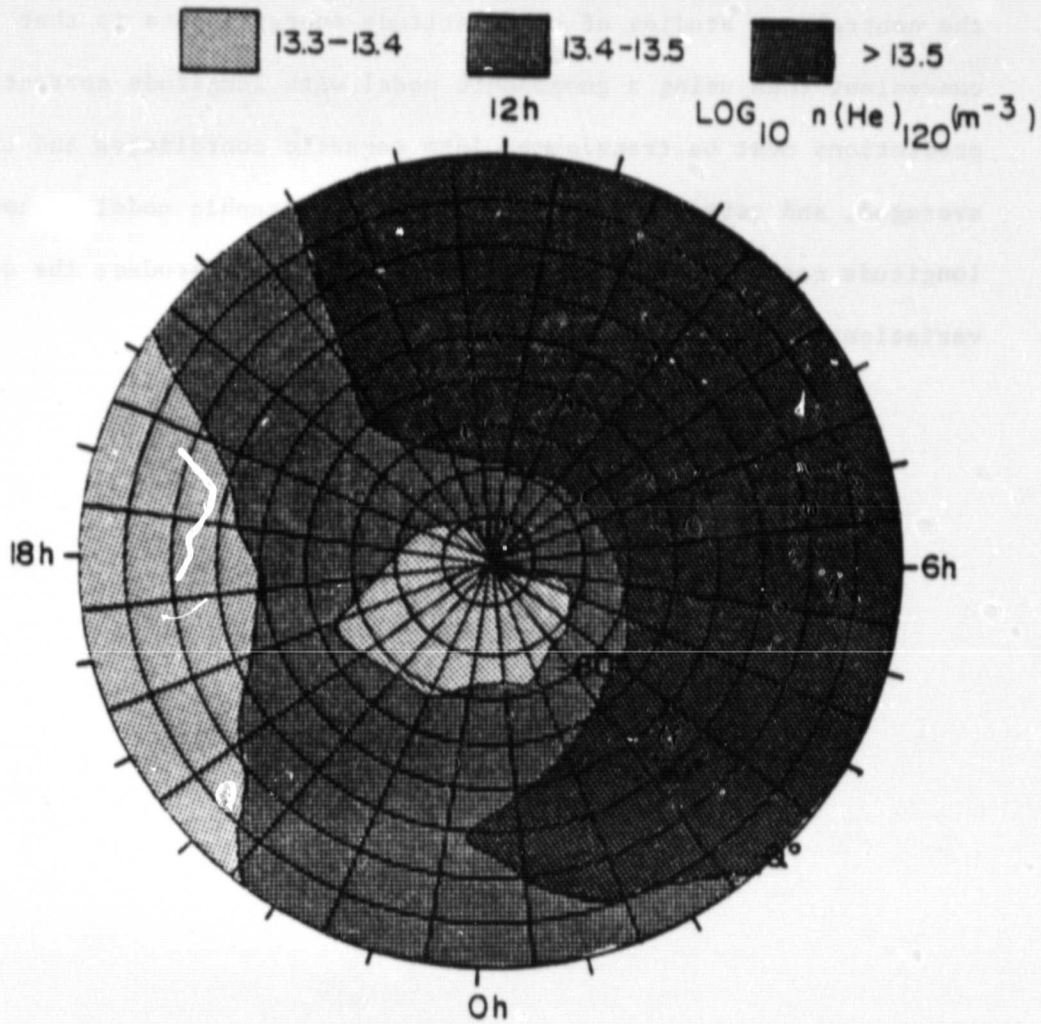

Figure 24 Contour representation of $\log_{10}$ n(He) at 120 km in the southern hemisphere for the MSIS geographic model without longitude terms at spring equinox for $F_{10.7}$ = 100 and Ap = 4.

model which uses magnetic coordinates to estimate the concentrations of the neutrals in studies of high latitude energy inputs is that it is more convenient than using a geographic model with longitude corrections whose predictions must be transformed into magnetic coordinates and then averaged, and more accurate than using a geographic model without longitude corrections which does not adequately reproduce the density variations.

CHAPTER VI

EFFECTS OF MAGNETIC ACTIVITY ON THE NEUTRAL COMPOSITION

6.1 Response of Atomic Oxygen to Enhanced Magnetic Activity in the Region of the Westward Auroral Electrojet

Joule heating in the regions of the auroral electrojets increases markedly during magnetic disturbances. Fluctuations in magnetic activity throughout these disturbances can be monitored by the auroral electrojet indices (AE, AL, and AU), which attempt to measure the B field perturbations produced by the electrojet currents and by the 3-hour ap or daily Ap indices, which reflect global changes in magnetic activity, so that changes in the neutral atmosphere with magnetic activity variations may be modeled. Direct use of these indices in modeling has, however, several problems. There is a time delay between the Joule heating and the winds and density perturbations and a further time delay before these affect densities at lower latitudes, and this results in time delays and storage phenomena (Wydra, 1975; Hedin et al., 1977c). Therefore the temperature and composition of the neutral thermosphere cannot be represented on a one-to-one basis with changes in the magnetic activity indices. This is particularly important in the polar regions where the energy input from magnetic storms is large and the density variations are substantial. Large errors occur in these areas in empirical models because data taken when the magnetic activity level is low immediately after a storm are used to develop quiet time models without the time history of the atmosphere being considered.

This problem is illustrated in Figure 25 where the atomic oxygen density at 120 km and the 3-hour ap index have been plotted through the magnetically disturbed period 16 March, 1974 to 21 March, 1974. The O densities were determined in the same manner as in the long-term analysis and were restricted to 55 to 60° MLAT and 0400 to 0700 MLT in order to reduce density variations with magnetic position. Although the 3-hour ap index indicates the average trends in the density variations, the relations with the O density during the recovery from the disturbance of 16 March is very poor. The difference between the O densities here and those several days later after the atmosphere has recovered from the magnetic disturbance is greater than a factor of two, but no indication of this slow recovery is given by the 3-hour ap index which is nearly constant over this period.

The same type of behavior was found in the recovery phase of another magnetic storm. Figure 26 shows the O density at 120 km between 55 and 60° MLAT and 0000 and 0300 MLT and the 3-hour ap index for the period 10 April, 1974 to 12 April, 1974. The densities do not return to quiet time values for approximately 24 hours after the 3-hour ap shows low activity. Again, there is more than a factor of two difference in the O values over this period, but essentially no change in the 3-hour ap index. Because such wide density variations with almost no change in ap values are responsible for very large errors in the empirical models, it would be desirable to include the atmospheric storage phenomenon in a magnetic activity indicator which could be used in modeling so that better estimates of the neutral densities throughout and during recovery from

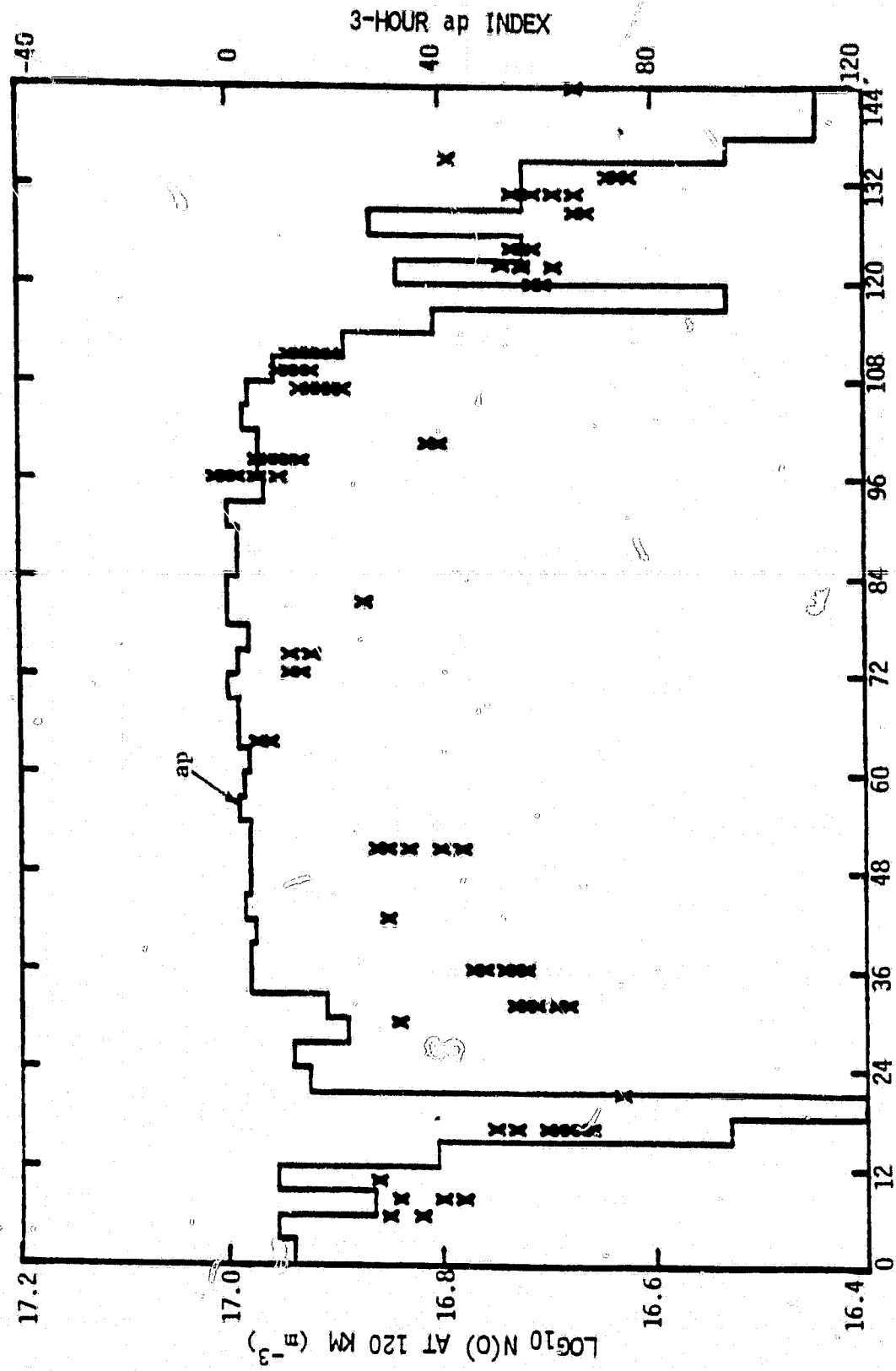

Figure 25 Log_{10} n(O) at 120 km and 3-hour ap index as a function of universal time from 16 March 1974.

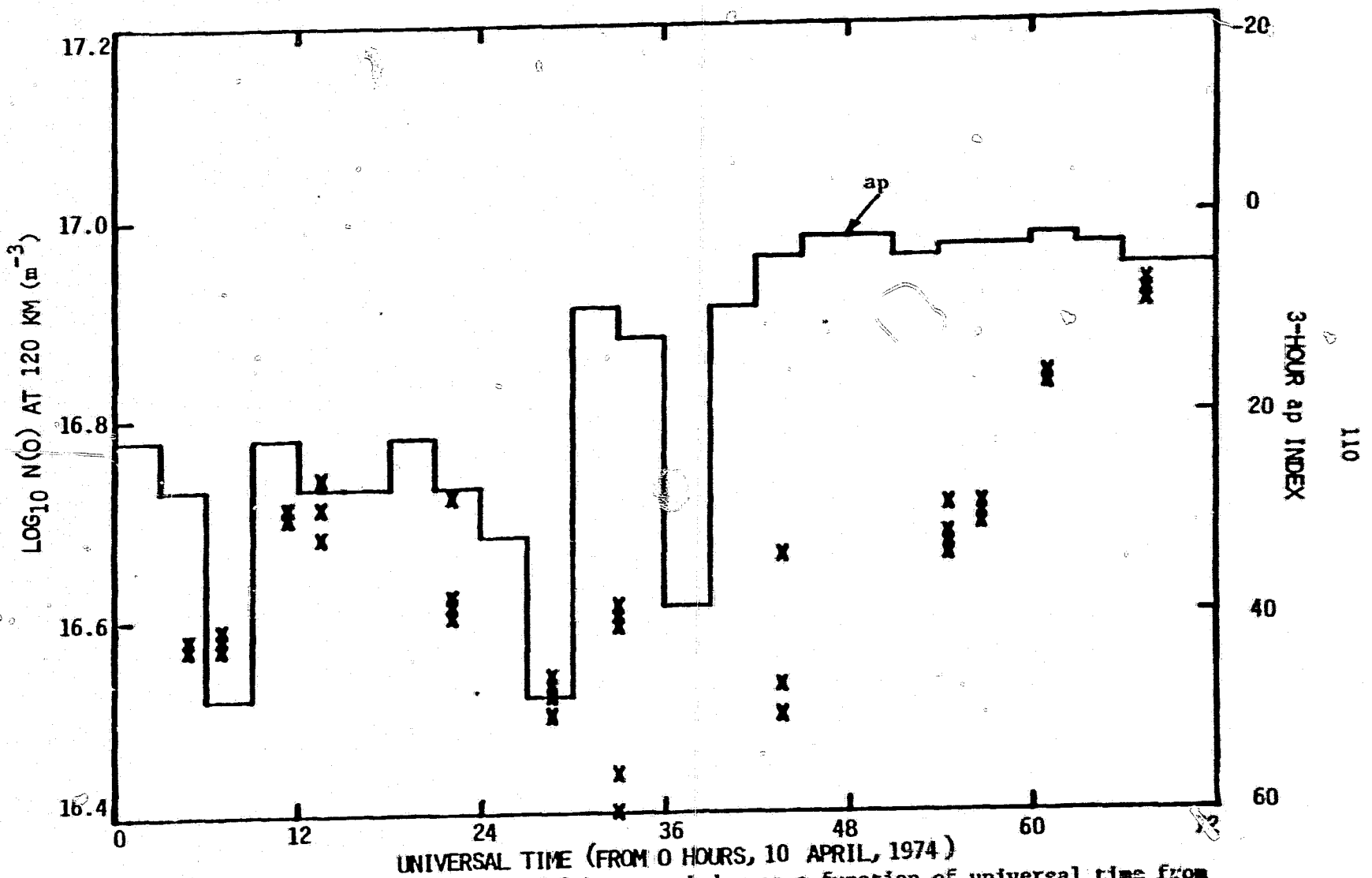

Figure 26 Log10 n(O) at 120 km and 3-hour ap index as a function of universal time from 10 April 1974.

magnetic storms could be determined. In the region of the westward electrojet, the AL index is most nearly related to the ionospheric current system responsible for Joule heating and consequent density changes in the neutral atmosphere. Therefore, this index will be used exclusively in developing a magnetic activity indicator which will be related to atomic oxygen density changes near the westward electrojet for the two periods examined previously.

6.2 Relation of a Magnetic Activity Indicator Based on the Auroral Electrojet Index AL to the Atomic Oxygen Density During Magnetic Disturbances

An indicator of magnetic activity which is closely related to the neutral density variations which occur during magnetic storms must include both time delay and energy storage effects. At high latitudes, the delay between a magnetic disturbance and the resulting changes in the neutral atmosphere appears to be on the order of one hour (Prölss and Fricke, 1976). To a first approximation of a magnetic storm lasting more than a few hours, this delay time can be neglected.

Storage effects can be approximated by using the AL index in an equation of the form

$$ML(t)_\tau = \frac{1}{\tau}\int_{-\infty}^{t} AL(t')e^{-(t-t')/\tau}\,dt' \qquad (6.1)$$

where the time constant, τ, can be adjusted to obtain closest agreement between this magnetic activity index and the neutral density variations.

The atomic oxygen densities at 120 km for the period 16 March, 1974 to 21 March, 1974 and this index for τ=1 hour are shown in Figure 27. The index responds as quickly as the atomic oxygen densities to magnetic activity increases but returns to quiet time values much more rapidly than n(O) increases after the disturbance, suggesting a value of τ which is much too small. For τ=12 hours (Figure 28), the agreement between the ML index and the O densities at storm onset remains good and the relation during recovery is much closer, although the densities still increase more slowly than the ML index decreases after the disturbance has passed. A value of 24 hours for τ (Figure 29) causes some delay in the ML index to the onset of the storm, but gives an even closer relation between the index and the atomic oxygen densities during recovery. This relation is significantly better than that obtained using the 3-hour ap index to model the density variations.

The ML index for τ=12 hours also agrees more nearly with the O densities than did the 3-hour ap index during the recovery phase of the storm of 10 April, 1974 to 12 April, 1974 (Figure 30) although the ML index returns to quiet time values more rapidly than the O densities increase. When τ is lengthened to 24 hours, however, the atomic oxygen density values increase more quickly than the ML index decreases during recovery (Figure 31). An upper limit of less than 24 hours for τ in the ML index is thus indicated for this storm. This value is consistent with that obtained for the recovery phase of the first storm, though it appears to be larger than required to represent the onset. A value of τ not exceeding 12 hours appears to characterize this phase more closely.

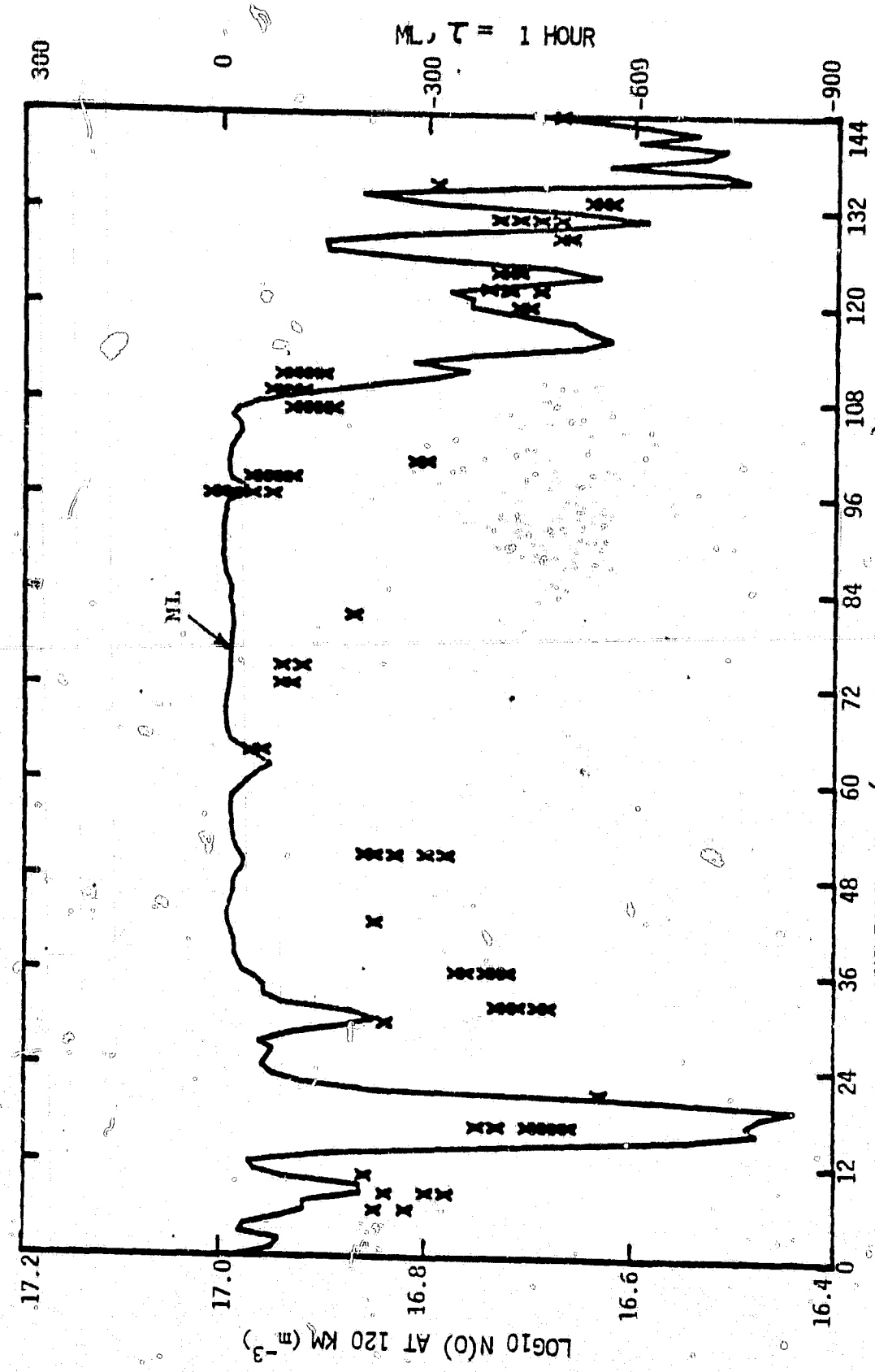

Figure 27 Log_{10} n(O) at 120 km and the ML index (τ = 1 hour) versus universal time from 16 March 1974.

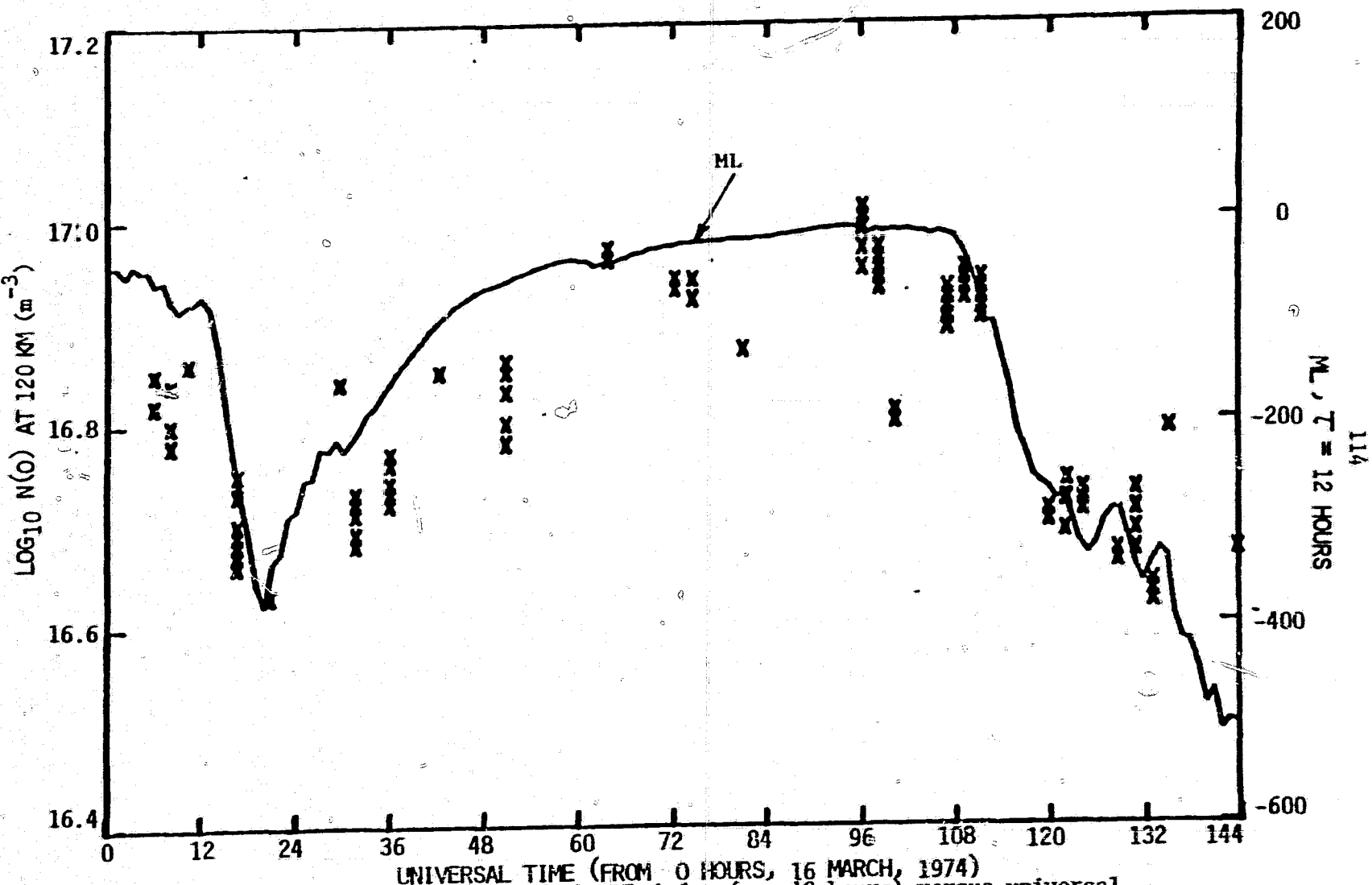

Figure 28 Log_{10} n(O) at 120 km and the ML index (τ = 12 hours) versus universal time from 16 March 1974.

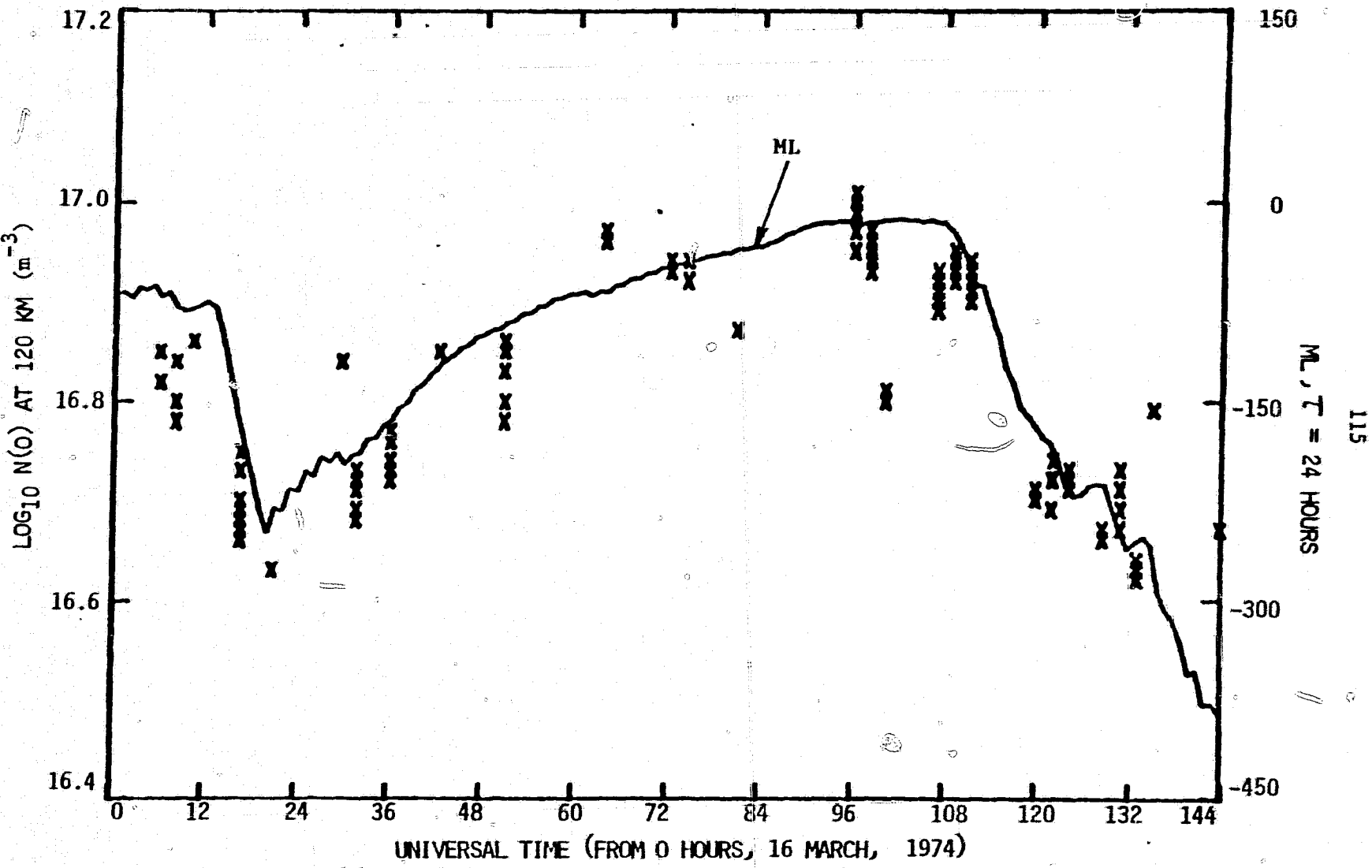

Figure 29 Log_{10} n(O) at 120 km and the ML index (τ = 24 hours) versus universal time from 16 March 1974.

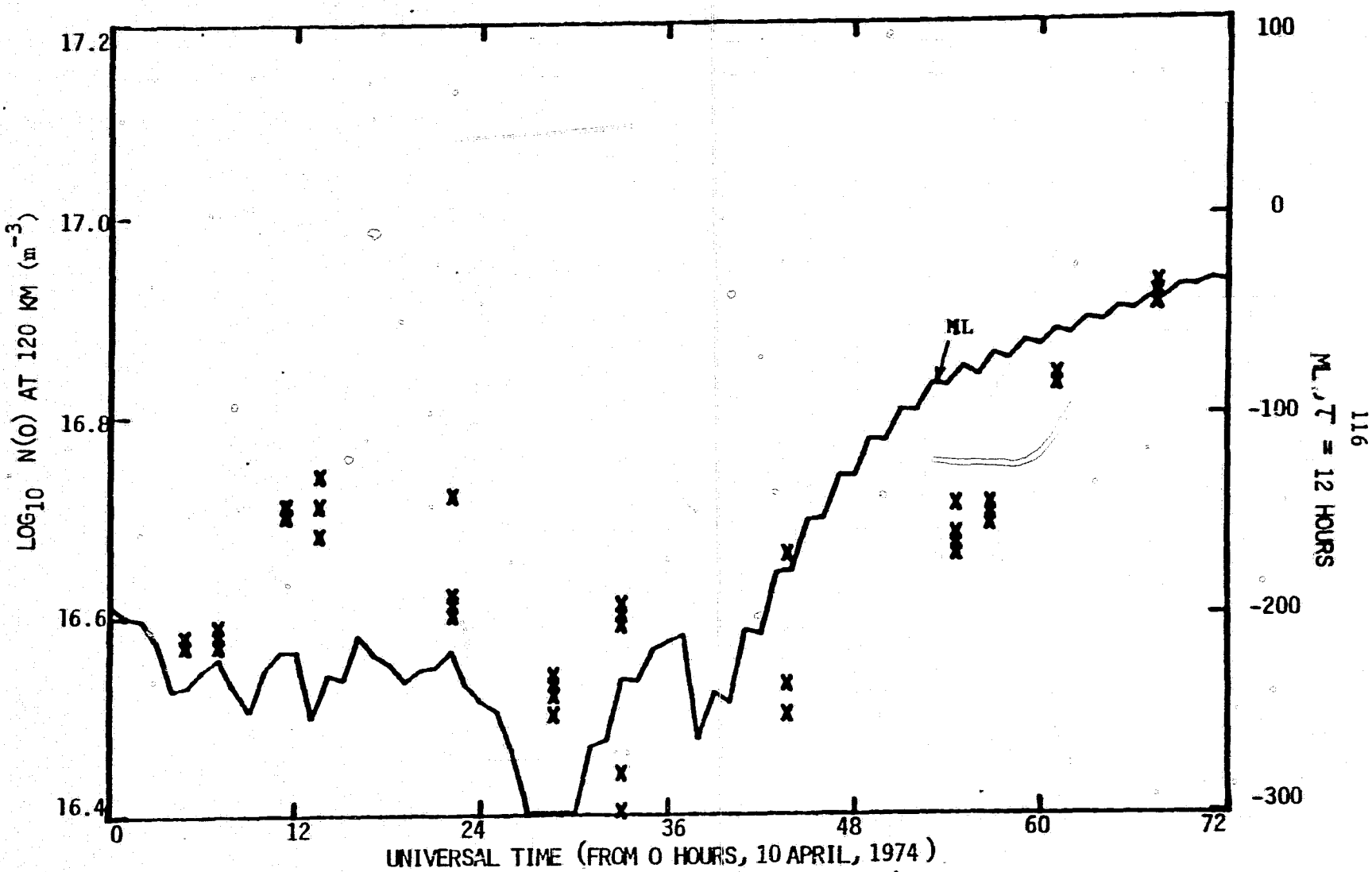

Figure 30 Log_{10} n(O) at 120 km and the ML index (τ = 12 hours) versus universal time from 10 April 1974.

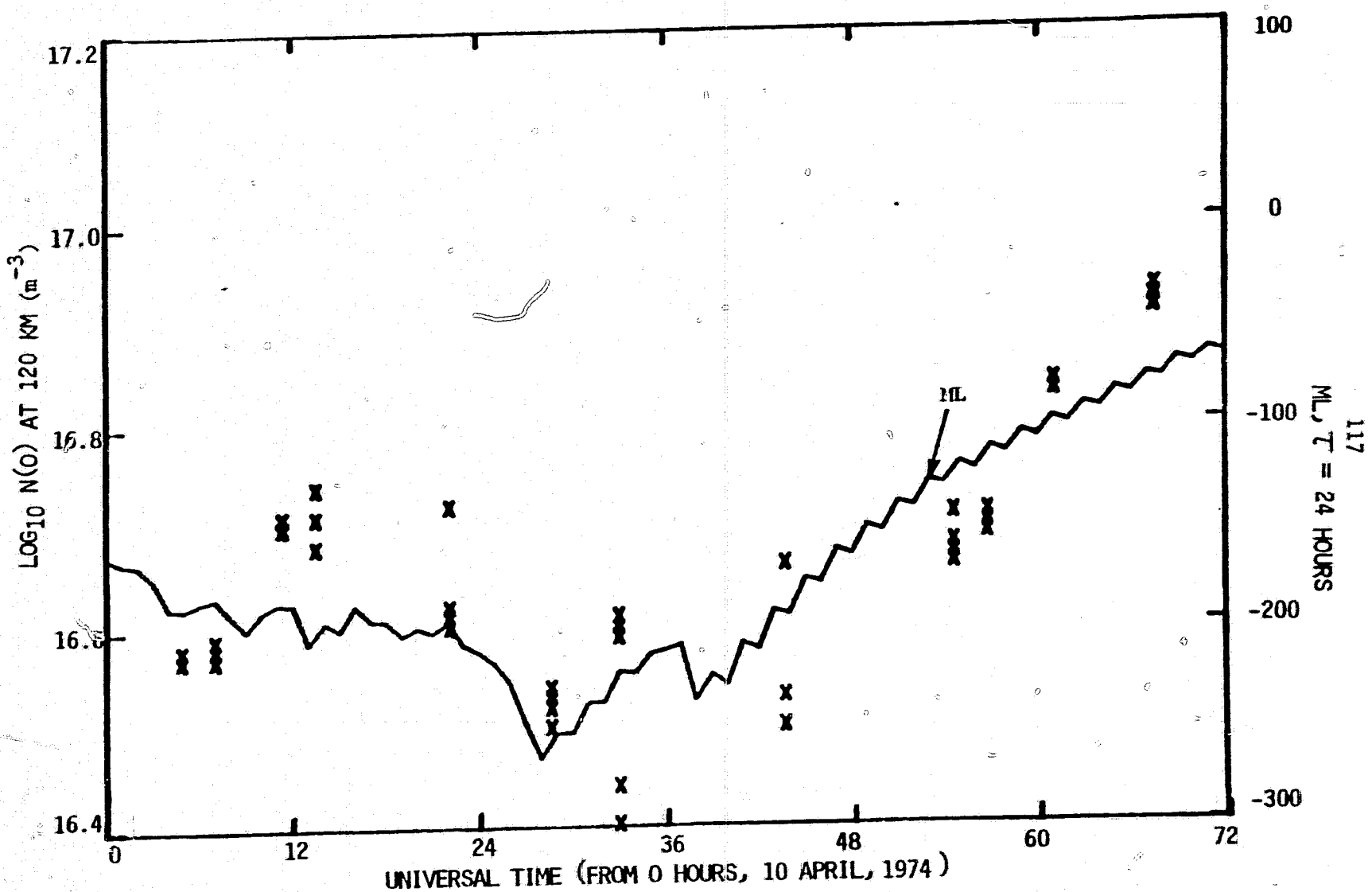

Figure 31 Log_{10} n(0) at 120 km and the ML index (τ = 24 hours) versus universal time from 10 April 1974.

In spite of the difference in the time constants for the onset and recovery phases of the two magnetic storms, the ML index is much more directly related to the 120 km atomic oxygen densities than is the 3-hour ap index. Use of this index in empirical modeling could markedly reduce the errors in density estimates caused by the atmospheric response to magnetic heating. This is an important aspect of modeling since these errors can exceed a factor of two.

CHAPTER VII

CONCLUSIONS

7.1 Long-term Averages of Atomic Oxygen and Helium

Averages of the atomic oxygen densities reduced to 120 km and the helium densities normalized to 300 km for each season have been examined in a magnetic coordinate system for various magnetic activity levels under both low and high solar activities. A persistent depletion region for both constituents has been identified at high magnetic latitudes (>60°) in the postmidnight magnetic local time sector for all seasons and all magnetic activity levels examined, except for helium in winter. It is believed that the large seasonal variation in helium, at least a 25:1 ratio of winter to summer densities at 300 km, obscures this prominent feature. This region of low densities seems to be a permanent feature of the polar thermosphere since it is present under both high and low solar activity conditions.

The location of the depletion region near the westward electrojet supports the theory that Joule heating due to electric currents flowing in the ionosphere causes upwelling of the neutral gas and a density decrease in the region of heating for constituents having less than the mean molecular mass (Mayr and Volland, 1972c; Reber and Hays, 1973).

Large density gradients in magnetic latitude and magnetic local time near the area of low densities suggest that the localized energy sources are comparable to or even greater than solar UV and EUV inputs in these regions.

The relation of the density minima to magnetic coordinates indicates that this coordinate system is well suited for modeling the neutral polar thermosphere.

7.2 Global Empirical Density Model

An empirical model of the atomic oxygen and helium distributions above 120 km has been developed in magnetic coordinates and compared to similar models based on the geographic coordinate system.

The magnetic model and the MSIS geographic model with longitude terms make similar predictions over the globe and show nearly equivalent structure towards the magnetic poles. The MSIS geographic model without longitude terms does not show the same structure as these models at high magnetic latitudes, but rather gives highly averaged density estimates.

Although the MSIS model with longitude terms has the capability of reproducing both longitude and universal time variations of the densities simultaneously, the magnetic model predicts very similar density values while using fewer parameters. The magnetic model is also based on a coordinate system in which many important high latitude energy inputs are organized which makes it a very convenient tool for use in a wide variety of studies of the polar thermosphere.

7.3 Auroral Activity and the Atomic Oxygen Distribution

A magnetic activity index based on the auroral electrojet index AL was developed for comparison with the atomic oxygen data taken during two magnetic storms. The auroral electrojet index is a measure of the high latitude ionospheric current and hence of the Joule heating in this region. The magnetic activity index was of the form,

$$ML(t)_\tau = \frac{1}{\tau}\int_{-\infty}^{t} AL(t')e^{-(t-t')/\tau}\,dt' \qquad (7.1)$$

Values of the time constant, τ, were found to range from 12 to 24 hours for storm recovery but less than 12 hours for storm onset.

7.4 Suggestions for Future Research

One of the most important areas where further work in global empirical modeling is needed lies in the response of the thermosphere to magnetic disturbances. Current magnetic activity indices such as ap and Kp are not well correlated with the energy input to the auroral regions and to the resultant Joule heating. Major improvements in magnetic activity corrections must be based on indices more directly related to the actual energy deposition processes. The best current indices are the auroral electrojet indices AU, AL, and AE. Work should be done on the theoretical and experimental relations of these indices to the spatial and temporal variations of the energy inputs and on the atmospheric response (Nisbet, 1980).

Measurements of lower altitude thermospheric temperatures over the entire globe which are direct would also be of tremendous value. Such information would permit variable lower boundary conditions based on actual data to be employed in the models and, thereby, expand enormously the altitude range over which model predictions would be realistic.

Density and wind velocity data in the same region would be instrumental in determining the effects of turbulence on the composition and would serve as a valuable link between photochemical equilibrium models at lower heights and diffusive equilibrium models at satellite altitudes.

REFERENCES

Agy, V., Geomagnetic coordinates and geomagnetic time, NBS Report, No. 8789, 1965.

Amayenc, P. and G. Vasseur, Neutral winds deduced from incoherent scatter observations and their theoretical interpretation, J. Atmos. Terr. Phys., 34, 351-364, 1972.

Banks, P. M. and G. Kockarts, Aeronomy Part B, p. 43, Academic Press, New York, 1973.

Barlier, F., C. Berger, J. L. Falin, G. Kockarts, and G. Thullier, A thermospheric model based on satellite drag data, Ann. Geophys., 34, 9-24, 1978.

Barlier, F., C. Berger, J. L. Falin, G. Kockarts, and G. Thullier, Comparisons between various semi-empirical thermospheric models of the terrestrial atmosphere, J. Atmos. Terr. Phys., 41, 527-541, 1979.

Bartels, J., The eccentric dipole approximating the earth's magnetic field, Terr. Mag., 41, 225-250, 1936.

Bates, D. R., Some problems concerning the terrestrial atmosphere above about the 100 km level, Proc. Roy. Soc., Ser. A, 253, 451-462, 1959.

Blamont, J. E. and J. M. Luton, Geomagnetic effect on the neutral temperature of the F-region during the magnetic storm of September 1969, J. Geophys. Res., 77, 3534-3556, 1972.

Blamont, J. E., J. M. Luton, and J. S. Misbet, Global temperature distributions from Ogo 6 6300 A airglow measurements, Radio Sci., 9, 247-251, 1974.

Blum, P. W. and I. Harris, Full non-linear treatment of the global thermospheric wind system - I. Mathematical method and analysis of forces, J. Atmos. Terr. Phys., 37, 193-212, 1975a.

Blum, P. W. and I. Harris, Full non-linear treatment of the global thermospheric wind system - II. Results and comparison with observations, J. Atmos. Terr. Phys., 37, 213-235, 1975b.

Brekke, A., J. R. Doupnik, and P. M. Banks, A preliminary study of the neutral wind in the Auroral E region, J. Geophys. Res., 78, 8235-8250, 1973.

Brekke, A., J. R. Doupnik, and P. M. Banks, Observations of neutral winds in the Auroral E region during the magnetospheric storm of August 3 - 9, 1972, J. Geophys. Res., 79, 2448-2456, 1974.

Carignan, G. R. and W. H. Pinkus, OGO-F04 experiment description, Technical Note 08041-31T, University of Michigan, Ann Arbor, MI., 1968.

Carru, H., M. Petit, and F. Waldteufel, On the diurnal variation of the thermosphere temperature, Planet. Space Sci., 15, 944-945, 1967.

Chandra, S. and P. Stubbe, Ion and neutral composition changes in the thermospheric region during magnetic storms, Planet. Space Sci., 19, 491-502, 1971.

Chandra, S. and N. W. Spencer, Exospheric temperature inferred from the Aeros A neutral composition measurement, J. Geophys. Res., 80, 3615-3621, 1975.

Chanin, M. L. and G. F. Tulinov, The polar thermospheric temperature behavior during the 11-year solar cycle, J. Geophys. Res., 84, 406-410, 1979.

Ching, B. K. and Y. T. Chiu, A phenomenological model of the global electron density in the E, F1 and F2 regions, J. Atmos. Terr. Phys., 35, 1615-1630, 1973.

CIRA 1972, COSPAR International Reference Atmosphere, Akademie-Verlag, Berlin, 1972.

Cole, K. D., Joule heating of the upper thermosphere, Aust. J. Phys., 15, 223-235, 1962.

Cole, K. D., Magnetic storms and associated phenomena, Space Sci. Rev., 5, 699-770, 1966.

Cole, K. D., Electrodynamic heating and movement of the thermosphere, Planet. Space Sci., 19, 59-75, 1971.

Creekmore, S. P., J. M. Straus, R. M. Harris, B. K. Ching, and Y. T. Chiu, A global model of thermospheric dynamics - I. Wind and density fields derived from a phenomological temperature, J. Atmos. Terr. Phys., 37, 491-515, 1975.

Dickinson, R. E., E. C. Ridley, and R. G. Roble, Meridional circulation in the thermosphere, I, Equinox conditions, J. Atmos. Sci., 32, 1737-1754, 1975.

Dickinson, R. E., E. C. Ridley, and R. G. Roble, Meridional circulation in the thermosphere, II, Solstice conditions, J. Atmos. Sci., 34, 178-192, 1977.

Engebretson, M. J., K. Mauersberger, D. C. Kayser, W. E. Potter, and A. O. Nier, Empirical model of atomic nitrogen in the upper thermosphere, J. Geophys. Res., 82, 461-471, 1977.

Evans, J. V., Observation of F region vertical velocities at Millstone Hill, 1, Evidence for drifts due to expansion, contraction, and winds, Radio Sci., 6, 609-626, 1971.

Fedder, J. A. and P. M. Banks, Convection electric fields and polar thermospheric winds, J. Geophys. Res., 77, 2328-2339, 1972.

Finch, H. F. and R. B. Leaton, The earth's main magnetic field-epoch 1955.0, Monthly Notices Roy. Astron. Soc. Geophys. Suppl., 7, 314-317, 1957.

Forbes, J. M. and F. A. Marcos, Thermospheric density variations associated with auroral electrojet activity, J. Geophys. Res., 78, 3841-3847, 1973.

French, J. B., N. M. Reid, A. O. Nier, and J. L. Hayden, Rarified gas dynamic effects on mass spectrometric studies of upper planetary atmospheres, AIAA Journal, 13, 1641, 1975.

Geisler, J. E., A numerical study of the wind system in the middle thermosphere, J. Atmos. Terr. Phys., 29, 1469-1482, 1967.

Gurnett, D. A., Critical problems of magnetospheric physics, p. 123, IUCSTD Secretariat, Washington, D.C., 1972.

Gustafsson, G., Latitude and local time dependence on precipitated low-energy electrons at high latitudes, J. Geophys. Res., 78, 5537-5552, 1973.

Harper, R. M., Dynamics of the neutral atmosphere in the 200-500 km height region at low latitudes, Thesis, Rice University, Houston, Texas, 1971.

Harris, I. and H. G. Mayr, Diurnal variations in the thermosphere 1. Theoretical formulation, J. Geophys. Res., 80, 3925-3933, 1975.

Harris, I. and W. Priester, Time dependent structure of the upper atmosphere, J. Atmos. Sci., 19, 286-296, 1962.

Hays, P. B., R. A. Jones, and M. H. Rees, Auroral heating and the composition of the neutral atmosphere, Planet. Space Sci., 21, 559-573, 1973.

Hays, P. B. and R. G. Roble, Direct observations of thermospheric winds during geomagnetic storms, J. Geophys. Res., 76, 5316-5321, 1971.

Hedin, A. E. and C. A. Reber, Longitudinal variations of thermospheric composition indicating magnetic control of polar heat input, J. Geophys. Res., 77, 2871-2879, 1972.

Hedin, A. E., H. G. Mayr, C. A. Reber, and N. W. Spencer, Empirical model of global thermospheric temperature and composition based on data from the Ogo 6 quadrupole mass spectrometer, J. Geophys. Res., 79, 215-225, 1974.

Hedin, A. E., J. E. Salah, J. V. Evans, G. P. Newton, S. Chandra, C. A. Reber, P. Bauer, L. Cogger, J. P. McClure, and D. C. Kayser, Global model of thermosphere temperatures based on incoherent scatter and in-situ N_2 density measurements, EOS, 56, 1030, 1975.

Hedin, A. E., J. E. Salah, J. V. Evans, C. A. Reber, G. P. Newton, N. W. Spencer, D. C. Kayser, D. Alcayde, P. Bauer, L. Cogger, and J. P. McClure, A global thermospheric model based on mass spectrometer and incoherent scatter data, MSIS 1. N_2 density and temperature, J. Geophys. Res., 82, 2139-2147, 1977a.

Hedin, A. E., C. A. Reber, G. P. Newton, N. W. Spencer, H. C. Brinton, H. G. Mayr, and W. E. Potter, A global thermospheric model based on mass spectrometer and incoherent scatter data, MSIS 2. Composition, J. Geophys. Res., 82, 2148-2156, 1977b.

Hedin, A. E., P. Bauer, H. G. Mayr, G. R. Carignan, L. H. Brace, H. C. Brinton, A. D. Parks, and D. T. Pelz, Observations of neutral composition and related ionospheric variations during a magnetic storm in February, 1974, J. Geophys. Res., 82, 3183-3189, 1977c.

Hedin, A. E., N. W. Spencer, H. G. Mayr, I. Harris, and H. S. Porter, Direct evidence of transport processes in the thermospheric diurnal tide, J. Geophys. Res., 83, 3355-3357, 1978.

Hedin, A. E., C. A. Reber, N. W. Spencer, H. C. Brinton, and D. C. Kayser, Global model of longitude/UT variations in thermospheric composition and temperature based on mass spectrometer data, J. Geophys. Res., 84, 1-9, 1979.

Hernandez, G. and R. G. Roble, Direct measurements of nighttime thermospheric winds and temperatures 3. Monthly variations during solar minimum, J. Geophys. Res., 82, 5505-5511, 1977.

Hodges, R. R. Jr. and F. S. Johnson, Lateral transport in planetary exospheres, J. Geophys. Res., 73, 7307-7317, 1968.

I.G.R.F. 1975, IAGA Division I Study Group, International geomagnetic reference field 1975, EOS Trans. A.G.U., 57, 120-121, 1976.

Jacchia, L. G., Static diffusion models of the upper atmosphere with empirical temperature profiles, Smithson. Astrophys. Observ. Spec. Rept., No. 170, 1964.

Jacchia, L. G., Static diffusion models of the upper atmosphere with empirical temperature profiles, Smithson. Contrib. Astrophys., 8, 215, 1965.

Jacchia, L. G., Smithson. Astrophys. Observ. Spec. Rept., No. 332, 1971.

Jacchia, L. G., Thermospheric temperature, density, and composition: New models, Smithson. Astrophys. Observ. Spec. Rept., No. 375, 1977.

Jacchia, L. G., and J. W. Slowey, The shape and location of the diurnal bulge in the upper atmosphere, Space Res. VII, 1077-1090, 1967.

Jacchia, L. G., J. W. Slowey, and U. von Zahn, Latitudinal changes of composition in the disturbed thermosphere from Esro 4 measurements, J. Geophys. Res., 81, 36-42, 1976.

Jacchia, L. G., J. W. Slowey and U. von Zahn, Temperature, density, and composition in the disturbed thermosphere from Esro 4 gas analyzer measurements:A global model, J. Geophys. Res., 82, 684-688, 1977.

Kasprzak, W. T. and G. P. Newton, Comparison of the San Marco 3 Nace neutral composition data with the extrapolated OGO-6 empirical model, J. Geophys. Res., 81, 1404-1406, 1976.

Kayser, D. C. and W. E. Potter, Molecular oxygen measurements at 200 km from AE-D near winter solstice, 1975, Geophys. Res. Letters, 3, 455-458, 1976.

Kayser, D. C., Private Communication, University of Minnesota, 1977.

Kent, G. S., Measurement of ionospheric movements, Rev. Geophys. and Space Phys., 8, 229, 1970.

Kirchoff, V. W. J. H. and L. A. Carpenter, Dominance of the diurnal mode of horizontal drift velocities, J. Atmos. Terr. Phys., 37, 419-428, 1975.

Knutson, J. R., D. C. Kayser, and W. E. Potter, Mass spectrometric measurement of thermospheric wind, J. Geophys. Res., 82, 5253-5256, 1977.

Kohl, H. and J. W. King, Atmospheric winds between 100 and 700 km and their effects on the ionosphere, J. Atmos. Terr. Phys., 29, 1045-1062, 1967.

Köhnlein, W., D. Krankowsky, P. Lämmerzahl, W. Joos, and H. Volland, A thermospheric model of the annual variations of He, N, O, N_2, and Ar from the Aeros Nims data, J. Geophys. Res., 84, 4355-4362, 1977.

Krankowsky, D., P. Lämmerzahl, F. Bonner, and H. Wieder, The Aeros neutral and ion mass spectrometer, J. Geophys. Res., 79, 601-611, 1974.

Laux, U. and U. von Zahn, Longitudinal variations in thermospheric composition under geomagnetically quiet conditions, J. Geophys. Res., 84, 1942-1946, 1979.

Maeda, H., Neutral winds and ion drifts in the polar ionosphere caused by convection electric fields - 1, J. Atmos. Terr. Phys., 33, 197-205, 1976.

Mahajan, K. K., Diurnal variation of the ion temperature, J. Atmos. Terr. Phys., 31, 93-101, 1969.

Matsushita, S. and W. H. Campbell, eds., Physics of Geomagnetic Phenomena, Volume 2, Academic Press, Newyork and London, 1967.

Mauersberger, K., W. E. Potter, and D. C. Kayser, A direct measurement of the winter helium bulge, Geophys. Res. Letters, 3, 269-271, 1976.

Mayr, H. G. and I. Harris, Variations in eddy diffusion and associated transport processes, Geophys. Res. Letters, 4, 25-28, 1977.

Mayr, H. G., I. Harris, and H. Volland, Theory of the phase anomaly of the thermosphere, J. Geophys. Res., 78, 7480-7489, 1973.

Mayr, H. G. and A. E. Hedin, Significance of large-scale circulation in magnetic storm characteristics with application to AE-C neutral composition data, J. Geophys. Res., 82, 1227-1234, 1977.

Mayr, H. G. and H. Volland, Temporal variations in the atmospheric composition, paper presented at National Fall Meeting, A.G.U., San Francisco, California, 1970.

Mayr, H. G. and H. Volland, Semiannual variations in the neutral composition, Ann. Geophys., 27, 513-522, 1971.

Mayr, H. G. and H. Volland, Theoretical model for the latitudinal dependence of the thermospheric annual and semiannual variations, J. Geophys. Res., 77, 6774-6790, 1972a.

Mayr, H. G. and H. Volland, Diffusion model for the phase delay between thermospheric density and temperature, J. Geophys. Res., 77, 2359-2367, 1972b.

Mayr, H. G. and H. Volland, Magnetic storm effects in the neutral composition, Planet. Space Sci., 20, 379-393, 1972c.

Mayr, H. G. and H. Volland, A two-component model of the diurnal variations in the thermospheric composition, J. Atmos. Terr. Phys., 35, 669-680, 1973a.

Mayr, H. G. and H. Volland, Magnetic storm characteristics of the thermosphere, J. Geophys. Res., 78, 2251-2264, 1973b.

Mayr, H. G. and H. Volland, Composition waves in the thermosphere, J. Geophys. Res., 81, 671-675, 1976.

Meriwether, J. W., J. P. Heppner, J. D. Stolarik, and E. M. Wescott, Neutral winds above 200 km at high latitides, J. Geophys. Res., 78, 6643-6661, 1973.

Nagy, A. F., R. J. Cicerone, P. B. Hays, K. D. McWatters, J. W. Meriwether, A. E. Belon, and C. L. Rino, Simultaneous measurement of ion and neutral motions by radar and optical techniques, Radio Sci., 9, 315-321, 1974.

Newton, G. P., W. T. Kasprzak, S. A. Curtis, and D. T. Pelz, Local time variation of equatorial thermospheric composition determined by the San Marco 3 Nace, J. Geophys. Res., 80, 2289-2299, 1975.

Nicolet, M., Structure of the thermosphere, Planet. Space Sci., 5, 1-32, 1961.

Nier, A. O., W. E. Potter, D. R. Hickman, and K. Mauersberger, The open-source neutral-mass spectrometer on Atmosphere Explorer-C, -D, -E, Radio Sci., 8, 271-276, 1973.

Nier, A. O., W. E. Potter, D. C. Kayser, and R. G. Finstad, The measurement of chemically reactive atmospheric constituents by mass spectrometers carried on high-speed spacecraft, Geophys. Res. Letters, 1, 197-200, 1974.

Nier, A. O., W. E. Potter, and D. C. Kayser, Atomic oxygen and molecular oxygen densities in the lower thermosphere, J. Geophys. Res., 81, 17-24, 1976.

Nisbet, J. S., Neutral atmospheric temperature from incoherent scatter observations, J. Atmos. Terr. Phys., 24, 586-593, 1967.

Nisbet, J. S., On the construction and use of the Penn State MK 1 ionospheric model, PSU-IRL-SCI-355, The Pennsylvania State University, 1970.

Nisbet, J. S., Theoretical relationships between the Birkeland currents and the AL, AU, and AE magnetic indices, submitted to J. Geophys. Res., January, 1980.

Nisbet, J. S. and D. A. Glenar, Thermospheric meridional winds and atomic oxygen depletion at high latitudes, J. Geophys. Res., 82, 4685-4693, 1977.

Nisbet, J. S., B. J. Wydra, C. A. Reber, and J. M. Luton, Global exospheric temperatures and densities under active solar conditions, Planet. Space Sci., 25, 59-69, 1977.

Nisbet, J. S., M. J. Miller, and L. A. Carpenter, Currents and electric fields in the ionosphere due to field-aligned auroral currents, J. Geophys. Res., 83, 2647-2657, 1978.

Offermann, D., Composition variations in the lower thermosphere, J. Geophys. Res., 79, 4281-4293, 1974.

Oran, E. S. and D. Strobel, Photochemically-induced departures of O and O_2 from diffusive equilibrium distributions, J. Geophys. Res., 81, 257-259, 1976.

Parkinson, W. D. and J. Cleary, The eccentric geomagnetic dipole, Geophys. J. Roy. Astron. Soc., 1, 346, 1958.

Pelz, D. T., C. A. Reber, A. E. Hedin, and G. R. Carignan, A neutral atmosphere composition experiment for the Atomsphere Explorer-C, -D, -E, Radio Sci., 8, 277-283, 1973.

Prölss, G. W. and K. H. Fricke, Neutral composition changes during a period of increasing magnetic activity, Planet. Space Sci., 24, 61-67, 1976.

Reber, C. A. and P. B. Hays, Thermospheric wind effects on the distribution of helium and argon in the earth's upper atmosphere, J. Geophys. Res., 78, 2977-2991, 1973.

Reber, C. A. and A. E. Hedin, Heating of the high-latitude thermosphere during magnetically disturbed periods, J. Geophys. Res., 79, 2457-2461, 1974.

Reber, C. A., A. E. Hedin, and S. Chandra, Equatorial phenomena in neutral thermospheric composition, J. Atmos. Terr. Phys., 35, 1223-1228, 1973.

Reber, C. A., A. E. Hedin, D. T. Pelz, W. E. Potter, and L. H. Brace, Phase and amplitude relationships of wave structure observed in the lower thermosphere, J. Geophys. Res., 80, 4576-4580, 1975.

Reddy, C. A., Evidence of a meridional circulation cell in the lower thermosphere during a magnetic storm, J. Atmos. Terr. Phys., 36, 1561-1564, 1974.

Roble, R. G., B. A. Emery, J. E. Salah, and P. B. Hays, Diurnal variation of the neutral thermospheric winds determined from incoherent scatter radar data, J. Geophys. Res., 79, 2868-2876, 1974.

Roble, R. G., R. E. Dickinson, and E. C. Ridley, Seasonal and solar cycle variations of the zonal mean circulation in the thermosphere, J. Geophys. Res., 82, 5493-5504, 1977a.

Roble, R. G., J. E. Salah, and B. A. Emery, A seasonal variation of the diurnal thermospheric winds over Millstone Hill during solar cycle maximum, J. Atmos. Terr. Phys., 39, 503-511, 1977b.

Roper, R. G., The dynamics of the turbopause, paper presented at Symposium on Dynamics, Chemistry and Thermal Processes in the Ionosphere and Thermosphere, Int. Assn. of Geomagn. and Aeron., Kyoto, Japan, 1973.

Salah, J. E. and J. V. Evans, Measurements of thermospheric temperatures by incoherent scatter radar, Space Res. VIII, 267-286, 1973.

Spencer, N. W., H. B. Niemann, and G. R. Carignan, The neutral atmosphere temperature experiment, Radio Sci., 8, 284-296, 1973.

Stehle, C. G., J. S. Nisbet, and E. Bleuler, A global model of the neutral thermosphere in magnetic coordinates based on Ogo 6 data, submitted to J. Geophys. Res., November, 1979.

Straus, J. M., Departures from hydrostatic equilibrium in the global distribution of thermospheric argon, J. Geophys. Res., 82, 5249-5252, 1977.

Straus, J. M. and L. Christopher, Dynamical effects on the global distribution of thermospheric atomic oxygen, J. Geophys. Res., 84, 1241-1252, 1979.

Straus, J. M., S. P. Creekmore, and B. K. Ching, A dynamical model of upper-atmospheric helium, J. Geophys. Res., 82, 2132-2138, 1977.

Taeusch, D. R., G. R. Carignan, and C. A. Reber, Neutral composition variation above 400 kilometers during a magnetic storm, J. Geophys. Res., 76, 8318-8325, 1971.

Taeusch, D. R. and B. B. Hinton, Structure of electrodynamic and particle heating in the undisturbed polar thermosphere, J. Geophys. Res., 80, 4346-4350, 1975.

Thuillier, G., J. L. Falin, and C. Wachtel, Experimental global model of the exospheric temperature based on measurements from the Fabry-Perot interferometer on board the Ogo 6 satellite - Discussion of the data and properties of the model, J. Atmos. Terr. Phys., 39, 399-414, 1977.

Trinks, H., K. H. Fricke, U. Laux, G. W. Prölss, and U. von Zahn, Esro 4 gas analyzer results 3. Spatial and temporal structure of the mid-latitude atmosphere during a geomagnetic storm, J. Geophys. Res., 80, 4571-4575, 1975.

Trinks, H. and U. von Zahn, The Esro 4 gas analyzer, Rev. Sci. Instrum., 46, 213-217, 1975.

Vest, R., A three-dimensional model of the thermosphere with auroral heating, PSU-IRL-SCI-412, The Pennsylvania State University, 1973.

Volland, H. and H. G. Mayr, The degeneration of the Hough functions within the thermosphere, Space Res. XII, Akademie-Verlag, Berlin, 1095-1099, 1972.

Volland, H. and H. G. Mayr, A numerical study of three-dimensional diurnal variations within the thermosphere, Ann. Geophys., 29, 61-75, 1973.

von Zahn, U., K. H. Fricke, and H. Trinks, Esro 4 gas analyzer results, 1., First observation of the summer argon bulge, J. Geophys. Res., 78, 7560-7562, 1973.

von Zahn, U., W. Köhnlein, K. H. Fricke, U. Laux, H. Trinks, and H. Volland, Esro 4 model of global thermospheric composition and temperature during times of low solar activity, Geophys. Res. Letters, 4, 33-36, 1977.

Waldteufel, P. and J. P. McClure, Preliminary comparisons of middle and low latitude Thomson scatter data, Ann. Geophys., 25, 785-792, 1969.

Walker, J. C. G., Analytic representation of upper atmosphere densities based on Jacchia's static diffusion models, J. Atmos. Sci., 22, 462, 1965.

Wydra, B. J., Global exospheric temperatures and densities under active solar conditions, PSU-IRL-SCI-436, The Pennsylvania State University, 1975.